DEPARTMENT OF FOOD SCIENCE
FACULTY OF LIFE SCIENCES
UNIVERSITY OF COPENHAGEN

Optimization of Dairy Processes

Applied Spectroscopy and Chemometrics

PhD thesis · 2010

Christian Bøge Lyndgaard

Optimization of Dairy Processes

Applied Spectroscopy and Chemometrics

PhD thesis by
Christian Bøge Lyndgaard

2010

Optimization of Dairy Processes
Applied Spectroscopy and Chemometrics
PhD thesis 2010 © Christian Bøge Lyndgaard

ISBN 978-87-7611-390-2

Printed by SL grafik, Frederiksberg C, Denmark (www.slgrafik.dk)

Preface

This PhD thesis was carried out at the Quality & Technology Group, Department of Food Science, Faculty of Life Science, University of Copenhagen. The project was sponsored by the Danish Dairy Board as part of the research project "PAT in the Dairy Industry. The thesis was supervised by Professor Søren Balling Engelsen and Associated Professor Frans van den Berg from the University of Copenhagen.

Many people have been involved in this project. Most importantly I am grateful to my supervisors Søren and Frans. The combination of your competences has provided ideal supervision. A special thanks goes to Søren for helping me in structuring the thesis and for his constructive criticism during preparation of papers. I am most indebted to Frans for helping me in all phases of the project: introducing me to Matlab, setting up experiments (with Lego), many discussion and preparation of papers.

Fonterra invited me to work in New Zealand for seven months. It was a most rewarding stay where I experienced many facets of a very well functioning dairy industry; especially within application of Process Analytical Technology. My special thanks go to my supervisor Steve Holroyd for introducing me to people around the company as well as wineries of Hawke's Bay. Furthermore, Scott Fisherman Thomsen, Rob Crawford and Tristan Hunter are also thanked for making the stay a good experience both professionally and socially.

I am thankful to my colleagues at Q&T for contributing to a great working environment both socially and academically. A special thanks goes to both Åsmund Rinnan and Morten Arendt Rasmussen for being the victims of my endless questions regarding chemometrics. The company of my office mate Franscesco Savorani has been greatly appreciated despite his numerous humiliations of me in table tennis. Anders Lawaetz is thanked for good companionship, sick jokes and for suffering in parallel with me during the finalization of our theses.

Finally, the warmest of thanks goes to my lovely fiancée Lotte Bøge Sørensen (soon-to-be-Lyndgaard) for proof-reading this thesis and most of all for her care, support and patience during this mission.

Christian Lyndgaard Hansen

August 2010

Abstract

This thesis describes some applications of spectroscopic and chemometric methods for analysis of dairy processes. The approach has been to measure during processing and thereby take advantage of the rapid and non-invasive nature of spectroscopic methods. The work is presented in six papers that make up the core of the thesis. The thesis furthermore gives an introduction to the processes investigated, the concept of PAT and the methods applied.

The cheese manufacturing process was studied by TD-NMR, specifically the syneresis step i.e. whey separation (**PAPER I**). This process is important as it is the cheese producer's main way of controlling the moisture content of the final cheese. The process is however complex to evaluate due to the fact that it is a heterogeneous dynamic system sensitive to physical handling. TD-NMR can be successfully applied as it is non-invasive and sufficiently rapid to capture the dynamics. It was possible to quantify the moisture content inside and outside the syneresis curd at all times during the process. The approach makes it possible to study dynamics and influencing factors of syneresis.

Ultrafiltration of milk yields the by-product UF permeate, which is extensively re-used in the other dairy processes. Factory-to-factory variation in permeate composition can be a potential problem when permeate from multiple factories is used as ingredient in one product. In **PAPER II** permeate compositional variation between six dairy factories was surveyed using infrared spectroscopy. PCA revealed that permeate samples had a unique infrared signature based on the factory of origin, and that variation in total solids and protein explained a large part of the differences between factories. To further investigate if other factory specific variation existed, protein and total solids information were removed from the IR spectra by orthogonalization. After orthogonalization, neither PCA nor ECVA could classify the factory origin. The study demonstrated the benefit of IR and chemometrics in exploring unknown variations in a production environment.

In-line monitoring of rennet milk coagulation was studied by fiber optic near infrared spectroscopy (**PAPER III**). Terminating milk coagulation at the right coagulum firmness is critical for yield and moisture of the final cheese. The cheese maker's knife test is still the dominating method of evaluating coagulum firmness, even at large modern dairies. Results of the present thesis showed that NIR measurements are sensitive to coagulation since underlying coagulation reactions could be identified in the NIR signal. A model capturing coagulation dynamics during micelle aggregation and network formation was proposed. The model showed near perfect fit to NIR data. Furthermore, an algorithm was designed to extract the two-stage model parameters in real-time. The approach makes it possible to predict the optimal end-point of coagulation in real-time. Where PAPER III considers the production aspect of coagulation, **PAPER IV**

focuses on understanding the NIR light scattering properties of milk. The main observation was that scatter changes are highly wavelength dependent in the beginning of coagulation and less in the later stages. The observations are discussed in relation to particle size and geometry changes occurring during milk coagulation.

An automatic algorithm for analyzing large TD-NMR datas set was developed in **PAPER I**. The algorithm is further discussed in **PAPER VI**. The approach was tested on TD-NMR measurements of potatoes in order to predict dry matter content (**PAPER V**).

This thesis has shown some advantages of spectroscopic and chemometric methods for analyzing three dairy processes. It has been shown that the combination of these two disciplines can provide process insight and control possibilities that classical analytical techniques cannot offer.

Resumé

Formålet med dette ph.d. studium har været, at udforske anvendelsen af nogle spektroskopiske og kemometriske metoder til analyse af mejeriprocesser. Fremgangsmåden har været at måle under selve processen og dermed udnytte spektroskopiske metoders høje analysehastighed og ikke-invasive karakteristika. Projektets resultater er præsenteret gennem seks artikler, der udgør kernen i afhandlingen. Afhandlingen giver endvidere en introduktion til de processer som er undersøgt, PAT konceptet og de anvendte metoder.

Syneresеprocessen under ostefremstilling blev undersøgt vha. TD-NMR (**ARTIKEL I**). Denne proces er vigtig, da det er her mejeristen har størst mulighed for at kontrollere vandindholdet af den færdige ost. Processen er dog meget kompleks at undersøge, idet ostmasse-valle systemet er meget heterogent, under konstant ændring, samt er følsom over for fysisk håndtering. TD-NMR som metode, blev fundet ideel til at undersøge syneresen, idet metoden er ikke-invasiv og tilpas hurtig til at kunne opfange processens dynamik. Studiet viste at TD-NMR kunne bruges til at kvantificere vandindhold indenfor og udenfor ostemassen løbende under synerese processen. Denne fremgangsmåde gør det muligt, at undersøge dynamikken i syneresen samt forskellige faktorers indflydelse på syneresen.

Ultrafiltrering af mælk giver bi-produktet UF permeat som i stort omfang genbruges i andre mejeriprodukter. Variation i permeats sammensætning mellem fabrikker kan blive et problem, når permeat fra forskellige fabrikker anvendes som ingrediens i samme produkt. I **ARTIKEL II** blev variation i permeat sammensætningen mellem seks mejerier undersøgt med infrarød spektroskopi. PCA viste at permeatprøverne havde en unik infrarød signatur alt efter hvilket mejeri de stammede fra, og at variation i total tørstofsindhold og protein forklarede en stor del af forskellene mellem mejerierne. For videre at undersøge om andre mejeri-specifikke variationer eksisterede, blev information om protein og totalt tørstofsindhold fjernet fra IR spektrerne vha. matematisk orthogonalisering. Efter orthogonalisering kunne hverken PCA eller ECVA klassificere prøverne i forhold til deres oprindelses mejeri. Studiet demonstrerer fordelene af IR og kemometri i forhold til at udforske ukendt variation i et produktions miljø.

In-line monitorering af løbekoagulering blev undersøgt vha. fiber optisk nær infrarød spektroskopi (**ARTIKEL III**). At stoppe mælke koagulering ved den rigtige koagel fasthed er særdeles kritisk for udbyttet og vandindholdet af den færdige ost. Mejeristens knivtest er stadig den mest anvendte metode til at bedømme mælke koagelets fasthed, selv på store moderne mejerier. Resultater fra den nærværende afhandling viser at NIR målinger er sensitive overfor koagulering idet de underlæggende koaguleringsreaktioner kan identificeres i NIR målinger.

En model der beskriver koaguleringsdynamikken under micelle sammenklumpning og netværks dannelsen blev formuleret. Modellen viste et næsten perfekt fit til NIR målingernes tidsudvikling. Endvidere blev en algoritme designet til at udtrække modellens parametre i real-tid, således at NIR kan anvendes som in-line prædiktionsmetode af sluttidspunktet. Mens Artikel III overvejer produktions aspektet ved koagulering, så fokuserer **ARTIKEL IV** på forståelse af de optiske egenskaberne af mælk under koaguleringen. Hoved observationen var at lysspredningsændringer er meget bølgelængde afhængig i begyndelsen af koaguleringen og mindre i de senere faser. Disse observationer er diskuteret i relation til de ændringer i partikelstørrelse og gel netværks geometri som opstår under mælke koagulering.

En automatiseret algoritme til analyse af store TD-NMR data sæt blev udviklet i Artikel I. Denne algoritme bliver diskuteret nærmere i **ARTIKEL VI**. Denne metode blev testet på TD-NMR målinger af kartofler med henblik på at bestemme tørstofsindholdet (**ARTIKEL V**).

Overordnet set har denne ph.d. afhandling vist en række fordele ved at anvende spektroskopi og kemometri til at analysere mejeri processer. Der er vist at kombinationen af disse to discipliner kan bidrage med proces indsigt og kontrol muligheder som klassiske analytiske teknikker ikke kan tilbyde.

List of publications

PAPER I

Hansen, C.L., Rinnan, Å., Engelsen, S.B., Janhøj, T., Micklander, E., Andersen, U. and van den Berg, F. (2010): Effect of Gel Firmness at Cutting Time, pH, and Temperature on Rennet Coagulation and Syneresis: An *in situ* 1H NMR Relaxation Study. Journal of Agricultural and Food Chemistry, 58 (1), 513-519.

PAPER II

Hansen, C.L., van den Berg, F., Rasmusen, M.A., Engelsen, S.B. and Holroyd, S. (2010): Detecting variation in ultrafiltrated milk permeates – Infrared spectroscopy signatures and external factor orthogonalization. Chemometrics and Intelligent Laboratory Systems, *In Press*

PAPER III

Hansen, C.L., van den Berg, F. and Engelsen, S.B. (2010): Real-time modeling of milk coagulation. Journal of Food Engineering, *Submitted*

PAPER IV

Dahm, D., Hansen, C.L., Hopkins, D. and Norris, K. (2010): NIR discussion forum: analysis of coagulating milk. NIR news, 21 (5), 16-17.

PAPER V

Hansen, C.L., Thybo, A.K., Bertram, H.C., Viereck, N., van den Berg, F. and Engelsen, S.B. (2010): Determination of dry matter content in potato tubers by low-field NMR. Journal of Agricultural and Food Chemistry, 58 (19), 10300-10304.

PAPER VI

Hansen, C.L.,. van den Berg, F. and Engelsen, S.B. (2010): Using PARAFAC core-consistency to estimate the number of components in LF-NMR data - application to in-situ studies of mechanically induced gel syneresis in cheese production. In Magnetic Resonance in Food Science, Renou, J.P.; Webb, G. A.; Belton, P. S.; Rutledge, D. N., Eds.; The Royal Society of Chemistry: 2010; *In Press*.

ADDITIONAL WORK BY THE AUTHOR

Hansen, C.L., Berg, F.v.d., Zacheriassen, C.B. and Engelsen, S.B. (2008): Proces Analytisk Teknologi i mejeriindustrien. Mælkeritidende, 6, 128-131.

Hansen, C.L., Berg, F.v.d., Ringgaard, S., Stødkilde-Jørgensen, H. and Karlsson, A.H. (2008): Diffusion of NaCl in meat studied by ^{1}H and ^{23}Na magnetic resonance imaging. Meat Science, 80, 851-856.

Hansen, C.L., Berg, F.v.d., Ringgaard, S., Stødkilde-Jørgensen, H. and Karlsson, A.H. (2007): Magnetisk resonans billed analyse til at undersøge saltning af kød. Dansk kemi, 88, nr. 8, 20-23.

List of Abbreviations

ALS	Alternating Least Squares
DWS	Diffuse Wave Spectroscopy
ECVA	Extended Canonical Variate Analysis
EFO	External Factor Orthogonalization
FT	Fourier Transform
FTIR	Fourier Transform infrared
*i*ECVA	Interval Extended Canonical Variate Analysis
*i*PLS	Interval Partial Least Squares
IR	Infrared
MIR	Mid Infrared
MLR	Multiple Linear Regression
MSC	Multiplicative Scatter Correction
NIR	Near Infrared
NMR	Nuclear Magnetic Resonance
PARAFAC	PARAllel FACtor analysis
PAT	Process Analytical Technology
PC	Principal Component
PCA	Principal Component Analysis
PLS	Partial Least Squares
R^2	Square root of the correlation coefficient
RMSEC	Root Mean Square Error of Calibration
RMSECV	Root Mean Square Error of Cross Validation
RMSEP	Root Mean Square Error of Prediction
SNV	Standard Normal Variation
SV	Singular Value
SVD	Singular Value Decomposition
TD-NMR	Time Domain Nuclear Magnetic Resonance

Table of Contents

CHAPTER 1
INTRODUCTION

Background

The subject of this thesis is spectroscopic analysis of dairy processes. Dairy processes are inherently complex since both large biological variation in starting materials and a multitude of process factors will influence end-product quality. The objective of this PhD project has been partly to understand the fundamental biological mechanisms, but foremost being able to *identify*, *measure* and *control* the critical-to-quality attributes and their relation to end-product quality.

The dairy industry has to ensure that the quality and safety of intermediates and end-products meets well-defined specifications. One strategy to achieve this is to thoroughly check the quality of each batch of the final product. The problem with this approach is that if the final product is out of specification this cannot be easily corrected. A more attractive strategy is therefore analysis of not only the process input and output, but also continues performance evaluation during the process. This will enable control of all relevant processing parameters in *real-time*. The benefit of this approach is rapid detection and correction of processes moving out of specification. This in turn makes it possible to minimize specification margins, yielding increased productivity and profitability.

In 2004 the US Food and Drug Administration (FDA) formulated a guidance to Process Analytical Technology (PAT) recommending pharmaceutical manufactures to move from strict end-product analysis to analysis of whole process chain – parts of this document will is used as guidance in this work. Over the last couple of decades the dairy industry has increasingly recognized the benefits of moving from strict end-product evaluation to continuous analysis of multiple steps throughout the entire process, albeit often in a fragmented manner.

Scope of thesis

This thesis investigates whether spectroscopy can be used as a tool in optimizing the production of dairy processes exemplified by the *coagulation* and *syneresis* step in cheese manufacturing, and *ultrafiltration of milk*:

Controlling the degree of syneresis, i.e. whey expulsion from coagulated milk, is the cheese producer's main way of controlling the moisture content of the curd, which in turn affect the ripening process and moisture content of the final cheese product. Thus, this process step is extremely important for the final yield and quality of the cheese. It is however complex to measure syneresis, mainly

because physical handling of syneresing curd in itself induces further syneresis. The objective of **PAPER I** was to investigate Time Domain Nuclear Magnetic resonance (TD-NMR) as a method for quantification of syneresis. The approach was to induce syneresis by cutting the coagulum inside the NMR spectrometer. The approach was tested in a factorial design, investigating the effect of milk pH, temperature, and gel firmness at cutting time on syneresis rate.

Ultrafiltration of milk yields a by-product UF permeate, which is extensively re-used in the other dairy processes. Factory-to-factory variation in permeate composition can be a potential problem when permeate from multiple UF factories is used as ingredient in one product. The objective of **PAPER II** was to survey UF permeate compositional variation between six dairy factories using infrared spectroscopy. Permeate composition was furthermore analyzed using uni-variate reference analysis. PCA and ECVA were used to investigate between-factory-variation and external factor orthogonalisation was used to remove compositional information in IR spectra.

The milk coagulation step in cheese production ends with cutting of the coagulum in dices. Cutting is the primary way of separating water from the coagulum as increased surface area and pressure induces syneresis. Timing the cut at the right coagulum firmness is important. If the coagulum is too weak it will scatter into small particles which will be lost during the later drainage. On the other hand if the coagulum is too firm, whey expulsion is inhibited resulting in cheese with too high moisture content. At present the dominating tool available for cheesemaker's is the *knife test*, where coagulum cuttability is determined based on visual appearance of small test cut. The objective of **PAPER III** was to investigate rapid NIR analysis in the cheese vat (in-line) as a method for prediction of optimal cutting time. The objective of **PAPER IV** was to understand the change in NIR scattering properties of coagulating milk.

The study described in **PAPER I** resulted in approximately 2000 NMR relaxation curves with varying number of exponential components. This extensive data set makes it natural to construct an automated algorithmic approach for analysis of the individual relaxation curves. The algorithm was based on DOUBLESLICING, a rapid technique with many validation possibilities, where a set of validation criteria limits automatically can select the appropriate number of components. DOUBLESLICING and its validation possibilities are described in **PAPER VI**. The objective of **PAPER V** was to investigate TD-NMR as a tool for determine dry matter in potatoes; the algorithm developed in **PAPER I** was applied.

Outline of thesis

This thesis can be considered as an introduction to PAT applied in the dairy industry with special emphasis on cheese production. The thesis consists of an

introductory part followed by a four peer-reviewed papers (**PAPER I, II, III and V**), a conference paper (**PAPER VI**) and one discussion paper (**PAPER IV**). The introductory part serves to guide the reader into the fundamentals of three dairy processes, the analytical methods used as well as the major results. The introductory part is composed of the following chapters:

Chapter 1 initially presents an overview cheese production. Subsequently, the processes milk coagulation and curd syneresis are described in details: molecular mechanisms, kinetics, and effect of process factors/parameters, plus classical methods used to evaluate these processes. This chapter provides a basic understanding of the dairy technology.

Chapter 2 considers dairy processes from a PAT point of view. First an introduction to PAT and control concepts are given, then results from the thesis and other PAT applications in the dairy industry are presented.

Chapter 3 describes fundamentals of the spectroscopic methods used in this thesis, TD-NMR, NIR and IR.

Chapter 4 presents the basic and advanced chemometric methods used in this thesis, with special emphasis on modeling TD-NMR data and external factor orthogonalization.

Chapter 5 summarizes the conclusions and challenges of the study, and presents the perspectives for further use of spectroscopic methods in analyzing dairy processes.

CHAPTER 2
DAIRY PROCESSES

This thesis considers dairy processes in particular the early stages of cheese manufacturing and the process of ultrafiltrating milk. This chapter is divided in three parts. The first part provides an overview the entire process of cheese manufacturing. The second and the third part consider two unit operations, coagulation and syneresis, respectively. Both operations are described with respect to underlying molecular mechanisms, kinetics and the effect of various process factors, including the classical reference methods used to study the processes.

2.1 Overview of cheese making

Cheese making can be summarized as an array of sub-processes as illustrated in Figure 1. The manufacturing of cheese is essentially a concentration process, where milk fat and casein are concentrated approximately ten-fold, while the whey proteins, lactose and water soluble salts are removed with the whey. Rennet coagulated cheeses are ripened for a period ranging from 2 weeks to 2 years, during which microbiological, biochemical, and physical changes occur (Fox and McSweeney, 1998). All varieties of cheese can be categorized in three *super families* based on the principal method used to coagulate the milk i.e. rennet coagulation (~75% of total production), isoelectric acid coagulation or coagulation based on a combination of heat and acid (Fox and McSweeney, 1998). In this thesis only rennet coagulation has been studied.

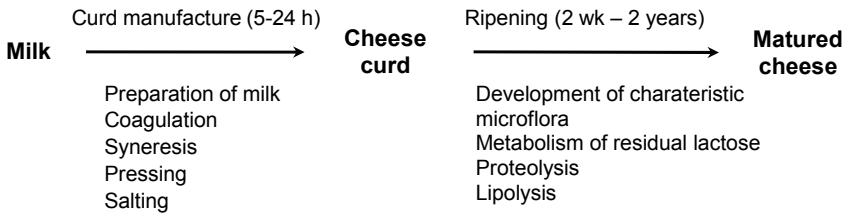

Figure 1. Summary of the cheese making process (adapted from Walstra *et al.*, 2004).

The focus of this thesis is on three different processes related to curd manufacturing, which is illustrated by the three blue boxes in Figure 2. The manufacturing of the curd is also the part of cheese making with the largest possibility of controlling the quality attributes of the final cheese.

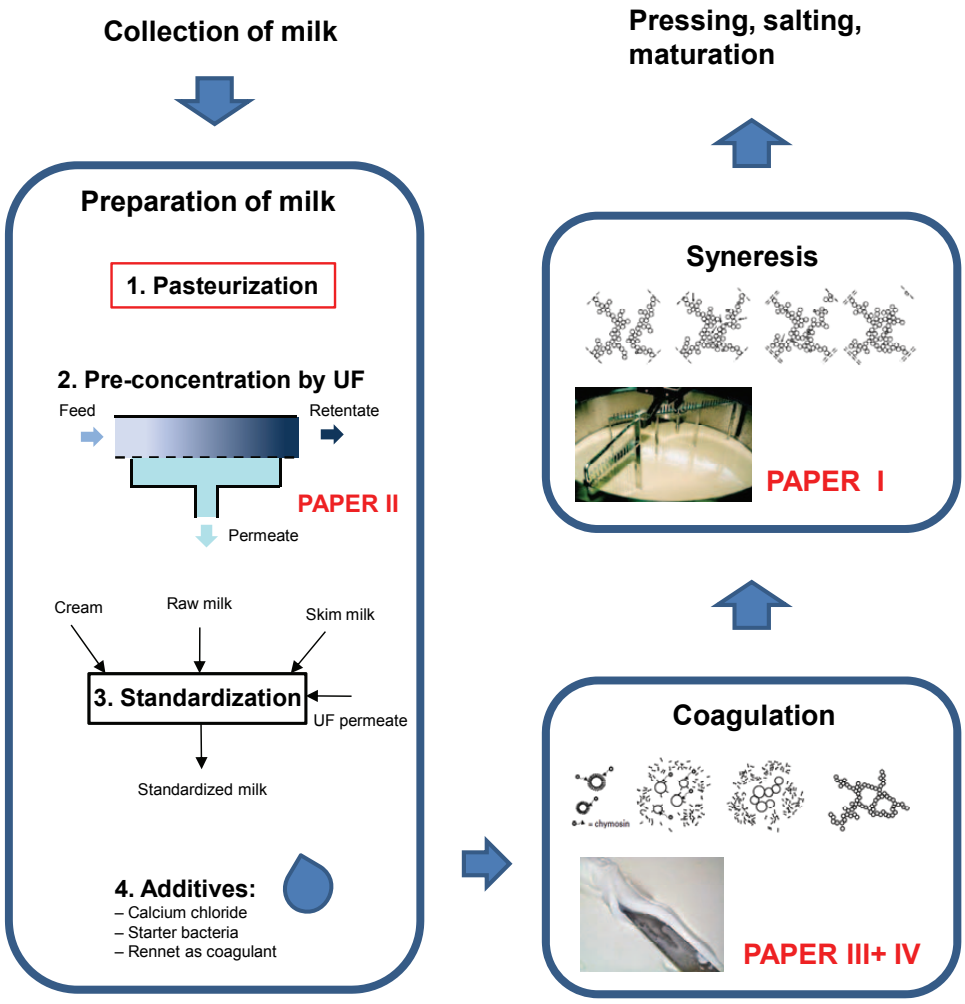

Figure 2. Overview of curd making.

Preparation of milk

The milk used to produce most cheese varieties undergoes some sort of pre-treatment. Concentration of fat and casein and the ratio of *fat-to-casein* are important parameters affecting cheese quality (Fox and McSweeney, 1998). The composition of milk will vary according to season and geography, but within the last two decades technological advancements, in ultrafiltration and on-line standardization have made it possible to level out these variations in milk composition and thereby improve or standardize curd characteristics and cheese quality. Ultrafiltration has made it possible to concentrate fat and casein content, which is important in the standardization of milk. On-line standardization has become widely used at large dairy plants. The principle in on-line standardization

is that the whole milk composition is rapidly determined typically by Infrared spectroscopy (IR) and feedback control of various feeding stream (skim, cream, UF permeate) ensures a constant fat-to-protein ratio (Fagan *et al.*, 2009; details are given in section 3.4.2). In the last decade UF permeate (a bi-product from ultrafilation of milk) has been re-used in large quantities as mixing ingredient in the standardization process. Factory-to-factory variation in permeate composition can be a potential problem when permeate from multiple UF factories is used as ingredient in one product. The objective of **PAPER II** was to survey UF permeate compositional variation between six dairy factories using infrared spectroscopy.

The majority of all cheese milk is pasteurized (72^{o}C at 15 s) shortly prior to coagulation with the purpose of inactivating pathogenic and spoilage bacteria. At some plants the milk is thermized (69^{o}C at 15 s) upon arrival to reduce the greater part of the bacteria before storage. The pH and concentration of calcium also varies in raw milk and both factors influence the characteristics of curd. Addition of $CaCl_2$ (0.02% aqueous solution) is widely used and standardization of pH can be done using the acidogen, gluconic acid-δ-lactone, although this is only practiced on a limited scale (Fox and McSweeney, 1998).

Conversion of milk to curd

Rennet coagulation is initiated by adding rennet to milk, where the principal proteinase chymosin in rennet modifies the casein micelles of the milk. κ-casein, which is a hairy-like peptide chain protruding the surface of the micelle, is cleaved very specifically by chymosin. When about 60-80% of the κ-casein has been proteolyzed, several of the repulsive forces between micelles are removed and the micelles start the form a gel (Fox and McSweeney, 1998). This process and the factors affecting it are described more detailed in section 2.2. The objective of **PAPER III** was to investigate rapid NIR analysis in the cheese vat (in-line) as a method for prediction of optimal cutting time. The objective of **PAPER IV** was to understand the change in NIR scattering properties of coagulating milk.

Curd syneresis

Rennet gels are very stable, and an essential process step of curd making is cutting the gel into cubes (called grains) to provoke syneresis (whey separation). Controlling the degree of syneresis is the cheesemaker's main way of controlling the moisture content of the curd, which in turn affect the rate of the ripening process and moisture content of the final cheese product (Fox and McSweeney, 1998). Thus, this process step is extremely important for the quality of the cheese. A detailed description of the syneresis process and the influencing factors is given in section 0. **PAPER I** investigates the use of Nuclear Magnetic Resonance (NMR) to quantify the extent of syneresis. The gel strength at cutting influences the progress of syneresis and optimal timing of cutting is therefore a

critical manufacturing step. **PAPER III** investigates the use of in-line NIR for finding the right time of the cutting at the optimal gel firmness.

2.2 Milk coagulation

This section serves to introduce the reader to an understanding of the biochemical processes behind coagulation as well as some of the classical methods used to study the process.

2.2.1 Structure of casein micelles

The structure and behavior of the casein micelles in milk are highly related to the coagulation process. Approximately 74-78% of milk protein is casein, which is not present in true solution but as a suspension of micelles which has a hydrophobic core and a hydrophilic surface. Figure 3 illustrates the structure of a casein micelle. The hydrophilic surface is due to the presence of κ-casein, which is a long peptide (build from 169 amino acid units) representing 12-15% of the total casein. κ-casein plays an important role in relation to coagulation because the rennet enzyme chymosin is extremely selective towards Phe_{105} – Met_{106} bond in κ-casein. It is precisely this event of κ-casein that initializes rennet coagulation (Fox and McSweeney, 1998).

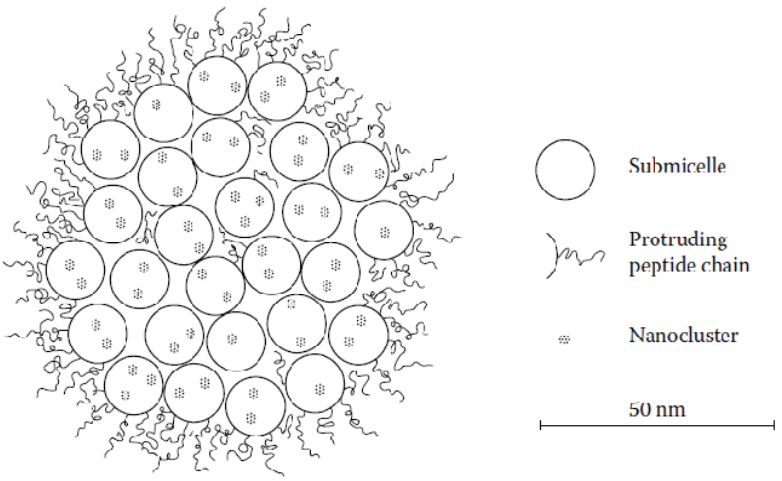

Figure 3. Cross section of the casein micelle (Walstra *et al.*, 2006).

2.2.2 Colloidal stability of milk

To understand why κ-casein cleavage induces coagulation, some colloidal aspect of milk are described. One of the phenomena in milk keeping casein micelles

from spontaneous aggregation is *steric repulsion* between micelles. Repulsion can occur when two micelles come close enough for their κ-casein hairy layers to interact. The reason for this repulsion is that the local concentration of polymers is increased, causing an increase in osmotic pressure. To counteract this process solvent is sucked into the gap between the micelles, which drives them apart. Steric repulsive forces can be quite strong if the polymer chain density is high (Walstra *et al.*, 2006)

Another closely related phenomenon is *electrostatic repulsion*. Particles in aqueous solutions most often bear an electric charge. In the micelle the *surface potential* is generally below 25 mV. At physiological pH the potential is, however, negative which causes the particles to repel each other, when they approach each other. As the pH decreases the surface potential approaches zero, which is one of main reasons why pH is a factor affecting coagulation rate.

There are not only repulsive forces in the colloidal system of milk. In fact, *Van der Waals attraction forces* along with calcium binding complex formation are believed to be the dominating reasons for micelle aggregation (Lucey, 2003).

2.2.3 Micelle Aggregation

Micelles start to aggregate when the greater part (60-80%) of the κ-casein hairs have been cleaved so that the steric (and electrostatic) repulsive forces have been diminished sufficiently. The more κ-casein chymosin has removed the greater the rate of flocculation, because a greater number of free non-hairy sites are available. Casein denuded κ-casein is referred to as para-casein, depicted below.

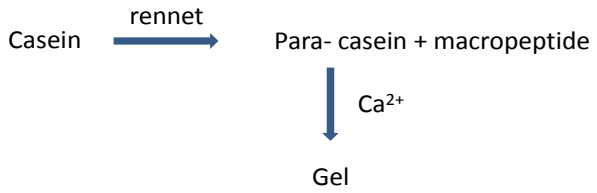

For aggregation to occur a sufficient Ca^{2+} concentration is also required because Ca^{2+} diminishes the electrostatic repulsion between micelles and Ca^{2+} ions can make bridges between negative sites in the para-casein micelles. In this process pH also plays an important role since lowering the pH will increase the Ca^{2+} activitiy (Walstra *et al.*, 2006).

Aggregation can also occur as a result of pH decrease without the presence of rennet. This happens when the milk pH is about 4.6, where the electrostatic repulsive forces are diminished, enabling micelle flocculation (Fox and McSweeney, 1998). The present project has not addressed acid coagulation and it will not be described further.

2.2.4 Kinetics of milk coagulation

In literature there seems to be consensus that rennet induced milk coagulation is the result of three underlying stages with different mechanisms (Figure 4): (I) initial enzymatic proteolysis of casein after which the altered casein micelles are referred to as para-casein; (II) subsequent aggregation of para-casein, where the aggregation rate depends on the concentration of free para-casein sites implying that this stage is dependent on rate and degree of casein proteolysis; III) gelation, formation of polymer networks where aggregated micelle strands are cross-linking, also referred to as gel firming (Storry & Ford, 1982; McMahon *et al.*, 1984; Carlson *et al.* 1987a; Castillo *et al.* 2003b).

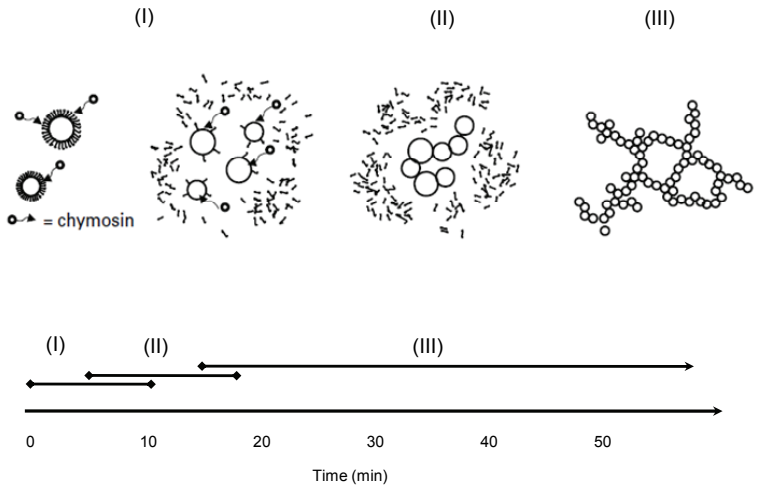

Figure 4. Illustration of the rennet coagulation process. (I) κ-casein removal by chymosin (II) para-casein aggregation and (III) gel network formation (modified from Dalgleish, 1993).

PAPER III describes a study, where milk coagulation is measured in-line by NIR reflectance spectroscopy. Figure 5 shows that the three phases can be identified from NIR measurements. The transition between stages is however not easily identified, because *head-and-tail* of the successive stage in the process overlap to some extent.

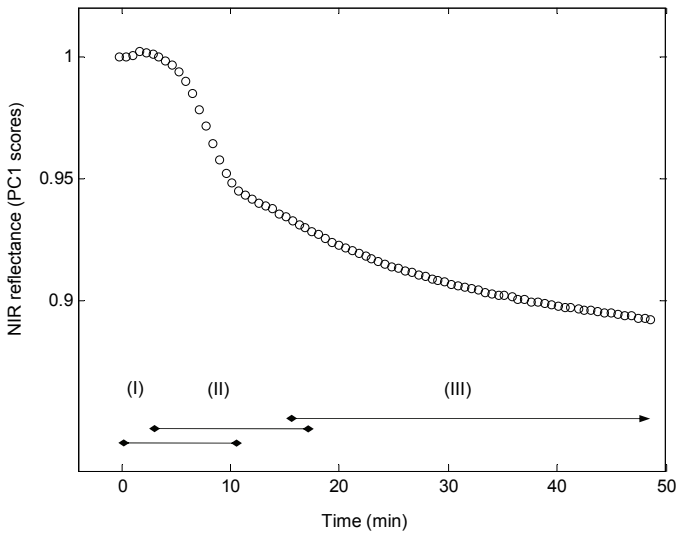

Figure 5. First principal component scores from NIR reflectance measurement during milk coagulation; (I) κ-casein proteolysis, (II) para-casein aggregation and (III) gel network formation (**PAPER III**).

Each of the three underlying coagulation phases (proteolysis, aggregation and network formation) is governed by its own reaction profile. **PAPER III** considers how to extract reaction kinetic parameters from NIR measurements of milk coagulation. The following sections serves to introduce the reader to the different rate equations that literature has suggested to explain the kinetics of each of the three phases.

Kinetics of κ-casein proteolysis

The proteolysis of κ-casein has been described by Michaelis-Menten kinetics (van Hooydonk *et al.* 1984) giving the rate of proteolysis by Equation 1:

Equation 1

$$\frac{-d[S]}{dt} = \frac{V_{\max}[S]}{K_m + [S]}$$

Where [*S*] is substrate (κ-casein) concentration, V_{max} is the maximum rate of proteolysis at infinite substrate concentration and K_m is the dissociation constant of the enzyme-substrate complex.

Although investigation of κ-casein proteolysis was not a special focus in the present thesis the proteolytic reaction causes a slight changes in NIR reflectance properties of milk. This is observed in Figure 5 (from **PAPER III**) where reflectance

increases slightly in the first 3-4 minutes after rennet addition. The same observation was made by Scher and Hardy (1993) using NIR reflectance and simultaneous measurements of casein micelle size distribution by quasi-elastic light scattering. They found that during a short initial period after rennet addition the micelle size distribution shifted slightly downwards and this was accompanied by a slight change in reflectance. Thus, the change in light scattering properties of the milk observed in the initial phase (Figure 5) seems to reflect the micelle size reduction by κ-casein cleavage.

Kinetics of aggregation and gel formation

In addition to κ-casein proteolysis **PAPER III** considers real-time modeling of the two next phases of the milk coagulation. The proposed kinetic models explaining micelle aggregation and gel formation will be reviewed in this section. Different suggestions have been made on which type of kinetics govern the aggregation reaction. Scott Blair (1970) stated that the reaction can be described by the autocatalytic logistic function, while other studies argue that second-order reaction kinetics are more appropriate to describe aggregation (Carlson *et al.*, 1987b; Castillo *et al.*, 2003b). After a certain extent of para-casein aggregation, studies have shown that the coagulation kinetics are altered to become a first order reaction (Carlson *et al.* 1987c; Castillo *et al.*, 2003b; Niki *et al.* 1994). The onset of first order kinetics has been interpreted as the gel point, defined as the point where network formation starts by cross-linking of polymer micelle strands. Carlson *et al.* (1987d) pointed out that to apply a network formation model based on first order reaction kinetics, it is necessary to determine the time at which "gelation" occurs.

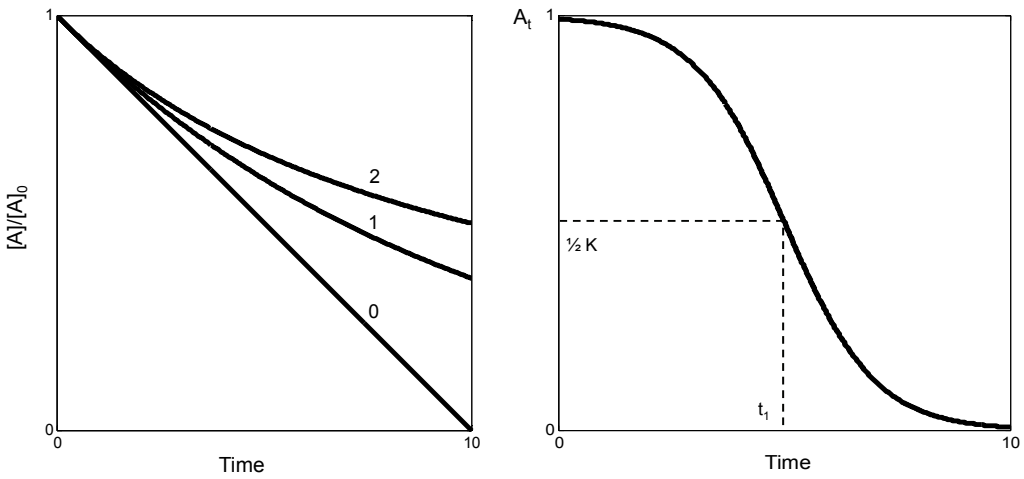

Figure 6. Change in concentration of reactant A with time for reactions of order 0, 1 and 2 (left) and the logistic function (right).

Table 1 provides an overview of rate equations and Figure 6 shows how the reactant concentration changes for reaction order 0, 1, and 2 and the logistic function. Thus, whereas the zero order reaction rate is independent of the concentration of the reactant, first and second order reactions are dependent on reactant concentration (Walstra, 2003).

Table 1. Overview of rate equations.

Order	Reaction type	Rate equation	Integrated form
0	A → B	$-\frac{d[A]}{dt} = k$	$[A]_0 - [A] = kt$
1	A → B	$-\frac{d[A]}{dt} = k[A]$	$[A] = [A]_0 \cdot \exp(-kt)$
2	A + A → AA	$-\frac{d[A]}{dt} = k[A]^2$	$\frac{1}{[A]} - \frac{1}{[A]_0} = kt$
	Autocatalytic growth/reduction	$-\frac{d[A]}{dt} = kA\left(1 - \frac{A}{K}\right)$	$[A]_t = \frac{K}{1 + \exp(-k \cdot (t - t_1))}$

2.2.5 Factors affecting kinetics

In this paragraph the main process factors influencing kinetic profiles for the different coagulation stages are discussed.

Factors that affect the rate of κ-casein proteolysis

The effect of temperature is relatively small and corresponds to the Brownian motion (the random diffusion) thereby increasing the encounter frequency between rennet molecules and the κ-casein.

pH has a large impact since lowing the pH increases the affinity of the rennet enzyme to the micelles, which increases the reaction rate. At a too low pH the reaction rate is smaller presumably because the elevated affinity is so high that it takes some time for the enzyme to release again.

Factors that affect the rate of aggregation

One of the reasons why milk coagulation is a complex process is that it involves a chain of interrelated reactions. An example of this complexity is para-casein aggregation that is depended on the degree of κ-casein proteolysis. It has been estimated that aggregation starts when 60–80% of κ-casein has been

proteolysed (Carlson *et al.* 1987a, b; Dalgleish, 1993). Castillo *et al.* (2003b) estimated that at the time of maximum aggregation rate (t_{max}) 78% of κ-casein has been proteolyzed.
Temperature has a big impact due to the increase of Brownian motion increasing the encounter frequency between para-casein micelles. E.g. at 20^{o}C aggregation does not occur at all.
Ca^{2+} concentration influences aggregation rate a lot because besides Van der Vaal attraction forces a sufficient Ca^{2+} concentration is required for two reasons: Ca^{2+} diminishes the electrostatic repulsion between micelles and Ca^{2+} ions can make bridges between negative sites in the para-casein micelles.
pH influences the aggregation rate in two ways: lowering pH increases Ca^{2+} activity and lowering pH increases affinity of the enzyme causing proteolysis to occur in concentrated regions of the micelle surface as opposed to random surface positions. In this way a *free* para-casein site become available sooner than when random surface proteolysis at higher pH occurs. Consequently, it has been observed that aggregation started at different degrees of proteolysis 70%, 60%, and 40% at pH values of 6.6, 6.2, and 5.6 respectively.

Factors affecting rate of gel formation
Temperature like in the other stages the temperature has an effect on Brownian motion. As a consequence of this the rate of gel formation is influenced. At low temperatures the joints between the particles of the gel are stronger than at high temperatures. Presumably, this is because the micelles are more swollen at low temperatures, which leaves a larger connection area with more bonds.

2.2.6 Methods of evaluating milk coagulation

Many different instruments and procedures have been developed with the aim of measuring milk coagulation or in some way get an indication of how milk gelation proceeds. There seems to be three motivations behind developing the methods:
- To test and optimize critical factors influencing coagulation such as rennet type and concentration, calcium concentration, temperature, pH, etc.
- To understand the underlying mechanisms of milk coagulation.
- As a process analytical tool with the aim of being able to act in near real-time and hereby optimize product quality (see Chapter 3).

This section of Chapter 2 provides an overview of classical reference methods used to evaluate coagulation. These methods have been used as reference for the in-line sensor methods described in Chapter 3.

The cheesemakers finger or knife test

Although a single point test method, the cheesemakers *knife test* is still the dominating method used to evaluate gel firming on the production floor. It is used in deciding when a gel is ready to be cut. The cheesemaker makes a slight cut in the coagulum with her/his finger or a knife and lifts the curd to see if there is a clean break and if clear whey is exuded. This indicates that the coagulum is ready for cutting (Lucey, 2002). This subjective method has the obvious disadvantages of requiring training and being a person-dependent source of variation. Bearing in mind that timing of cutting influences both moisture content and loss of curd fines, it seems to critical process step with room for improvement.

The Berridge methods or visual clotting

One of the simplest methods of evaluating milk coagulation semi-objectively is the method developed by Berridge (1952). It is also recognized as a standard method for testing rennet activity (IDF, 1992). Figure 7 schematically shows the setup used. The *clotting time* is determined by placing the milk in a tube, which is rotated in a water bath; a fluid film is initially formed inside the rotating tube and the clotting time is defined to be the time when when flocs of protein are visually observe in the film.

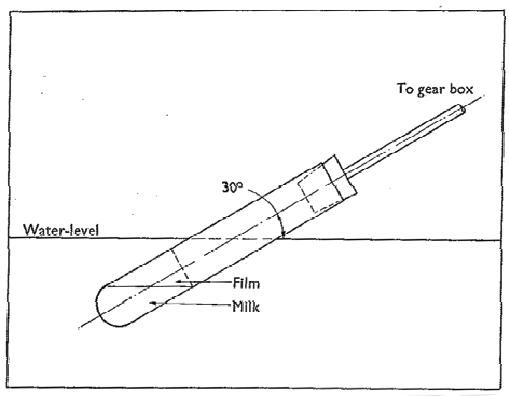

Figure 7. Setup in the Berridge clotting time method, where milk with rennet added is rotated in a tube until visible flocs are observed (Berridge, 1952).

Formagraph

Change in drag force is the measurement principle of the Formagraph, which is an older off-line instrument that is still widely used in dairy research (McMahon and Brown,1982; Heino *et al.*, 2009). The output of the Formagraph only comes on paper, and an example is shown in Figure 8. The time when the distance between two traces is 20 mm is considered a reference point in gel firmness (McMahon and Brown,1982).

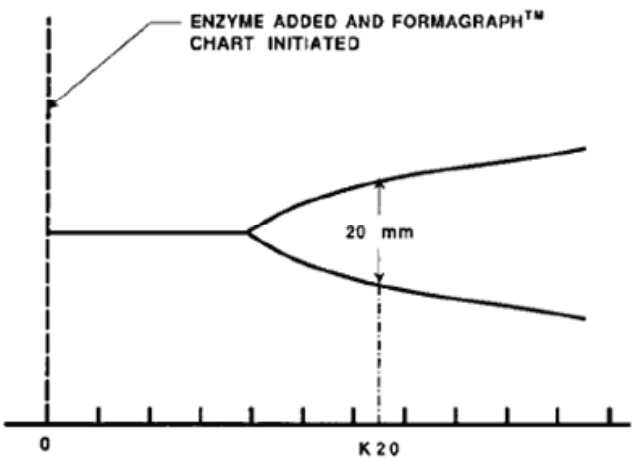

Figure 8. A typical output from the Formagraph.

Rheological methods

Rheological methods are widely used to understand the progress of milk coagulation. In **PAPER I** the effect of gel strength at cutting on syneresis rate was studied by TD-NMR. In order to compare the effect of different levels of gel firmness on syneresis, rheological measurements were carried out simultaneously by Free Oscillating Rheometry *(*FOR) using a ReoRox4 instrument.

Coagulating milk exhibit viscoelastic properties, which means that it cannot be described only as a Newtonian liquid (ideal viscous) nor as Hookean solid (ideal elastic). For a Newtonian liquid all the energy is *lost* as heat upon deformation, and for a Hookean solid all energy is *stored* upon deformation (Gunasekaran and Ak, 2003). Milk gels exhibit both an elastic behavior described by a so-called *storage module* (G') and a viscous behavior described by a *loss module* (G''). Low amplitude oscillation experiments can estimate the metrics G' and G'' by applying a small amplitude of strain τ to the sample, measuring the amplitude of the resulting stress γ (Equation 2 and Equation 3):

Equation 2

$$G' = \left(\frac{\tau}{\gamma}\right)\cos(\delta)$$

Equation 3

$$G'' = \left(\frac{\tau}{\gamma}\right)\sin(\delta)$$

Where δ is the phase angel i.e. the delay between applied strain and measured stress (Gunasekaran and Ak, 2003). In **PAPER I** 20 milk gels were cut at three different levels of G' in order to investigate if gel strength at cutting influenced syneresis. At some point during milk coagulation G' will be equal to G'', which is referred to as the *gel point* (Gunasekaran and Ak, 2003). Figure 9 shows the typical changes in viscoelastic moduli G' and G'' of coagulating milk in **PAPER I**. In this paper the viscoelastic moduli were determined in using FOR (ReoRox4) at an oscillation frequency of 10 Hz. The attentive reader might have noticed that moduli shown in Figure 9 are considerably higher (up to 600 Pa) than classical 1 Hz measurements. This is because the strain-to-stress ratio is frequency dependent i.e. increase at a higher frequency (Gunasekaran and Ak, 2003).

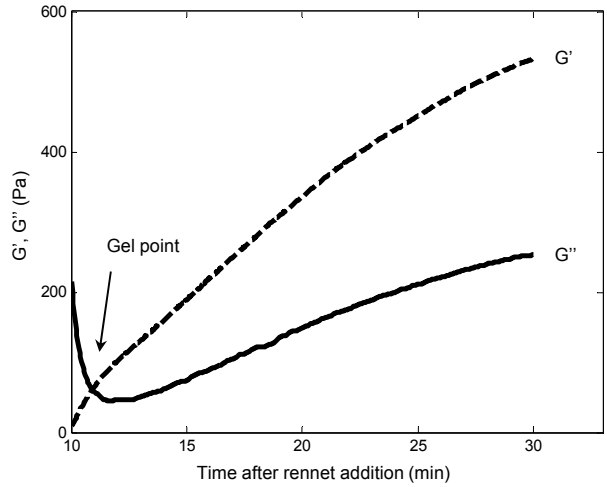

Figure 9. Changes in the storage (G') and loss (G'') moduli during rennet coagulation of milk. The gel point is identified as the cross point between G' and G''.

2.3 Curd syneresis

Syneresis is the expulsion of water and water soluble components from milk curd. During storage of dairy products e.g. yoghurt or cream cheese syneresis is undesirable, but in making cheese syneresis is an essential step. Since syneresis regulates the water content of the cheese, it is useful to understand and quantify the syneresis as a function of process conditions and milk properties. The ultimate result of syneresis is reflected in the water content of the cheese after pressing. Determining this quantity, however, yields little understanding. It is much more interesting to follow syneresis while it is going on, but this is not easy to do in a reliable and unbiased way. The research carried out in this thesis is concerned with estimating syneresis by TD-NMR (**PAPER I**). This chapter focuses on syneresis: the fundamental mechanisms, factor effects, production aspects, and especially methods of estimating syneresis.

2.3.1 Mechanisms

A milk gel that is left undisturbed will usually not show any apparent syneresis The aggregation of para-caseins forms a particle network with relatively large pores consisting of whey and fat globules. On average a micelle will link to three other micelles, but it may form junctions to additional micelles since its total surface area is reactive. As a consequence of this a higher bond energy is obtained and thereby a driving force is provided. However, for most parts the formation of new junctions are sterically hindered as the micelles are immobilized in the gel network. Nevertheless the immobilization is not complete as Brownian motion can be exhibited by some strands of the micelles. This type of motion will lead to occasional creation of new junctions, which will induce a tensile stress in the strands involved. This in turn is may lead to the breakage of such a strand (Figure 10, Dejmek *et al.*, 2004). The expected rate at which water leaves a milk gel when cut (i.e. syneresis) has been found to follow first-order reaction kinetics (Fox, 1998), which implies that the rate is dependent on the concentration of water in the gel. During enzymatic coagulation of milk water is kept in the gel as whey. The major part of the water, found in the interstices of the gel, is easy released if the interstices open. Another part of water is kept by capillary forces between the casein micelles whereas a third part is chemically bound hydrate water. Removing capillary and bound water is difficult and the majority of this water will pertain in the remainder of the cheese process (Dejmek *et al.*, 2004).

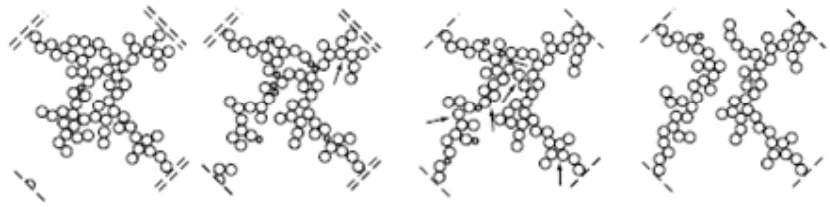

Figure 10. Illustration of strands of the para-casein micelles forming new links, causing breaking of a strand elsewhere in the gel network (reproduced from Walstra, 2006).

2.3.2 Factors affecting curd syneresis

Cutting the milk coagulum in dices (curd grains) is the event that affects syneresis most. After cutting, the coagulum is referred to as curd. There are many of factors influencing syneresis, which makes the process difficult to understand and control. The main factors are *gel firmness at cutting, surface area of the curd, stirring, pH, temperature and milk composition.*
If the coagulum is weak when being cut it will synerese slowly at first but then rapidly increase. More important is that curd fines (small fat and protein particles) are released into the whey decreasing the cheese yield. As a rule of thumb, the shear modulus should be 30 Pa at cutting (Walstra *et al.*, 2006). Optimization of cutting time using in-line NIR measurements is studied in **PAPER III** and described in detail elsewhere in the thesis (3.4.1).

Syneresis rate is proportional to the area of the surface between the curd and the whey. Therefore syneresis is enhanced by cutting the gel in cubes, which increases the surface area. This implies that smaller grains synerese faster than large. Hence, if there is a large variation in the curd grain size it can cause moisture inhomogeneity in the final cheese. Soft-type cheeses like Camembert are cut in large cubes, which lead to high moisture content. A cheese like Emmentaler is cut in smaller cubes, which lead to low moisture content (Walstra *et al.*, 2006). Stirring induces pressure, which make the curd grains collide and thereby condense each other. This implies that increasing the stirring speed increases syneresis rate. Stirring also prevent sedimentation of the grains (Everard *et al.*, 2007). It is experimentally observed that if pH is decreased the syneresis rate increases, but a clear explanation for this effect has not been found. By increasing the temperature the rate of syneresis is also increased. Finally, milk composition also has an effect, since a higher fat content causes the curd can shrink less, thereby retarding syneresis.

2.3.3 Analytical methods of evaluating syneresis

The most simple methods of evaluating syneresis are based on determining the weight or volume of the curd and whey. One way is simply to determine the volume of whey drained off. The result is very depended on conditions regarding curd handling, since it is often hard to standardize the external pressure applied, which therefore can easily give biased results (Pearse and Mackinlay, 1989). In a study by Lawrence (1959) it was demonstrated why measuring the volume or weight of whey and curd is difficult. It was observed that the rate of syneresis was affected by the volume of whey, surrounding curd particles and that when removing curd from whey, there was an increase in the rate of syneresis. Because of this numerous studies have tried to develop methods that can measure syneresis *in situ,* without physical interference.

Dilution of tracers

In order to avoid physical handling of curd, syneresis has been studied by adding a tracer compound, right after cutting, and then following the dilution of the tracer as more and more whey is expelled from the curd. One requirement for tracer methods to work is that the tracer compound does not affect the syneresis. Blue Dextran is the most used tracer compound. It has a large molecular weight ($2 \cdot 10^6$ Da), which prevents it from diffusion into and absorbing to the curd. Tracer monitoring is usually done by measuring the visual absorbance, where e.g. Blue Dextran has a maximum at 620 nm (Talens *et al.*, 2009). Another problem is to ensure homogenous distribution of the tracer without disturbing the curd with too excessive mixing (Pearse and Mackinlay, 1989). As an alternative approach Castillo *et al.* (2006) used fat content in the whey as an intrinsic tracer compound and measured dilution during syneresis using a fiber optic spectrometer in the spectral range 300–1100 nm. The obvious requirement for this approach is that all the fat is expelled at the start of syneresis and not continues during the process.

Time Domain NMR

Several TD-NMR relaxation studies have been reported on milk gel formation and syneresis (Hinrichs *et al.*, 2007; Lelievre & Creamer, 1978; Tellier *et al.*, 1993). The effect of milk gel syneresis on water proton relaxation has so far been studied on undisturbed gels (without cutting) that only exhibit spontaneous syneresis i.e. syneresis caused by pressure being built up by network formation within the gel. This is different from actual cheese manufacturing, where the coagulum is cut. In **PAPER I** syneresis, induced by cutting, was studied using TD-NMR. The results showed that after cutting the curd-whey system contained three types of water (Figure 11). The whey fraction was easily identified by its high T_2 value (1.2 - 2 s, not shown) and the approach enable continuous quantification of the water inside and outside the curd. The two remaining water

populations originates from water inside the curd; one population presumably being water tightly associated with the polymer nuclei in the curd network, and the other population being water trapped between the polymers in some way e.g. by capillary forces. In cheese production a typical target curd moisture of 55% is desirable (Walstra *et al.*, 2006), but this is not possible to measure. In the experiment shown in Figure 11 the water content of the curd can be estimated as ~60% after 110 minutes. At the present state of technology TD-NMR remains a laboratory method, but perhaps future advances will enable on-line installations, where the advancement of rapid curd moisture quantification could be utilized.

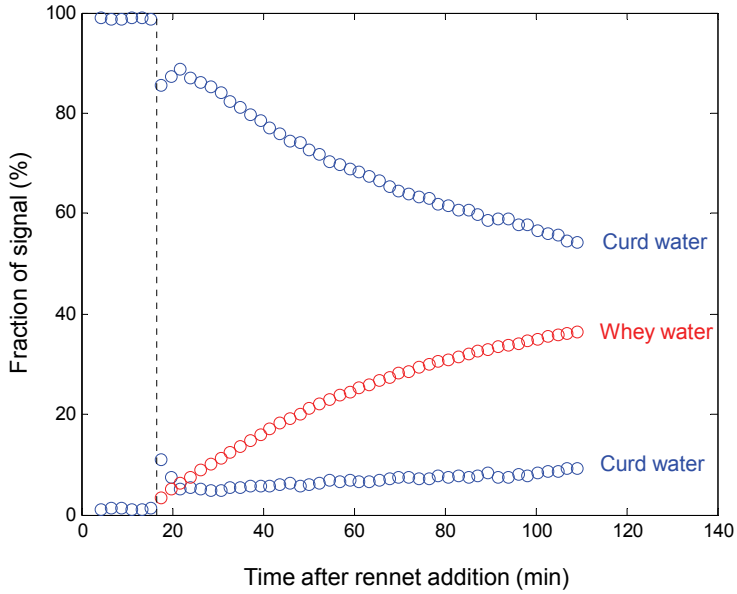

Figure 11. The evolution of three types of water during coagulation and subsequent syneresis quantified by TD-NMR. Broken line indicates time of cutting.

2.4 Summary

In this chapter cheese production has been described from different perspectives. The structure of the casein micelle is essential for understanding coagulation of milk. Rennet coagulation of milk is the result of rennet destabilization of repulsive forces in casein micelles. Destabilization of micelles in the presence of calcium will eventually cause micelles to aggregate and subsequently form a large polymer network. The underlying coagulation reactions are κ-casein proteolysis, micelle aggregation and network formation and these reactions are governed by their own kinetics. The coagulation process is complex because factors like temperature, pH, Ca^{2+} and milk composition affect kinetics of each underlying

reaction in different ways. Classical methods of evaluating milk coagulation include the knife test, Berridge clotting method, Formagraph and rheometry.

Syneresis is the expulsion of whey from milk curd, and syneresis step is the main way for the cheese producer to control moisture content of curd and the final cheese. Like coagulation, syneresis is highly dependent on a number of factors: gel firmness at cutting, temperature, pH, stirring speed, cube size and milk composition. Measuring syneresis is challenging, partly due to the heterogeneity of the curd-whey system, and partly because physical handling of curd in itself induces syneresis causing biased measurements. Methods include volumetric measurements, tracer dilution and TD-NMR. Results of **PAPER I** showed that TD-NMR can quantify syneresis non-invasively and in real-time.

CHAPTER 3
PROCESS ANALYTICAL TECHNOLOGY

3.1 Introduction

The focus of this thesis has been on analysis of dairy processes. The aim has been to understand the fundamental molecular mechanisms, but foremost with the starting point of being able to *identify*, *measure* and *control* the *critical-to-quality* attributes and their relation to end product quality. The key source of inspiration for this working approach has been ideas from Process Analytical Technology (PAT). The concept PAT can be boiled down to strategies for optimizing processes through timely measurements, control regimes, robust process design and data handling. To completely describe what PAT covers is beyond the scope of this thesis, but this chapter will provide the reader with conceptual elements, basics of control theory and some examples of PAT applications in the dairy industry.

3.2 What is PAT?

Process analytical chemistry (PAC) or process analytical technology (PAT, Box 1) originates from a specialized form of analytical chemistry over 70 years ago, and has been practices ever since to monitor activity in a process. However, what once was a sub-category of analytical chemistry or measurement science has developed into a much broader field of process understanding and control (Workmann *et al.*, 2009). The idea of monitoring processes by means of measurement technology is not new (McMahon and Wright, 1996), and traditionally PAT was implemented in order to move the analytical instrumentation from the laboratory to the production site and thereby get rapid on-line and in-line analyses (Koch, 2006). The importance of real-time measurements became clear, as it was realised that taking samples and transporting them to an analytical laboratory was costly, but it also resulted in inaccurate representation of the process, since the dynamics of the process were often missed because of the time required to perform the measurement. The field of process analytics has matured and it has been broadened to include all aspects of a process in order to enhance productivity, quality, and for environmental purposes. The developments have made PAT a multidisciplinary field that involves combining analytical

chemistry, engineering, biology, process control and technology with multivariate data analysis.

Box 1. The definition of PAT framework (FDA, 2004)*:*

"A system for designing, analyzing, and controlling manufacturing through timely measurements (i.e., during processing) of critical quality and performance attributes of raw and in-process materials and processes with the goal of ensuring final product quality."

In September 2004, the FDA published the PAT guidance document where a short definition of PAT was given (Box 1). Together with this guidance document FDA has trained a set of inspectors in PAT. This team of inspectors performs operational visits at pharmaceutical sites and approves PAT applications throughout the world.

3.3 Process Control Theory

A key element in improving any production is to gain control of the process. From a conceptual point of view a manufacturing process can be controlled as illustrated in Figure 12. Some raw materials generate an end-product or intermediate product under the influence of some controlled and uncontrolled parameters. Prior to introducing any form of control action a robust process is designed either based purely on traditional practice or by a systematic investigation of controllable factors (design of experiments) to find the optimal process settings. Different types of control strategies can be introduced to further optimize the process output (minimizing bias and/or variation compared to the target output/product properties). Feed-back control is the most common form of control where the actual output is compared with a target and control actions are taken to correct differences. In feed-forward control the process is adjusted according to information about the process input. To the authors knowledge this form of control is rarely used as producers prefer to standardize the input and keep the process parameters constant (like a recipe).

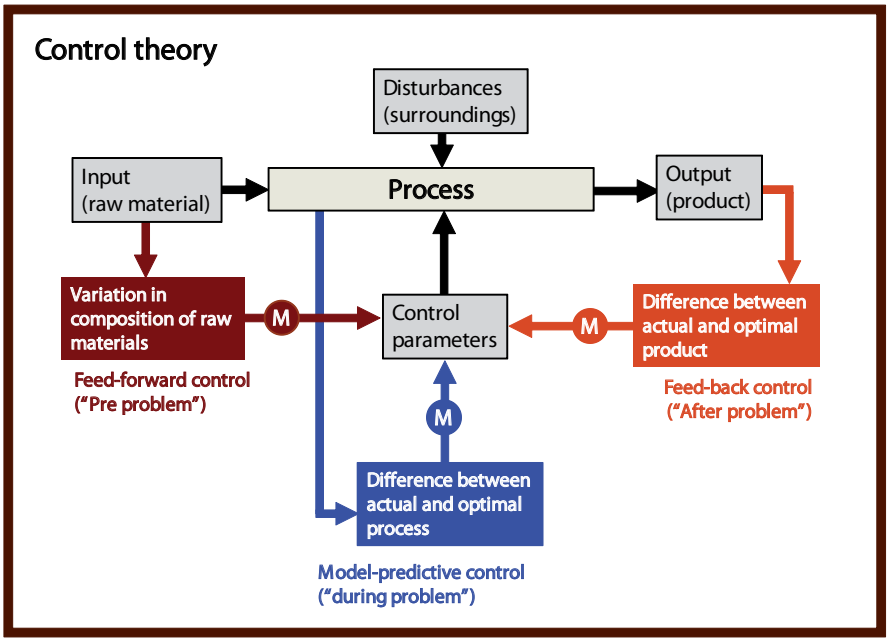

Figure 12. Control concepts.

In model-predictive control the actual process is continuously compared with the optimal process and control actions are taken to correct the differences. Model-predictive control requires some kind of measurements reflecting the state of the process. Model-predictive control is especially suitable for batch processes or processes that in some way are dependent on time (with a slow response to control actions). For fast responding continuous processes (near independent of time), model-predictive control is the same as feed-back control. **PAPER III** investigates NIR reflection as a method for monitoring for milk coagulation. There is an optimal end-point in the coagulation process. The time profile of NIR measurement reflects the state of the process and could therefore be used a decisive tool for end-point detect. End-point detection is a special variant of model-predictive control; because it only offers one control action being when the process should be terminated.

Often processes cannot be completely controlled due e.g. biological variation in raw materials. For instance in a process like cheese manufacturing depending on a large number of factors such as slight variations in milk composition, starter activity, rennet activity or temperature can alter the process dynamics substantial. IN such cases model predictive control is especially relevant as it allows for detection and correction of the process.

3.4 Potential and present PAT application in the dairy industry

3.4.1 In-line prediction of cutting

In modern dairy manufacturing there is an increased interest in automation of processes, while maximizing the yield at consistent quality. Timing of milk coagulaum cutting in cheese manufacture can be critical to the yield and quality of the final cheese. An industrial study of 80 batches showed that the loss of curd fines (curd particles) was high if the gel was cut too early (Figure 13). In the same study it was estimated that up to 0.7% (w/w) milk protein and fat could be lost due to early cutting, which must be considered a substantial economic loss. Longer cutting times result in slightly smaller loss, but the disadvantage of postponing the cutting is reduced production throughput (Ten Grotenhuis, 1999). Furthermore, postponing the cutting step increases the risk that the gel network becomes too strong. A too strong gel network withholds moisture (hinders syneresis), which in turn results in high moisture cheeses with undesirable sensory and microbiological effects (Payne *et al.* 1993). Thus, timing of cutting is indeed a critical-to-quality step in cheese manufacture, but at present the dominating tool available for cheesemakers is the knife test. While the test is based on the cheesemaker's solid experience, it is still person dependent and does not enable automation of the process.

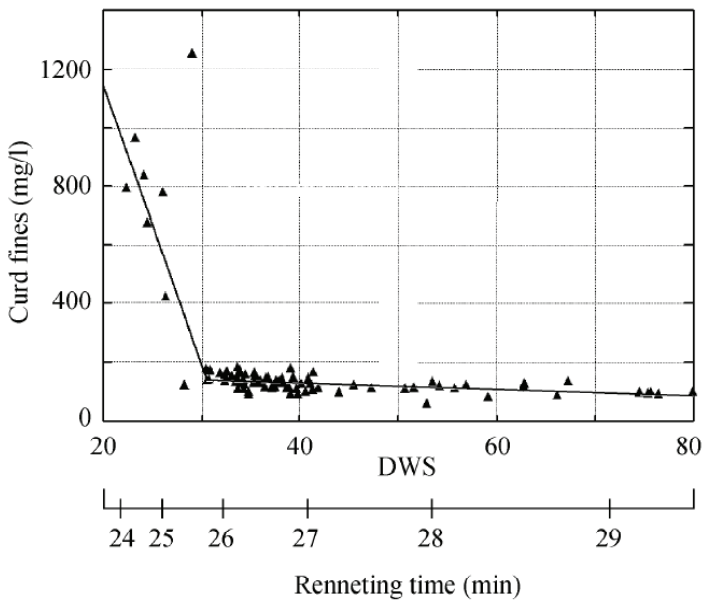

Figure 13. Curd fines in whey depending on gel strength (measured by DWS) and renneting time in cheese manufacturing (reproduced from Ten Grotenhuis, 1999).

As timing of gel cutting is a critical parameter for cheese yield and quality, many researchers have searched for methods to predict this optimal cutting time. O'Callaghan *et al.* (2002) reviewed sensor techniques for monitoring coagulum formation with the main emphasis on the ability to optimal predict cutting in real-time.

Reference methods for optimal cutting time

Any sensor potential for predicting optimal cutting time must be evaluated against some sort of reference of what *optimal* is. The optimum cutting time can be defined as the point where curd fine loss is minimized while syneresis rate is maximized. Quantifying the optimal cutting point is difficult, because measuring fine loss and syneresis rate, while at the same time controlling all influencing factors, is far from trivial. It is difficult to pin point the optimal cutting point, since the coagulation and syneresis processes are complex multi-factorial processes. Therefore, researchers have compared and calibrated sensors against various reference methods. These references methods include *Berridge clotting method*, *Formagraph*, *low amplitude dynamic shear measurements* and the *knife test*, which were described earlier in this thesis. Besides the knife test, these reference measurements are made on grab samples while the sensor measures in the cheese vat. This of course demands that all conditions affecting coagulation are strictly standardized between the reference method and the sensor method. Variations in milk composition are often handled in such studies by mixing rennet with a bulk volume of milk, which is then immediately distributed between the cheese vat with in-line sensor and the reference apparatus. Dynamic shear measurement has an advantage over the other three reference methods as it measures a rheological property in engineering units (Pascal), while the other methods gives an empirical measurement which is influenced by viscous and elastic properties. Table 2 provides an overview of studies investigating performance of in-line sensors versus reference methods for predicting optimal cutting time.

Table 2. Studies of in-line sensors for predicting optimal cutting time found from reference methods.

Study	In-line sensor(s)	Reference method
Payne *et al.* (1993)	NIR^{r} (860 nm)	Formagraph
Laporte *et al.* (1998)	NIR^{r} (1100-2500 nm)	Thermal probe
Crofcheck *et al.* (1999)	NIR^{r} (880 nm)	Plant operators (knife test)
O'Callaghan *et al.* (1999, 2000)	NIR^{r} (880 nm), NIR^{t} (680 ,850 nm), hot wire, torsional vibration, tunning fork	Rheometry
Passos *et al.* (1999)	Hot wire	Plant operator (knife test)
Castillo *et al.* (2000, 2002, 2003)	NIR^{r} (880 nm)	Berridge clotting method Knife test
Castillo *et al.* (2005)	NIR^{r} (880 nm)	Plant operators (knife test)
Mertens *et al.* (2002)	NIR^{r} (880 nm)	Rheometry

^{r} Reflectance; ^{t} Transmission

Hot wire sensor

Before describing the principles of the most successful sensor for prediction of cutting time, NIR reflection, the hot wire will be briefly discussed. An instrument that has already been installed in-line in an industrial production is the hot wire sensor (Lucey, 2002). Figure 14 shows a schematic illustration of the sensor and a graph of the response during coagulation. The sensor takes advantage of the fact that the thermal conductivity changes in coagulating milk. A constant current is passed through the wire, generating heat which is dissipated readily while the milk is liquid. As milk coagulates the heat transfer decreases and the temperature of the wire steadily increases (Hori, 1985). Calibration models between the temperature time profile and optimal cutting time have shown good predictive performance at tightly controlled conditions i.e. fixed temperature and milk composition. That said, O'Callaghan *et al.* (1999) found that the hot wire is only sensitive to the early part of coagulation (proteolysis and aggregation), but not the later part (network formation). This represents a problem because e.g. milk protein variation affects the later part of coagulation.

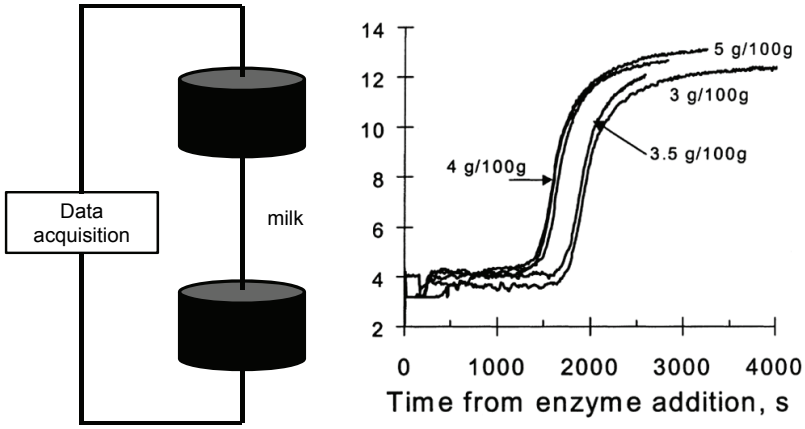

Figure 14. Illustration of the hot wire sensor and typical measurement traces of milk during coagulation with different levels of protein content (reproduced from O'Callaghan *et al.*,1999).

NIR reflection sensors

Sensors using NIR reflection are by far the most studied method for cutting time prediction. A study by Castillo *et al.*, (2005) will be used to illustrate the main principle behind the cutting time prediction using NIR reflection. In this the reflection sensor was placed in the cheese vat from the top and connected to a spectrometer with optic fibers (Figure 15). As the milk coagulate the light scattering properties change; an exact explanation has yet to be given. There seems however to be consensus that light scattering is a function of size of casein micelle aggregates, but also the geometrics of the formed gel network changes (O'Callaghan *et al.*, 2002). **PAPER IV** discusses NIR scattering properties of coagulating milk.

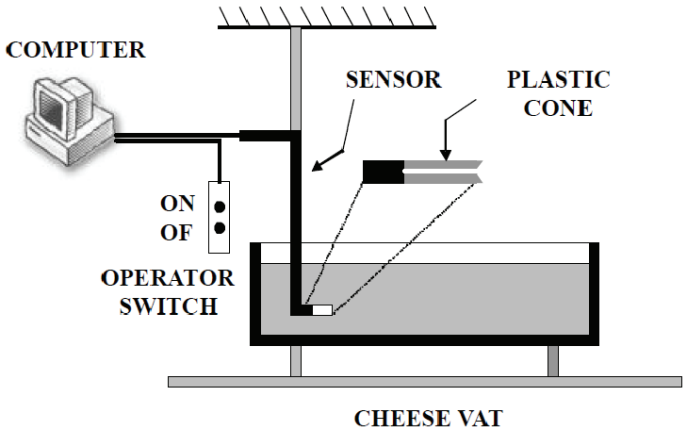

Figure 15. Schematic of fiber optic sensor installed in a cheese production (Castillo *et al.*, 2005).

In the study of Castillo *et al.* (2005) reflection at a single wavelength is used. A representative result of (short wave) NIR single wavelength measurements of one batch is shown in Figure 16. As input for cutting time prediction models various time- and response-based parameters are extracted from the NIR time profile and derivatives of the profile. The prediction models are made by regressing sets of time- and response-based parameters *X* (predictor data) against corresponding cutting times t_{cut} (response)

Equation 4

$$t_{cut} = Xb$$

Where *b* is the regression vector estimated by multiple linear regression. Some of the later studies of predicting cutting time using NIR (Castillo *et al.*, 2003a,

2005;Mertens *et al.*, 2002) pointed out that none of the time- and response-based parameters extracted from reflectance profiles describe changes occurring in the later part of milk coagulation. This is unfortunate as variation in protein content of milk have a marked effect of firming rate in the late stage (network formation) of milk coagulation. Findings of Castillo *et al.* (2003) showed that the Standard Error of Prediction (SEP) of 6.2 minutes (CV = 17.0 %) could be reduced to a SEP of 2.5 minutes (CV = 6.9%) by adding a protein concentration term to Equation 4. Likewise Castillo *et al.* (2005) showed that a SEP of 1.4 minutes (CV = 5.0 %) could be reduced to a SEP of 1.1 minutes (CV = 3.9%) by adding a protein concentration term. If an accurate value of milk protein content is readily available, it is an advantage to include this information for cutting time prediction. However, this is not always the case and not easy to implement in dairy automation systems.

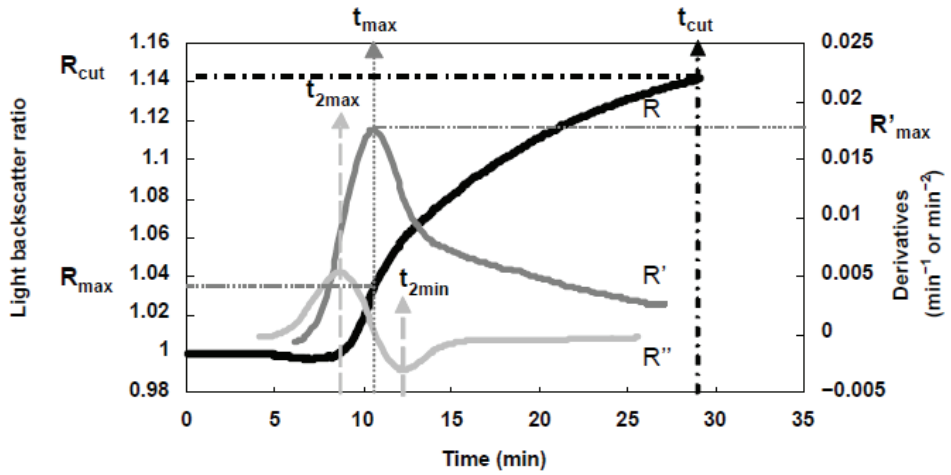

Figure 16. Typical NIR (880 nm) reflection profile during milk coagulation (R), the first derivative (R' and the second derivates (R''). Time-based (t_{max}, t_{2max}, t_{2min}, t_{cut}) and response-based (R_{max}, R_{cut}) parameters are extracted from the profile and derivatives.

In the present thesis a study (**PAPER III**) is conducted for extraction of parameters of NIR measurements that capture the kinetics of the entire coagulation period up to cutting. During a lab-scale rennet coagulation of milk NIR reflection spectra (1000 – 1900 nm) were recorded using a sensor connected to a FT-NIR spectrometer by fiber cables. Typical spectra and their subsequent conversion in to one sample/time score by PCA is shown in Figure 17. The development in PC1 scores is clearly a function of coagulation properties and the development can be divided into three stages (I-III) representing κ-casein proteolysis, micelle aggregation and network formation, respective. Figure 17

(bottom) shows that measurements in stage II follow an S-shape and in stage III an exponential decrease. The observation of these two shapes led to the formulation of a two-stage model for describing the measurement profile (Box 2).

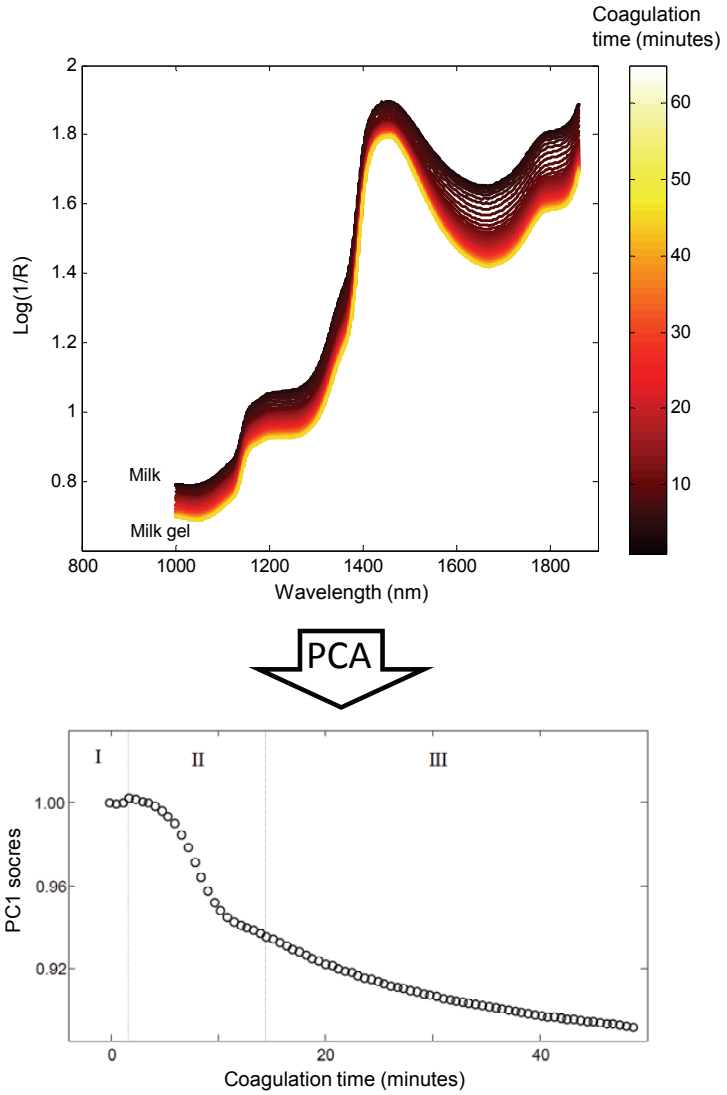

Figure 17. Top: NIR spectra recorded during milk coagulation. Bottom: Principal component scores during milk coagulation time. (I) κ-casein proteolysis, (II) para-casein aggregation and (III) gel network formation (**PAPER III**).

Two stage coagulation model

$$x(t) = \frac{\alpha_1}{1+exp(-k_{aggre}(t_{max}-t))} + \alpha_2 \qquad t < t_{transition}$$

$$x(t) = \alpha_3 exp(-k_{network}t) + \alpha_4 \qquad t > t_{transition}$$

x(t): PC1 scores a time t
$\alpha_1, \alpha_2, \alpha_3, \alpha_4$: relates to profile magnitude
k_{aggre} , $k_{network}$: rate constants
t_{max}: time of maximum aggregation rate
$t_{transition}$: time of transition between stages

The two stage model showed an almost perfect fit to the experimental data (Figure 18);it seems to fully capture the coagulation kinetics. In **PAPER III** an automated algorithm was made, designed to extract the two stage model parameters while NIR measurements are made of the coagulation process. The modeling approach used in **PAPER III** for extracting profile parameters differs from Castillo *et al.* (2005) as it takes advantage of the full time trajectory of measurements. Consequently, more information (through model parameters) can be used for prediction of cutting time. Future studies must compare the two ways of extracting information from the time trajectory on cutting time prediction.

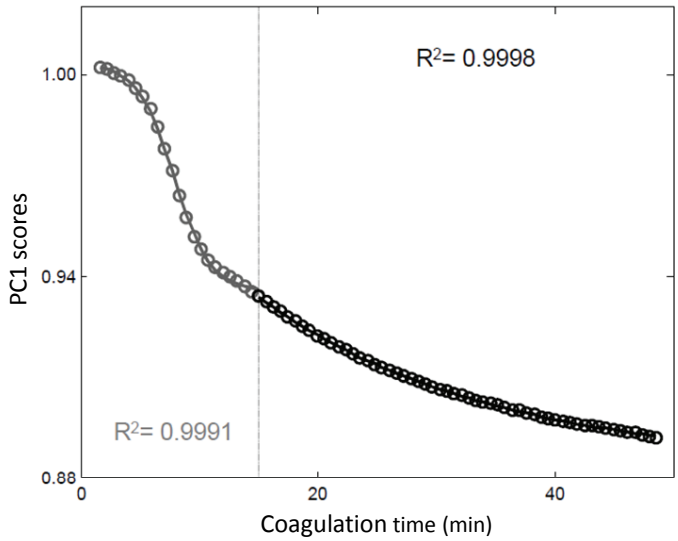

Figure 18. Fit (solid lines) of the two stage model to NIR measurements (o) acquired during coagulation. The vertical line denotes the stage transition time (**PAPER III**).

3.4.2 On-line standardization of milk

The motivation for on-line milk standardization is to minimize variation in fat and protein content in dairy products. No standardization or manual standardization based on at/off-line analysis will result in higher compositional variance (Figure 19, curve 1). By on-line standardization the variation is reduced (curve 2), which makes it possible to move closer to the limiting values (curve 3; Ellen and Tudos, 2003). By moving the average closer to the specification limit, milk components like fat, protein and lactose can be saved resulting in a better production economy.

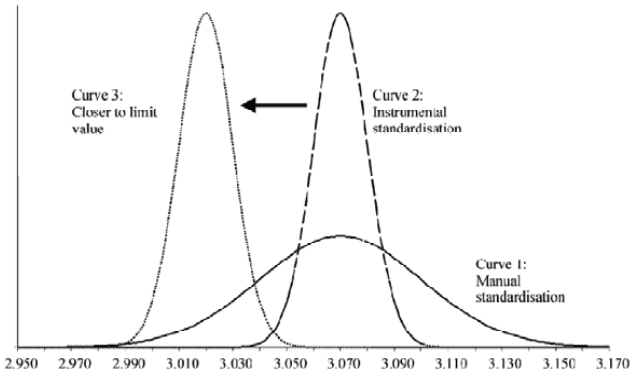

Figure 19. Effect of improving standardisation accuracy on the economy of production (reproduced from Ellen and Tudos, 2003).

The principle in the actual on-line standardization is that the whole milk composition is rapidly determined by on-line FT-IR (by-pass) and feedback control of the flow of various feeding streams (skim milk, cream and UF permeate) ensures a constant fat and protein content (Fagan *et al.*, 2009). Depending of the utilization of the milk different standardizations are used. Milk used for milk powder is standardized to a certain ratios of fat-to-total solid and protein-to-total solids as this will determine the resulting fat and protein content of the powder coming out of the drier. Milk for cheese manufacture is standardized to a certain ratio of fat-to-protein content as this is this ratio determines the fat and protein composition of cheese.

Figure 20. On-line FT-IR process instruments for milk standardization measuring fat, protein and lactose and dry matter (Foss, 2010).

3.4.3 On-line vs. off-line determination of milk powder composition

Many different powders (milk, skim milk, whey and other special powders) are manufactured in the dairy industry. Powders are mainly produced by spay drying or in fluid bed driers. The water content of these powders is very important as there are specifications with regard to maximum amount of water that must be obeyed. However, it is profitable to make products which narrowly match the specifications. In order to achieve this a rapid and precise method for analysis is required. In Holroyd (2002) it is demonstrated that an on-line analysis of milk powders enable the moisture content to be closely controlled. A NIR sensor was applied in a fluid bed drier and by mean of a grab arm a sample is collected and presented to the sensor. In Figure 21 on-line NIR results are compared to an off-line reference method (IDF 26A:1993). Generally the two methods match, but as indicated there is one time region where a serious deviation from the target value occurs. This deviation is not captured by the reference method as a result of low sampling frequency. In addition it takes more than 3 hours for the results of reference analysis to become available, whereas the NIR measurement provides data instantaneously; the economically advantages are obvious.

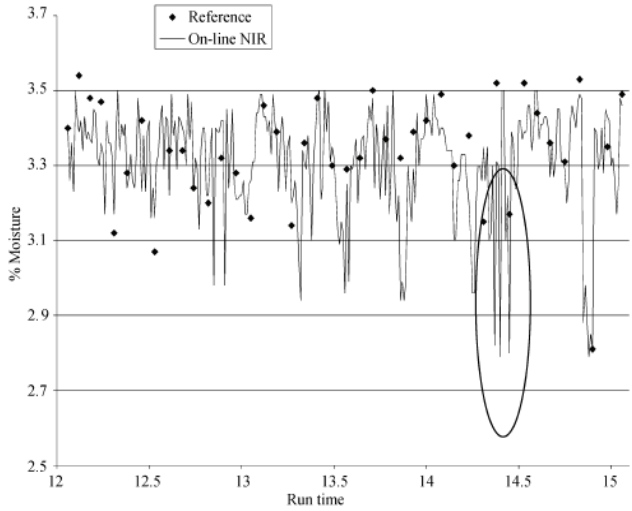

Figure 21. Comparison of on-line NIR and reference (IDF 26A:1993) measurements of moisture in milk powder (Holroyd, 2002).

Milk powder is also used for baby formula. Recently, several thousand babies in China became ill after being fed formula milk powder contaminated with industrial chemical melamine. In order to avoid this kind of adulteration and ensure milk product safety there is a need for a simple, accurate, rapid and low-cost technique to detect contaminants in milk. In Lu *et al.* (2009) showed that a NIR together with LS-SVM showed promising results for fast detection of melamine in milk products.

3.4.4 At-line determination of butter composition

In-line options are not always preferred over at-line solutions. Sometimes at-line measurements are sufficient and cheaper than in-line (Holroyd, 2002). An example is determination of moisture, salt and fat in butter which takes less than one minute is shown in Figure 22.

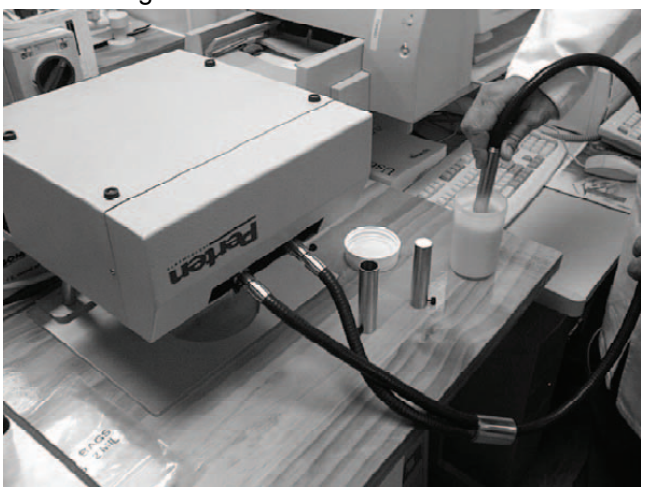

Figure 22. At-line determination of moisture, salt and fat in butter (Holroyd, 2002)

3.4.5 On-line determination of raw milk composition from individual cows

For the dairy business milk composition is very important in all stages. At farm level it is essential to be able to determine the milk composition in order to manage dairy herds efficiently e.g. the lactose content can be used to detect mastitis (an udder decease), which also reduce fat and protein content of milk (Tsenkova *et al.*, 2001). Therefore, it would be to advantage for the farmer if the composition of milk from individual cow could be determined on-line during milking. Both IR and NIR technology can be used to determine milk composition, and therefore an experimental on-line NIR sensing system for real-time assessment of milk quality during milking has been constructed (Kawamura *et al.*, 2007). The system was installed next to the milk bucket of the milking machine allowing a continuous flow of milk to be measured by the NIR sensor. PLS calibration models were developed for fat, protein, lactose and other key constituents (Kawamura *et al.*, 2007).

3.4.6 At-line determination of raw milk composition directly at the milk tanker

All raw milk is transported from the farms to the dairies by milk tankers. When the milk tanker arrives at the dairy it typically contains mixed milk from five to ten different farms. For payment schemes to the farmer, it is interesting to know the composition of the milk from the individual sources. A way to accomplish this is to construct a system to determine milk composition during the transportation into the milk tanker. In a feasibility experiment milk samples were collected before going into the milk tanker, and NIR and Raman measurements were carried out. The results from these measurements were compared to results from reference analysis, and PLS calibrations models for all the major milk constituents were constructed. The set-up is shown in Figure 23.

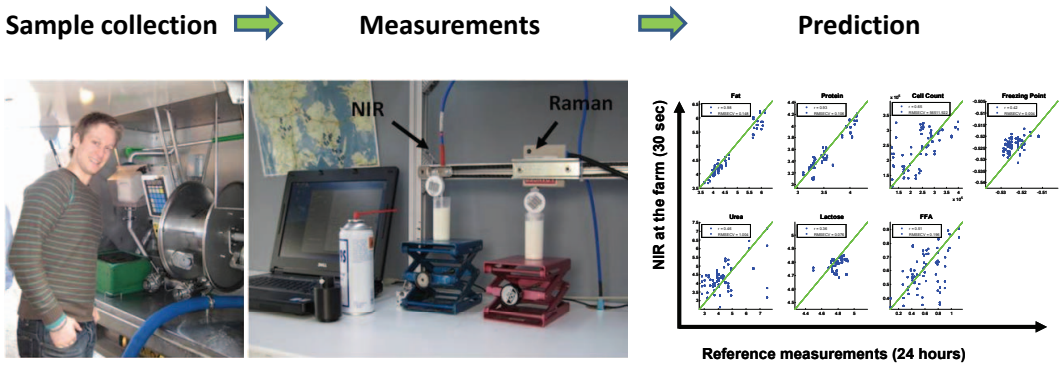

Figure 23. Measurement of milk composition at the farm. Samples collection by the author from milk tanker, NIR and Raman measurement in at the farm, and prediction of seven milk compositional parameters.

3.5 Summary

In this chapter the concept of PAT has been introduced as defined by FDA (2004). Control concepts *feed-forward*, *feed-back* and *model predictive* control have been described. Over the last couple of decades the dairy industry has gradually recognized the benefits PAT. A potential PAT application is in-line NIR measurement of milk coagulation and prediction of optimal cutting time. Several lab and industrial-scale studies have demonstrated the feasibility of NIR spectroscopy as a tool for predicting optimal coagulum cutting time. The approach has been to regress indices from the time profile of NIR measurements to optimal cutting time. Unfortunately, this approach does not capture kinetics late in the coagulation phase. **PAPER III** demonstrated an alternative approach of extracting information from NIR coagulation profiles, capturing the kinetics of the entire coagulation phase up to cutting. Rapid on-line IR measurements of whole

milk composition have made it possible to standardize milk using feed-back control of various mixing streams (skim milk, cream and permeate). As a result on-line IR improves dairy product quality consistency and production economy. On-line and at-line NIR analysis is widely used for determination of milk powder composition. Moreover, recently IR has been shown to detect milk powder adulteration. Finally a field study where milk composition is determined by NIR at the farm was described.

CHAPTER 4
SPECTROSCOPY

4.1 Introduction

Spectroscopy is the study of interaction between electromagnetic (EM) radiation and matter. The origin of the word (*spectrum* = image in Latin; *skopia* = to view in Greek), describes how spectroscopic measurements offers one to view an image of the measured sample (Miller, 2001). The development of spectroscopic methods is closely related to the quantum theory formulate by Maxwell, Einstein and Bohr. Maxwell described in 1864 that EM radiation (light) is in fact a wave. Later, in 1905, Einstein showed that light can be described as streams of particles named photons. To solve this apparent discrepancy Bohr formulated the wave-particle duality principle (1913) that EM radiation has characteristics of both a wave (continuous energy) and a particle (photons, discrete energy). EM radiation can be quantified and an atom or molecule can absorb or emit energy and change between a ground state (*i*) and an excited state (*j*) if the frequency (ν) of radiation matches the energy difference (ΔE) between states (Equation 5).

Equation 5

$$\Delta E = E_i - E_j = h \cdot \nu = h \cdot \frac{c}{\lambda}$$

Where *h* is Planck's constant. The frequency (ν) is related to the wavelength of radiation and the speed of light *c* in vacuum. The phenomenon of matching states and energy of radiation is called resonance. The energy of states is specific to molecules or atoms and may be influenced by the surrounding environment.
For practical and phenomenological reasons electromagnetic radiation is divided into smaller frequency/wavelength regions with their own names: gammas rays, X-rays, ultraviolet, visible, near infrared, infrared, and microwaves (Figure 24). For each of the spectral regions in Figure 24 radiation has a different kind of interaction with matter. Spectroscopic analytical techniques can evaluate these excitations properties in a molecule and thereby map the energy transition present.

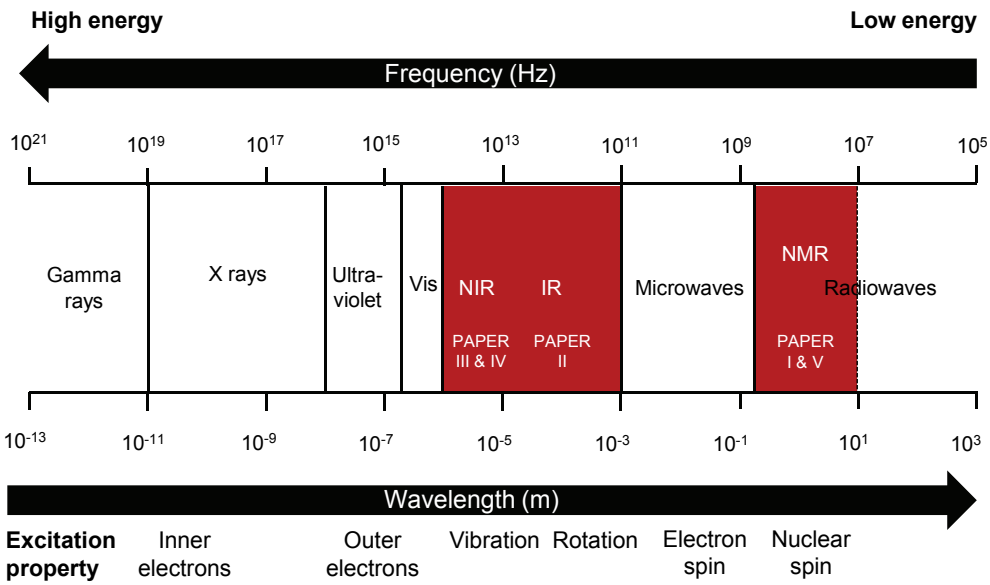

Figure 24. The electromagnetic spectrum divided into smaller wavelength regions with different effects of the molecule. The wavelength regions used in the present study is NIR, IR and NMR.

4.2 Time Domain NMR

Nuclear magnetic resonance (NMR) spectroscopy is widely used as analytical technique in research of e.g. foods (Belloque & Ramos, 1999; Rutledge, 2001), metabolomics (Cevallos-Cevallos, 2009) and pharmaceuticals (Holzgrabe, 2010). Actually NMR can be considered indirect spectroscopy as it requires an external magnet field. NMR spectroscopy can be divided into two main types: analysis in the time domain (TD) and in the frequency domain. Only ^{1}H TD-NMR will be described here as it has been applied to study milk coagulation and subsequent curd syneresis in the present thesis (**PAPER I**). The main characteristics of ^{1}H TD-NMR are: 1) it is a non-destructive method making it possible to perform different or repetitive analysis of the same sample, 2) it is sensitive to the physical state of water and 3) it is sensitive to the structural organization of the sample on a microscopic and macroscopic level (Belloque & Ramos, 1999). The fundamental theory behind ^{1}H TD-NMR has been extensively described in textbooks and research papers (Berendsen, 1992; Hemminga, 1992; Hills, 1990; Storey, 2006) and its use in dairy applications has recently been reviewed by Karoui and De Baerdemaeker (2007). Thus, only a summarized presentation will be given here.

In 1952 Bloch and Purcell received the Nobel prize in Physics for discovering that some atomic nuclei in a magnetic field absorb electromagnetic radiation (resonate) and radiate back out energy at a specific resonance frequency (Bloch

and Packard, 1945; Purcell *et al.*, 1946). Nuclei possess a property called *spin*, that can be thought of a spinning movement around an axis. Because nuclei carry electric charges, the spinning results in the formation of a small magnetic field and in this way the nuclei can be thought of as small magnets *spins* (Figure 25). In an NMR spectrometer the sample is placed in strong magnetic field (0.2 – 21 Tesla; earth magnetic field: 0.000005 Tesla), which causes all spins to align themselves parallel according to the magnetic field direction (B_0). If we consider the ^1H spins in a magnetic field, they will be divided into two groups according the Boltzmann's distribution law: 1) spins pointing in one direction (parallel) and 2) spins pointing in the other direction, but still parallel (so-called *anti-parallel*). There will be a slight excess of parallel spins compared with anti-parallel spins, and is the parallel spin net difference that provides the measurement signal in an NMR experiment (Hemminga, 1992).

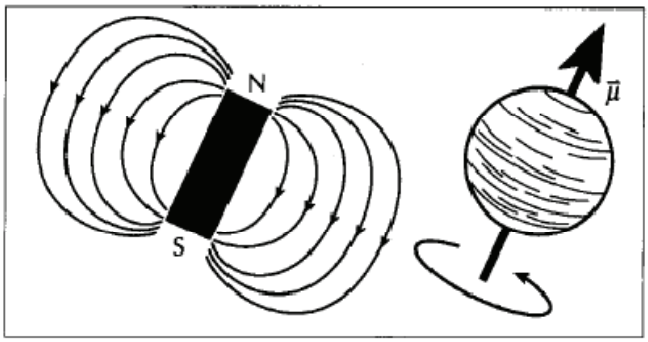

Figure 25. The spinning motion of nuclei generating a magnetic moment (Hemminga, 1992).

In an NMR experiment the aligned spins will be tilted down in a 90^o angle from their original position by exciting the spins with radiation (energy) of a frequency in the range of radiowaves (10 – 900 MHz). Because of the strong external magnetic field the spins will seek to return to the original position of alignment. This happens by the spins rotating around the axis of the external field while decreasing at an exponential rate. This returning motion is referred to as *relaxation* and inside the spectrometer a detector captures the signal from relaxing spins (Hemminga, 1992). The relaxation can be characterized by two types of behavior governed by time constants, designated T_1 and T_2 (Figure 26). The *spin-lattice relaxation* that is governed by T_1, is equivalent to restoring the *longitudinal* magnetization component parallel to the external magnetic field. In pure water, the proton spin-lattice relaxation time at room temperature is approximately 3 seconds. The *transverse* component of the magnetization is governed by the time constant, T_2, called the transverse or *spin-spin* relaxation time. In pure water, the proton spin-spin relaxation time at room temperature is approximately 2 seconds.

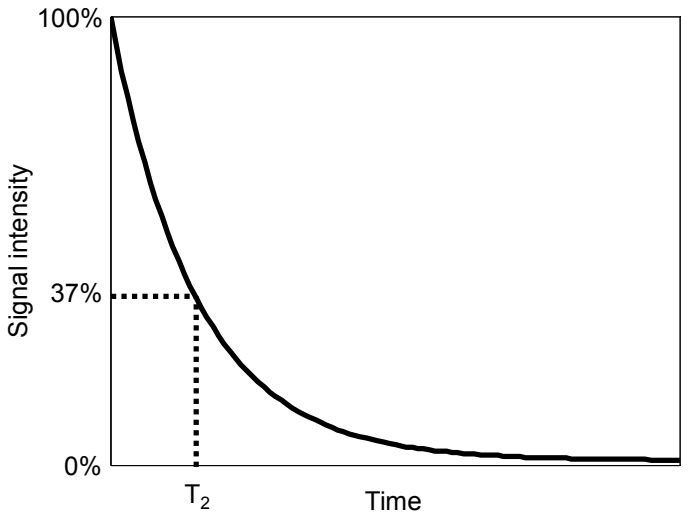

Figure 26. Graphical presentation of exponential decay of the transverse magnetization after excitation.

The relaxation of water protons in high water content biological systems such as foods is affected by the interaction with other protons in the microscopic surrounding media (Berendsen, 1992). In this way water protons act as small sensors probing the surrounding environment. For instance the relaxation rate of protons is low in pure water, where the only interaction is between neighboring water protons, while it is faster when water protons are interacting with protons (or other magnetic nuclei) in macromolecules (Berendsen, 1992). Because of the effect, the surrounding environment has, water proton relaxation is very sensitive to the physical compartmentalization present in many biological samples. This is related to self diffusion of water protons (Brownian motion) since water protons will experience fast relaxation if they move in the proximity of a physical barrier. Naturally, fast relaxation will only occur if the diffusion time for protons to reach the barrier is shorter than the intrinsic relaxation time of the protons and the time-scale of the NMR experiment (Hills, 1990).
Mathematically, the relaxation curve (e.g. Figure 26) can be described as a sum of N populations of protons decaying exponentially with their own relaxation time constant $T_{2,n}$ (Equation 6):

Equation 6

$$M(t) = \sum_{n=1}^{N} M_{0,n} \cdot exp\left(\frac{-t}{T_{2,n}}\right) + E$$

Where M(t) is the relaxation signal at time t, M_0 is the magnitude of the signal at excitation time (t=0) and E the instrumental noise. Analyzing relaxation curves in order to extract $M_{0,n}$ and $T_{2,n}$ values will be described elsewhere in this thesis (section 5.5). The origin of multiple proton populations (i.e. multi-exponential curves) with different relaxation behaviors (T_2) in biological samples comes from water and fat in different states within the sample. In **PAPER I** three populations of protons with different relaxation behavior were identified in synerezing milk curd (coagulated milk expelling whey). The population with the longest relaxation time (T_2 ~1.2 – 2 s) was identified as water protons in the expelling whey, which increased in volume as a function of syneresis time (quantified by the magnitude, M_0). The two remaining proton populations originated from water inside the synerezing curd; one population presumably being water tightly associated with the polymer nuclei in the curd network, another population being water trapped between the polymers in some way e.g. by capillary forces.

Determination of relaxation time by Hahn spin echo or Carr-Purcell-Meiboom-Gill (CPMG) sequence

The transverse relaxation time constant, T_2, can be determined be applying a radio frequency pulse sequence beginning with a 90° excitation pulse, followed by a pause and finalized by a 180° refocusing pulse (Figure 27). The reason why the 180° pulse is applied is that besides inhomogeneities in the magnetic field causes by spin-spin interactions there are also inhomogeneities in the main magnetic field, B_0, which are constant in time. By applying a 180° pulse after a 90° pulse a so-called spin-echo is formed, where the B_0 inhomogeneities are eliminated and only the inhomogeneities caused by spin-spin interactions are detected. By performing multiple experiments gradually incrementing the pause the signal amplitude as a function of time is measured i.e. the relaxation curve. This approach is called the spin echo sequence or the Hahn spin echo sequence since it was introduced by Hahn in 1950. The idea was further extended by Carr and Purcell (1954) and Meiboom and Gill (1958), who suggested using a series of 180° pulses added at an equidistant time 2τ after a single 90^o pulse. This pulse sequence produces a series of echoes, where the maximum value of each spin echo is exponentially decreasing and constitutes the measurement points of the relaxation curve. Only every second echo should be used because the 180° pulse will always contain a small inaccuracy. The precision of the consecutive 180° pulses is however high, which means that after two 180° pulses the direction of magnetization will be exactly back at 0^o.

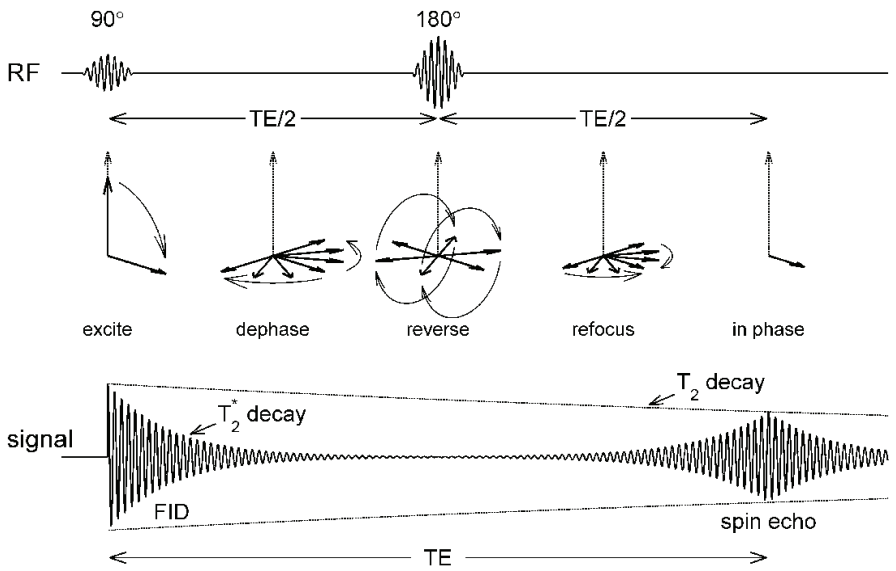

Figure 27. Formation of a spin echo by the Hahn sequence. The dephasing caused by inhomogeneities in the magnetic field can be reversed by applying a 180° pulse, which result in the formation of a spin echo. The amplitude of the spin echo depends on how much T_2 relaxation there is during the echo time (TE). Because T_2 relaxation originates from microscopical interactions and diffusion of the spins it cannot be reversed (Storey, 2003).

4.3 Vibrational spectroscopy

In 1800 William Hershel discovered an *invisible form of light* beyond the visible range, which today is referred to as infrared radiation (*infra* = below (the red) in Latin). In the period from 1800 to 1945 the theoretical understanding of vibrational spectroscopy in the infrared region was established, and the interpretation of the IR spectrum was achieved through the application of quantum theory. From 1945 instrumental developments enabled IR spectroscopy to contribute to qualitative and quantitative structural analysis of molecules in mixtures. As a result IR spectrometers for commercial applications arose, and the use of vibrational spectroscopy increased decade by decade. In 1980's Fourier transform spectrometers were introduced, which markedly reduced time of analysis and at the same time fiber optics was developed to enable in-line NIR analysis in real-time (Sheppard, 2002).
Today the majority NIR and IR applications are for off-line or at-line analysis, but a few applications of on-line or in-line analysis are also found. In this thesis off-line IR analysis was applied for UF permeate characterization (**PAPER III**) and in-line NIR analysis was applied to monitor milk coagulation (**PAPER II**).

4.3.1 The basic principles

At temperatures above the absolute zero all molecules exhibit oscillating motions called vibrations. Vibrational spectroscopy (IR and NIR) utilizes this molecular property by studying the interaction between infrared radiation and molecular vibration. For IR radiation at 4000-400 cm^{-1}, the radiation frequency corresponds to stretching and bending vibrations in covalent bonds in molecules. The IR spectrum reflects the fundamental vibrations, while overtones and combination tones are present in the NIR spectrum (Dufour, 2009). The exact matching of radiation frequency with bond vibrational frequency is called resonance and causes the radiation to be absorbed by the molecule. Bonds have different vibrational frequencies mainly depending on the mass of the involved atoms and the strength of the covalent bond. Consequently, the absorption frequency in an IR spectrum can be used to identify the presence of different bonds and in this way aid in finding out what substances are present in the samples (Griffiths, 2002). Stretching and bending are the main types of bondvibrations. Stretching vibrations can be symmetrical and anti-symmetrical, which have slightly different frequencies. The bending vibration can occur in different patterns recognized as scissoring, wagging, rocking and twisting, all occurring at different frequencies (Miller, 2001).

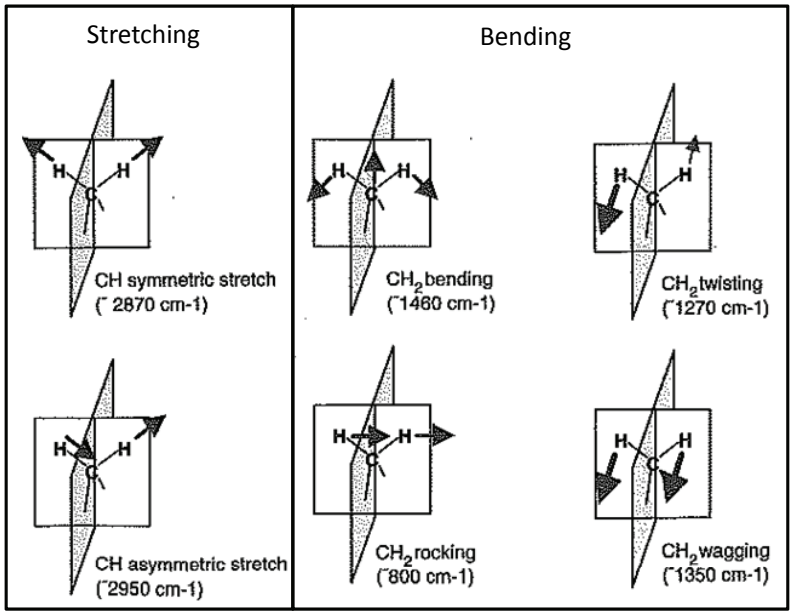

Figure 28. Geometric illustration of different vibrational patterns of the -CH_2- group and their approximate frequencies (modified from Miller, 2005).

Not all molecules absorb infrared radiation. Only the molecules that have a permanent dipole moment or an induced dipole moment during vibration are capable of absorbing infrared radiation. Homonuclear diatomic molecules such as N_2, Cl_2, and O_2 do not contain a dipole moment and are examples of molecules that do not absorb IR radiation (Miller, 2001). Low frequency molecular vibrations are of often difficult to assign. The frequency region below 1500 cm^{-1} is referred to as the fingerprint region. In this region each band found in the spectrum has multiple possible assignments. The complexity of this region makes it unique (as a fingerprint) for each sample (Dufour, 2009).

PAPER III applies IR to investigate compositional variation in UF permeate between several dairy production sites. Figure 29 shows a mid-IR spectrum of a permeate sample with various absorbance peaks of different *positions*, *width*, *height* and *shapes*. Correlation diagrams can be used to assign the peaks, but this does not provide an understanding of the underlying mechanisms nor explains differences in peak intensity and shape. Such an understanding is important to take full advantage of the information available in a mid-IR spectrum.

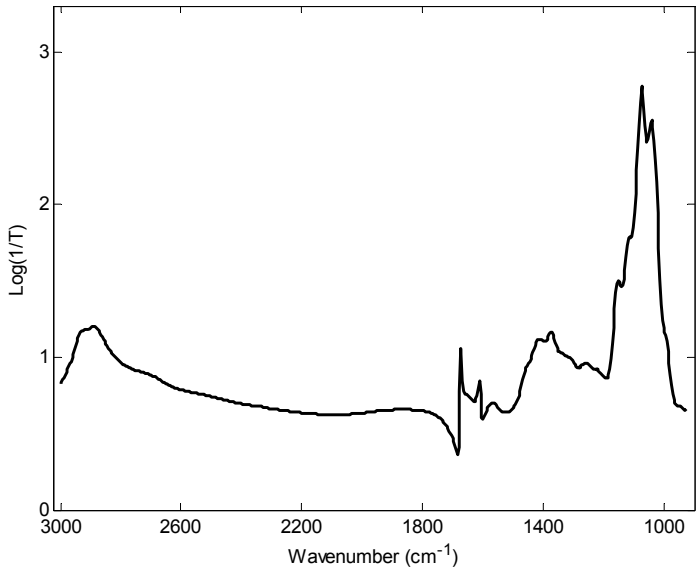

Figure 29. Mid-IR transmission spectrum of UF permeate.

4.3.2 Fundamental theory for spectral interpretation

To provide the reader with a more fundamental knowledge in understanding NIR and IR spectra, this section briefly describes phenomena which influence NIR and IR spectra: *dipole moment*, *electronegativity, hydrogen bonding, Hooke's law and anharmonicity.*

As previously mentioned a prerequisite for a molecule to absorb infrared radiation is that a dipole moment is present. A molecule made up of atoms that have different electronegativity will have a non-symmetrical distribution of charge. This difference is called the dipole moment and will change, when the distance between atoms vary by vibration (Ouellette, 1998).

Table 3. Extract of Pauling's electronegativity scale (Ouellette, 1998).

Atom	H	C	N	O	F	P	S	Cl	Br
Electronegativity	2.1	2.5	3.0	3.5	4.0	2.1	2.5	3.0	2.8

Peak height - *What determines how strongly various molecules absorb NIR and IR radiation?* If the difference in electronegativity between two atoms in a bond is less than 0.5 (see Table 1 for selected values), the dipole is weak and it will therefore interact poorly with electromagnetic radiation. This is the case for the C-H bonds where IR radiation consequently is weakly absorbed. O-H bonds have a difference in electronegativity of 1.4 and consequently IR is strongly absorbed. Hydrogen bonding also affects the intensity of absorption bands, but the effect is different for NIR and IR. Hydrogen bonding causes an increase in intensity of IR bands but decreases the NIR band intensity. The reason for this is that donor hydrogen vibrations become less anharmonic, which widely determines absorption intensity of overtones and combination tones (Miller, 2001).

Peak width - *What determines how broad an absorption band is?* The reason that the absorption band for O-H is broader than C-H bands is due to hydrogen bonding. Hydrogen bonds form when a hydrogen atom is electron poor and it is attracted to a electron lone pair on an acceptor atom. Donators of hydrogen bonds (mainly O-H and N-H) dampen the stretching frequency resulting in broader peaks. Bending vibrational frequency is however increased by hydrogen bond. C-H bonds are polar and cannot form hydrogen bonds and therefore there is only one form of C-H which results in a narrow band. O-H bonds can form multiple hydrogen bonds and thereby resonate at a broader range of frequencies, resulting in broad peaks (Miller, 2001).

Peak position - *What determines the position of absorption bands?* A covalent bond such as part of the O-H can be considered as a spring that can be stretched and compressed. The vibrational frequency of this system is especially dependents the mass of each atom. The relationship between frequency (ν), the so-called reduced mass (μ) and the force constant (k) is defined by Hooke's law (Equation 7 and Equation 8):

Equation 7

$$\nu = \frac{1}{2\pi}\sqrt{\frac{k}{\mu}}$$

Equation 8

$$\mu = \frac{m_1 m_2}{m_1 + m_2}$$

Where m_1 is the mass of atom one and m_2 is the mass of atom two (Sandorfy *et al.*, 2007; Pedersen and Rasmussen, 2004, Steele, 2004). Hooke's law is a simplified harmonic oscillator model since it only considers diatomic vibration and in reality multiple atoms affect vibration (Miller, 2001). It is however a good model for understanding what governs vibrational frequency. The force constant k is related to the bond enthalpy, which is the energy required to break the bond. Bonds involving hydrogen have the highest frequency because hydrogen has a small mass. The bond strength (i.e. enthalpy) in triple bonds is higher than in double bonds resulting in a higher frequency of triple bonds than double bonds. The fundamental division of the IR spectrum is shown in Figure 30.

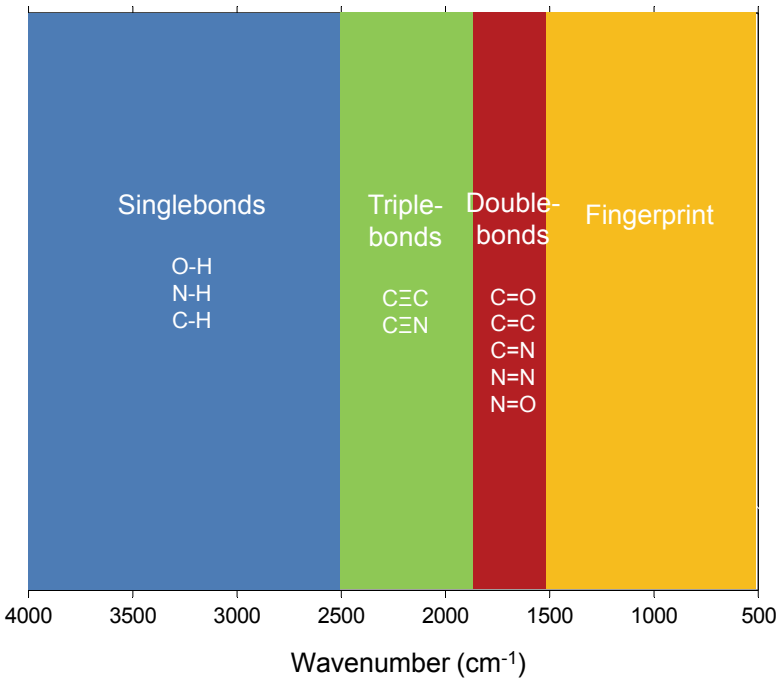

Figure 30. Fundamental structure (simplified) of the IR spectrum.

Peak position in NIR spectra

Most of what is written in the previous section holds for both NIR and IR. However, there are some fundamental differences. NIR radiation is absorbed by overtones and combination tones of fundamental IR vibrations, which are approximate integer multiples or summations of the fundamental vibrational frequency. A prerequisite for NIR radiation to be absorbed by a molecule is that the molecule deviates from the *harmonic* oscillating behavior, referred to as anharmonicity. Anharmonicity means that 1) the dipole moment is not exactly a linear function of interatomic distance and 2) when atomic nuclei are separated far enough they will eventually dissociate (Figure 31).

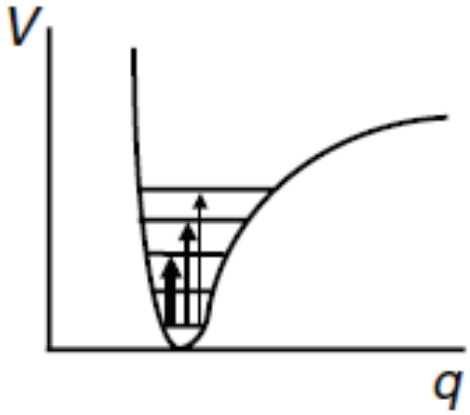

Figure 31. Graphical presentation of anharmonicity. As the inter-atomic distance (q) increase the potential energy does not increase linearly or symmetrically. The arrows indicate that several energy states (overtones) exist in NIR.

Mathematically, it means that the potential energy of a diatomic oscillator is not simply a quadratic function of interatomic, but can better be decribed by the Morse function (Figure 31). The absorption intensity of overtone and combination bands is depended of the degree of anharmonicity and dipole moment change. As a result the most intense band involve hydrogen stretches (O-H, C-H, N-H), which are very anharmonic (Miller, 2001).

4.3.3 Quantitative considerations

In NIR and IR transmission spectroscopy the relation between absorbance (A) and concentration (c) of the absorbing analyte is given by Lambert-Beers law (Equation 9 and Equation 10):

Equation 9

$$\mathbf{A = \varepsilon \cdot l \cdot c}$$

Equation 10

$$\mathbf{A = \log_{10}\left(\frac{I_0}{I}\right) = \log_{10}\left(\frac{1}{T}\right)}$$

Where ε is the molar absorptivity and l is the effective light path length, I_0 is intensity of incident light and I is intensity of light that has been transmitted through the samples. T is *transmittance*, the fraction of incident light that has passed through the samples ($T = I/I_0$) (Dahm and Dahm, 2001). Lambert-Beers law applies to transmission measurements on samples that have no scattering particles, however it is also frequently applied in diffusion reflection, where T is replaced by R in Equation 10, where R denotes the fraction of the reflected light out of the total incident light. A problem with using Lambert-Beers law for diffuse reflection measurements is that the effective path length is unknown. The Kubelka Munk (K-M) equation (Kubelka and Munk, 1931) provides a model of diffuse reflection (R) of samples with infinite thickness (Equation 11):

Equation 11

$$\mathbf{\frac{K}{S} = \frac{(1-R)^2}{2R}}$$

Where K and S are referred as K-M absorption and scattering coefficients, respectively.

4.3.4 NIR light scattering properties of coagulating milk

NIR measurements are more influenced by light scattering particles than IR measurement because the effective path length is longer for NIR radiation. In milk casein micelles and fat globules cause scattering of NIR radiation. These two components scatter light differently based on differences in size, number, and optical properties (e.g. the refractive index). Casein micelles are much smaller than the fat globules. The particle diameter of casein micelles falls in the range of 0.130 – 0.160 μm (Ruettiman and Ladisch, 1987) and fat globules are in the range of 0.1–10 μm for unhomogenized milk, with a mean diameter of 3.4 μm (Walstra et al., 2006). Skim milk appears slightly blue because the small casein micelles predominately scatter the shorter blue wavelengths of visible light. Whole milk appears white because the larger fat globules scatter all wavelengths of incident light (Crofcheck et al., 2002).

In **PAPER IV** NIR scattering properties of coagulating milk are discussed. In skim milk scatter caused by fat globules is presumably low as the fat concentration is very low (< 0.1%). Figure 32 (left) shows four spectra recorded during coagulation of milk. The dominating spectral change is a lowering of the baseline in the log(1/R) signal. A method of investigating baseline changes is *multiplicative scatter correct* (MSC). In MSC the spectra are plotted against a reference spectrum. In Figure 32 (right) the spectrum of a firm milk coagulum is plotted toward a reference spectrum, in this case of milk. The baseline change can be seen as the deviation from the target line. The non-linearities in the red spectral region (Figure 32) suggest that this spectral region is affected not only by scatter difference but also chemical differences.

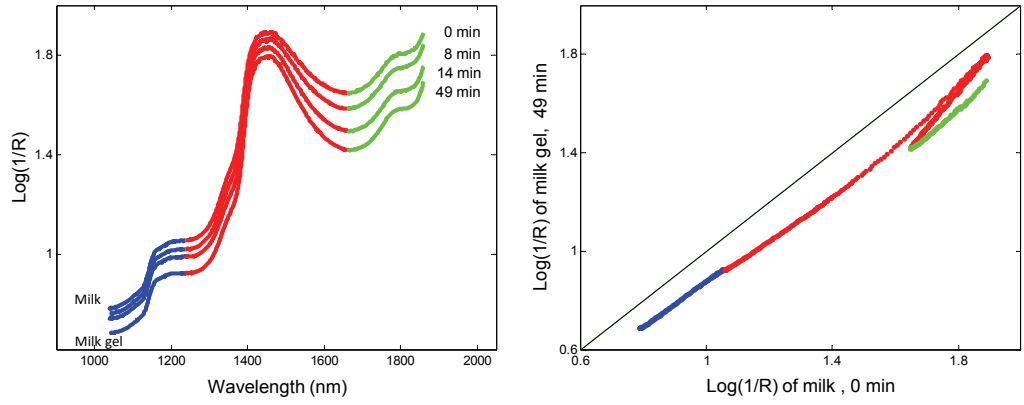

Figure 32. Left: four NIR reflection spectra (1050 – 1860 nm) recorded during rennet coagulation of skim milk and color coded in intervals. Right: spectrum of firm coagulum (49 min) vs. milk (0 min).

On the hand, the blue region (Figure 32, right) is linear throughout coagulation suggesting that only scatter changes affect this region.
In Figure 33 calculated slope and offset between the initial NIR spectrum of milk (t = 0 min) and spectra recorded during milk coagulation (t = 0.5 – 49 min) is shown for the region 1050 – 1250 nm (blue in Figure 32). These coefficients are equivalent to the MSC coefficient i.e. multiplicative and additive effects. The there is a large change in slope during the micelle aggregation phase (phase II, Figure 33), showing that scatter changes are particularly wavelength dependent in this phase. In the network formation phase (phase III, Figure 33), the scatter changes are slightly wavelength dependent. An explanation for the observation of wavelength dependence during micelle aggregation could be that in this periode the main particle size changes are occurring. More research in need to understand this scatter behavior.

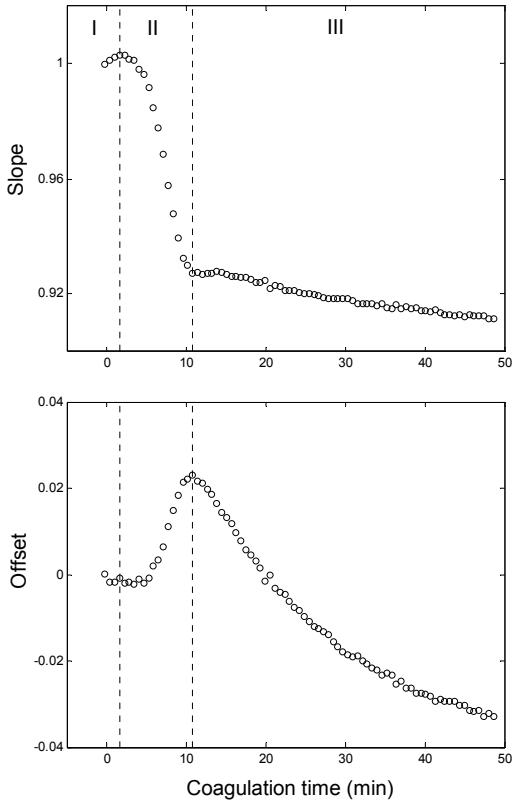

Figure 33. Slope and offset between the initial NIR spectrum (1050-1250 nm) of milk (t = 0 min) and the spectra recorded during coagulation (t = 0.5 – 49 min). (I) κ-casein removal by chymosin (II) para-casein aggregation and (III) gel network formation.

4.4 Summary

In this chapter the spectroscopic methods used in this thesis are described. This description includes fundamental quantum theory and overview of the electromagnetic spectrum. In addition, basic TD-NMR theory, magnetic moment, transverse and longitudinal magnetization, exponential relaxation and the CPMG sequence are explained. The chapter furthermore describes theory of vibrational spectroscopy including theory for spectral interpretation. Finally NIR scattering properties of coagulating milk are described.

CHAPTER 5
CHEMOMETRICS

5.1 Principal Component Analysis

There may be many motivations for using principal component analysis (PCA) on data: simplification, data reduction, outlier detection, classification and pattern recognition. PCA involves transformation of a number of correlated variables to a fewer number of uncorrelated "variables" called principal components (PC's). The first principal component account for the largest source of variability in the data, while the succeeding PC's account for the residual variation (Wold *et al.*, 1987). PCA is also called the Karhunen-Loèven transform (KLT), Hotelling transform or proper orthogonal decomposition (POD), depending on the field of use (Chatterjee, 2000).
In PCA each of the principal components (PC's) is the outer product of two vectors, a score vector (t_i) and a loading vector (p_i), where *i* denote the component number (Equation 12):

Equation 12
$$\hat{\mathbf{X}} = \mathbf{t_1 p_1^T} + \mathbf{t_2 p_2^T} + \cdots + \mathbf{t_i p_i^T} + \mathbf{E}$$

The number of PC's expresses the number of observed variations in the data and can be considered as the number of independent phenomena in the data. Often the number of PC's are many times smaller, than the number of variables of the original data, because variables co-vary. This is especially the case for spectroscopic data, where variables are higly co-linear. E.g. in **PAPER II** 40 UF permeate samples were measured at 220 IR wavelengths. Decomposition into PC's showed that two components explained 95% of the variation in spectra. In this way PCA can bring forth the essential information in data. The score vectors describe how the samples relate to each other and the loading vectors describe the variables relate to each other (Wold *et al.*, 1987).
The principal components are orthogonal to each other. Conceptually, orthogonality means that two vectors are completely uncorrelated with one another. Orthogonality is a nice property of PCA as it ensures simplifies interpretation. A downside of orthogonality is that variations in e.g. an individual specific chemical compounds (c_1) are not found if they are co-vary to some extend ($c_1^T c_2 \neq 0$) with another chemical compound (c_2). Models like PARAFAC (Bro, 1997) and MCR (Juan and Taulor, 2006) does not have the orthogonality constraint and can therefore handle co-varying variations of individual chemical compounds. Mathematically orthogonality can be written as shown in Table 4

Table 4. Mathematical properties of PCA.

	Scores	Loadings
Vectors	$t_i^T t_j = \begin{cases} 0 & for\ i \neq j \\ s_i^2 & for\ i = j \end{cases}$	$p_i^T p_j = \begin{cases} 0\ for\ i \neq j \\ 1\ for\ i = j \end{cases}$
Matrices	$\mathbf{T^T T = D(s^2)}$	$\mathbf{PP^T = I}$

Due to orthogonality of PC's the inner product of any combinations of score vectors will be zero except when PC's scores are multiplied with itself. In that case the inner product becomes the squared singular values. The inner product of any combinations of loading vectors will also be zero except when PC's are multiplied with itself. In that case the inner product becomes one.

PCA algorithms

Components can be calculated by the NIPALS algorithm, which sequentially (one at a time) seeks to minimize $\|X - t_i p^T_i\|^2_i$ in an iterative manner (Wold *et al.*, 1987). Components can also be calculated by SVD, which non-sequentially (all at once) uses eigenvalue decomposition of the covariance matrix (Equation 13 and Equation 14).

Equation 13

$$\mathbf{Cov(X) = \frac{X^T X}{m-1}}$$

Equation 14

$$\mathbf{Cov(X)V = VS^2}$$

where S^2 is the eigenvalues associated to the eigenvectors V. The notation in SVD is different than PCA (see box) but the eigenvectors V are the same as loadings P and in SVD the score matrix T is found as the linear combination of X and V (T = XV). In SVD eigenvalues S^2 are given as elements in a diagonal matrix ranked according to size. Since eigenvalues are related to explained variance of each component, this means that the first component explains most variance, the second component explains second most variance etc.

5.2 Partial least squares regression

PLS has become a standard method to solve multivariate regression problems. The following brief presentation of PLS is based on a selection from the exhaustive literature on the topic (Bro, 1996; Geladi and Kowalski 1986; Miller, 2005; Wold *et al.*, 2001).

The main motivation for developing PLS was that multiple least square regression (MLR) does not work properly when data has many more variables than samples such as in spectral data. A second essential problem is that many of the spectral variables co-vary. Conceptually, this means that there are a lot fewer independent phenomena in the data than there a variables. Mathematically this is called rank deficiency or singularity. MLR breaks down when a data matrix is singular, because it is not possible to take the inverse (i.e. $(X^TX)^{-1}$) of a singular matrix which is required to solve a regression problem (Equation 15 and Equation 16) :

Equation 15
$$\mathbf{y} = \mathbf{Xb}$$

Equation 16
$$\mathbf{b} = (\mathbf{X^T X})^{-1}\mathbf{X^T y}$$

where y is the response, X is the predictor data and b contains regression coefficients to be determined. The problem of co-varying variables is handled by the principal component regression (PCR), which uses principal component scores (T) as predictor data in MLR (Equation 17 and Equation 18):

Equation 17
$$\mathbf{y} = \mathbf{Tb}$$

Equation 18
$$\mathbf{b} = (\mathbf{T^T T})^{-1}\mathbf{T^T y}$$

The vectors in the score matrix are per definition uncorrelated (orthogonal), which makes it a non-singular matrix that MLR can handle. Since the variance compression of predictor data in PCR is done independently of the response y, it presents the problem that large variances (PC's) in predictor data might have little relevance for prediction of the response y. PLS deals with this problem by simultaneously maximizing variation in X and y and their mutual correlation. PLS can be considered as an *outer relation* (i.e. individual X and y decomposition) and *inner relation* linking the two. The outer relation of two blocks is like a PCA decomposition (Equation 19 and Equation 20):

Equation 19
$$\mathbf{X} = \mathbf{TP^T} + \mathbf{E}$$

Equation 20
$$\mathbf{y} = \mathbf{Uq^T} + \mathbf{E}$$

The *inner relation* links the two decompositions by relating the X and y scores for each component i and determining the regression coefficient (Equation 21 and Equation 22):

Equation 21

$$\mathbf{u_i} = \mathbf{b_i t_i}$$

Equation 22

$$\mathbf{b_i} = \mathbf{t_i^T}(\mathbf{t_i^T t_i})\mathbf{u_i}$$

This is however a suboptimal solution because the scores are calculated separately on each block. The inner relation can be improved by rotating the components. This can be done by letting t and u change places iteratively in the NIPALS algorithm (For further information see Geladi and Kowalski, 1986 or Wold *et al.*, 2001). The final step in PLS is to ensure that the scores are orthogonal, which is done by introducing loading weights.

5.3 Extended canonical variate analysis

ECVA is an extension of the standard canonical variate analysis (CVA) modified to deal with highly collinear data such as spectroscopic signals. ECVA has in some cases been found a superior classification method over PCA, partly because the principal components may not always be relevant to class differences (Nørgaard *et al.*, 2006; Savorani et al, 2010). The principle in standard CVA is to estimate a direction in space **w** (a weight vector) that maximizes the differences between sample classes and at the same time minimizes the differences within the sample classes (Equation 23).

Equation 23

$$\mathbf{max_w} \left\| \frac{\mathbf{w^T S_{between} w}}{\mathbf{w^T S_{within} w}} \right\|$$

where $S_{between}$ is the co-variance matrix between the classes, S_{within} is the sum of covariance matrices within the classes. The solution to this problem can be written as an eigenvalue problem (Equation 24 and Equation 25).

Equation 24

$$\mathbf{S_{between} w} = \lambda \mathbf{S_{within} w}$$

Equation 25

$$\mathbf{S_{within}^{-1} S_{between} w} = \lambda \mathbf{w}$$

where λ is the eigenvalue associated with the eigenvector w. Multiplication of the estimated weight vector w by the original mean centered predictor data (X) yields the canonical variates ($t_{cv} = X_{mc}w$). t_{cv} can then be used for classification. A problem with CVA however is that it does not work with co-linear data because

then it is not possible to do the inverse of S_{within} (Equation 25) just as MLR does not work with co-linear data (see PLS subchapter). In fact, the approach in ECVA is to turn Equation 25 into a regression problem, where PLS can handle the co-linearity problem. For a two-class classification problem it is solved by PLS(1) and for a multi-class problem it is solved by PLS2:

Two classes	Multiple classes
$(\bar{x}_1 - \bar{x}_2)k = \lambda S_{within} w$	$(\bar{x}_g - \bar{x})W = \lambda S_{within} W$
y = Xb + f	Y = XB + F
Solved by PLS	Solved by PLS2

For further details on the regression step see Nørgaard *et al.* (2006). The number of canonical weigth vectors (w) will always be one less than the number of classes and this vector can be used from a chemical point of view to inspect variables regions where differences between classes are largest. The regression problem in has so far only been solved by PLS, however other methods such as Ridge regression could also be used. Nørgaard *et al.* (2006) noted that the inner relation in PLS sometimes showed non-linearities, possibly because the predictor matrix S_{within} is a covariance matrix, which is symmetric. Perhaps, polynomian or spline PLS (Wold, 1992) could be used to improve the inner relations.
As with any supervised classification method it is very prone to overfitting and therefore validation (cross-validation and/or test set) is extremely important to validate the number of PLS components. Analog to *interval* PLS (Nørgaard *et al.*, 2000), *interval* ECVA has also been developed to provide better classification models and improve interpretation (Nørgaard *et al.*, 2007).

5.4 Parallel factor analysis

Parallel factor analysis (PARAFAC) was used in to decompose pseudo-upgraded TD-NMR relaxation curves in the present work (**PAPER I and V**). PARAFAC can be viewed as an extension of PCA to higher dimensions, but it has some special properties. There is no orthogonality constraint like in PCA. The non-orthogonality property means that components cannot be calculated successively as they are dependent on each other. Therefore the model is highly dependent on specifying the right number of components. The decomposition of a three-way data $\underline{X}$ (I x J x K), by the PARAFAC model can be written as

Equation 26

$$x_{ijk} = \sum_{c=1}^{C} a_{ic} b_{jc} c_{kc} + e_{ijk}$$

Where a_{ic} is the loading vector for samples (corresponds to score in PCA) for component c, b_{jc} and c_{kc} corresponds to loading vector for component c and C is the total number of components. The model is found by minimizing the sum of squares of residual e_{ijk} using alternating least squares (ALS; Bro, 1997). A model diagnostic in PARAFAC is *core consistency* and this diagnostic is used to determine the appropriate number of components in TD-NMR relaxation curves (**PAPER I and V**). To explain core consistency a little background regarding the structure of the PARAFAC model is required. The PARAFAC model in Equation **26** can be rewritten as a restricted form of a Tucker3 model with the added term t_{def}, which will be 1 for d = e = f and 0 otherwise:

Equation 27

$$x_{ijk} = \sum_{d=1}^{D} \sum_{e=1}^{E} \sum_{f=1}^{F} a_{id} b_{je} c_{kf} t_{def} + e_{ijk}$$

Where D = E = F and the remaining elements are the same as in Equation **26**. Figure 34 graphically shows the PARAFAC model written as a restricted Tucker3 model. In core consistency a core $\underline{G}$ is estimated by a Tucker3 model using PARAFAC loadings.

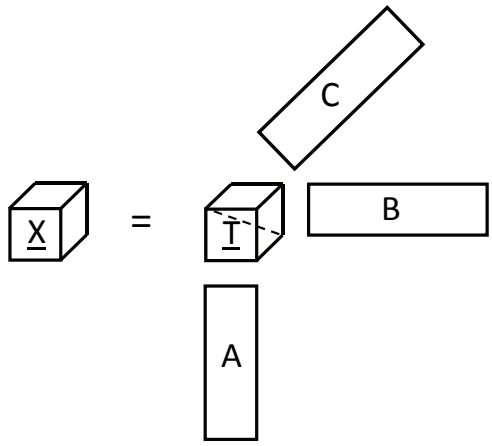

Figure 34. PARAFAC written as a Tucker3 model. The superdiagonal in T consist of ones and the remaining elements are zero.

For a perfect fitting PARAFAC model the Tucker3 core G based on PARAFAC loadings will be identical to superdiagonal array of one's the identity core I (Bro and Kiers, 2003). This lemma is used in the diagnostic tool core consistency where model core deviation from a superdiagonal array of one's T is quantified (Equation 28):

Equation 28

$$\textbf{Core consistency} = 100\left(1 - \frac{\sum_{d=1}^{F}\sum_{e=1}^{F}\sum_{f=1}^{F}(g_{def} - t_{def})^2}{F}\right)$$

Where g_{def} are elements in the modeled core G, with F components and t_{def} are elements in an array T with same dimension as G, but with ones in the superdiagonal elements and zeros in off-superdiagonal elements (Bro and Kiers, 2003). In this way core consistency can be used to validate the appropriate number of components in a PARAFAC model. Loss of residuals and shape of residuals can also be used to validate number of components in a PARAFAC model (Bro, 1997), but where residuals often decrease steadily when adding component, the core consistency will decrease dramatically if the model is overfitted (Bro and Kiers, 2003). Another diagnostic for PARAFAC models is split-half analysis. The idea is to split the data in two parts and due to the uniqueness of the PARAFAC model, one should get the same loading profiles in each spilt if the correct number of components are chosen (Bro, 1997). Specific to the analysis of TD-NMR relaxation is that required that loading vectors of the second dimension (B mode) should have an exponential shape; this is another validation diagnostic.

5.5 Modelling TD-NMR data

Proton TD-NMR relaxation measurement of biological samples often consist of contributions from multiple exponentials i.e. populations with their own characteristic magnitude and relaxation time constant (Equation 29, Figure 35):

Equation 29

$$M(t) = \sum_{n=1}^{N} M_{0,n} \cdot \exp\left(\frac{-t}{T_{2,n}}\right) + E$$

Where M(t) is the reduced magnetization at time t, $M_{0,n}$ is the concentration or magnitude parameter of the n^{th} exponential, $T_{2,n}$ is the corresponding transverse relaxation time constant, N is the number of exponential and E is the residual error.

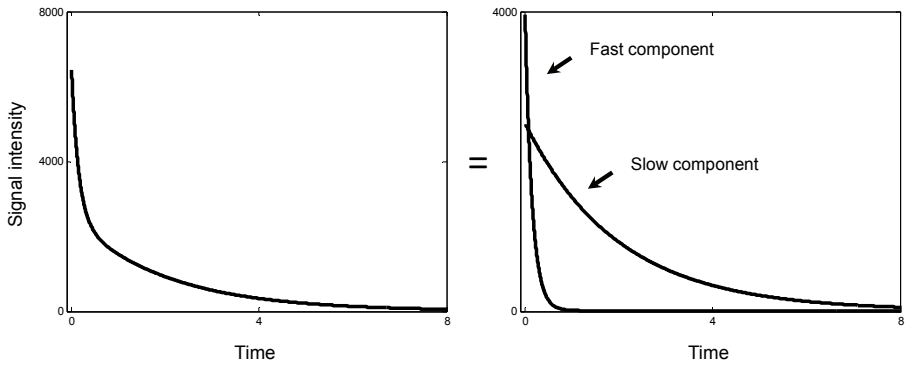

Figure 35. Illustration of the multi-exponential relaxation where two exponential contribute to the resultant signal.

One of the recurrent challenges when analyzing relaxation curves is to estimate the actual number of real components as opposed to random instrumental noise. If too few components are fitted the residuals will still contain information (Figure 36). If too many exponentials are fitted instrumental noise will be incorporated in the fit.

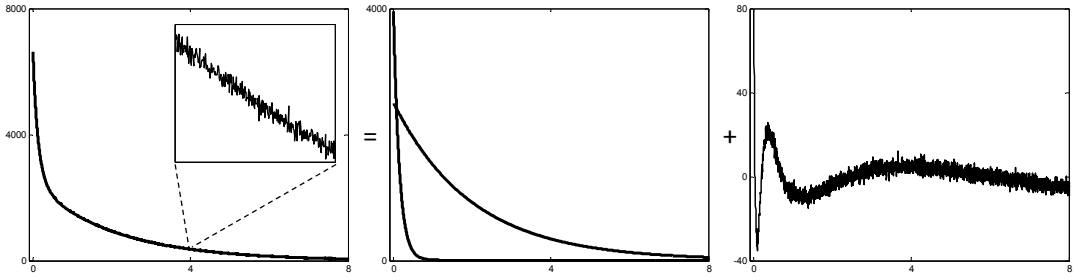

Figure 36. Illustration of bi-exponential fitting with systematic residuals.

Visual inspection of residuals can be a way to evaluate the appropriate number of exponentials; the solution should show a random distribution of residuals around zero (not the case in Figure 36). Relying solely of the loss of residuals for diagnosing the solution can be difficult as residuals per definition will continue to decrease when components are added.

Quite a few methods exist for analyzing TD-NMR, which have their own conceptual approach, solution diagnostics and computation speed. Three methods will be presented here.

5.5.1 Discrete Exponential Fitting

TD-NMR data are most frequently analyzed using discrete multi-exponential fitting using e.g. the Levenberg-Marquardt algorithm, which applies non-linear iterative curve-fitting to Equation 29 with N number of exponential to the relaxation curves. Solution diagnostics with regards to number of components are scarce. After fitting Equation 29 to the relaxation curve with N exponential components, inspection of the residuals (residuals vs. time) can reveal whether the curve has been modeled by too few, too many or the correct number of components. Other solution diagnostics are relative loss in fit and $\chi 2$ misfit tests. As previously mentioned, relative loss in fit can be a difficult criterion to base evaluation on, because the fit will always improve when adding exponentials (Bechmann *et al.*, 1999; Marquardt, 1963).

5.5.2 Distributed exponential fitting

This method is often perceived to be the more realistically appealing analytical approach to TD-NMR data compared to discrete exponential. Instead of trying to decompose the relaxation curve into a few exponentials with characteristic T_2's, the curve is considered a distribution of a set of many exponentials. The number of exponentials N and the time window they should be distributed across is pre-defined by the user. N corresponding M_0 values are then found and plotted as a

distribution over the T_2 values. The problem with this fitting procedure is that several distributions can give the same fit and the solution is therefore not stable (Provencher, 1982).

5.5.3 DOUBLESLICING

The DOUBLESLICING technique (Andrada *et al.*, 2007) utilizes the theoretical fact that in every part of a multi-exponential decaying curve each of the mono-exponentials are present, but in different amounts. The technique pseudo-upgrades a single relaxation curve to become tri-linear data, by cutting the relaxation curve into slices (Figure 37). By selectively removing parts of the signal curve (*slicing*), and using the remaining curve, the relaxation curve can be transformed from a one-dimensional signal (a vector x) into two-dimensional data (a matrix X). By repeating this procedure on the matrix, the data is transformed into three-dimensional data (a cube $\underline{X}$) and three-way mathematical methods can now be used (Figure 37). Dimensionality of the cube depends on the number of slicings I (vector slices) × J (measurement point) × K (matrix slices). Tri-linear models require the phenomena to be modeled to be present in all dimensions, which is exactly the case with the cube upgraded from a single relaxation curve.

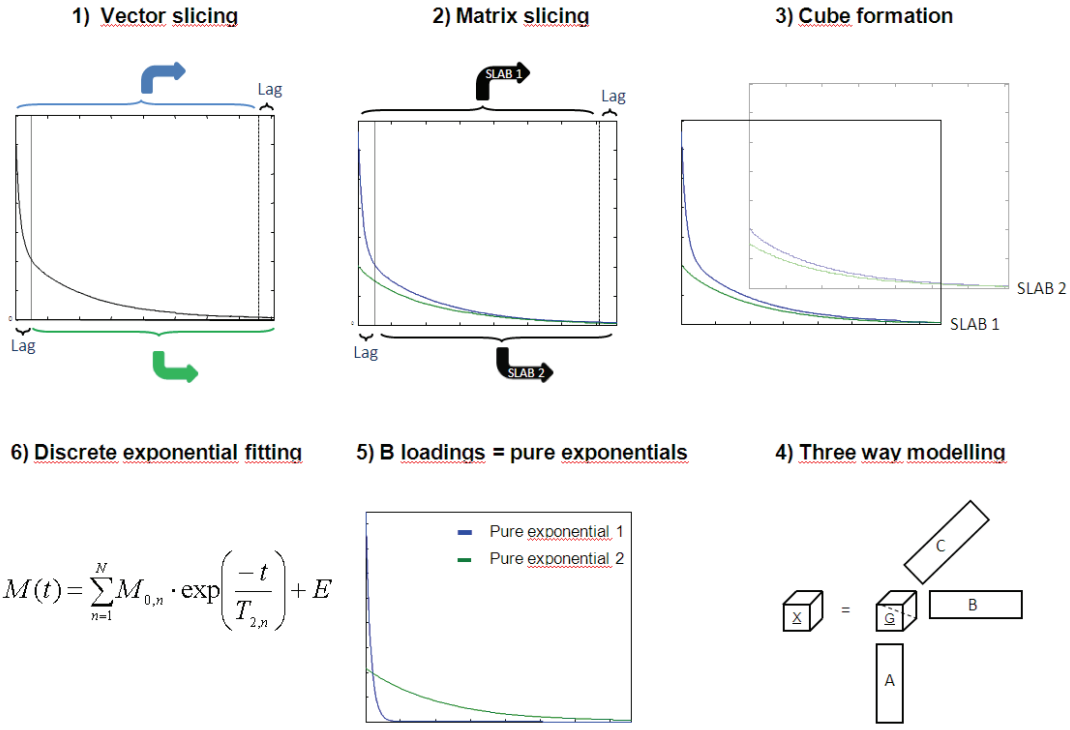

Figure 37. Illustration of the concept in DOUBLESLICING. Only two slices and slabs are shown, but this number can be greater.

The slicing points on the time axis of the decay curve are important because fast relaxing exponential components rapidly will contribute infinitesimal to the relaxation curve (e.g. Figure 35). To ensure that fast relaxing components are present in multiple slabs in each cube dimension Engelsen and Bro (2003) proposed to slice the vector and subsequent matrix at slicevariable = $2^{slicenumber-1}$ e.g. 1 2 4 8 … 2048. This slicing procedure called *powerslicing* ensures that fast components are represented in multiple slabs. The technique has been shown to be extremely rapid and has improved solution diagnostics. Andrade *et al.* (2007) tested the performance of DOUBLESLICING against existing methods and found that it was accurate in estimating relaxation times and that it outperformed discrete exponential fitting by a factor of four with regards to computation time. Solution diagnostics are diagnostics associated with multi-way models: loss of fit, core consistency and split-half. The solution can also be validated in the way that B-mode loadings follow an exponential shape.
DOUBLESLICING can be summarized as a rapid technique for analyzing TD-NMR relaxation curves with many possibilities to validate the appropriate number of exponential components. These characteristics make the technique superb for automatic algorithmic determination of the number of exponential components (based on a combination of several diagnostics) without *a priori* knowledge of the biological system. This is especially relevant when the number of measurements/samples is large and there is variation in the number of components between measurement. This is the case for dynamic systems like coagulating milk and synerezing curd as in **PAPER I** where 20 experiments resulted in ~2000 relaxation curves. MRI images are another example of large data sets where these concepts could be applied due to unknown pixel-to-pixel variation in the number of components.

5.6 External factor orthogonalization

Orthogonalization is the process of removing information from a data matrix X linearly related to an external factor. This mathematical process will be exemplified using a case study from the thesis. In an investigation of UF permeate variation between six dairy factories a PCA revealed that permeate samples had a unique infrared signature based on the factory of origin (Figure 38, **PAPER II**). The process of ultrafiltrating milk separates milk into UF retentate primarily containing large milk components (large whey proteins, casein, and fat), while UF permeate contain smaller milk components (water, minerals, vitamins, lactose and small whey proteins). The dominating solid fraction (w/w) of permeate is lactose followed by whey proteins. The loading spectra (corresponding to scores in Figure 38) showed that variation in total solids contributed largely to PC1 and variation in protein contributed largely to PC2. Reference analysis of permeate samples for protein and total solids content

confirmed this interpretation of the loadings. Moreover, operators at factories producing permeate with high protein content could confirm that UF membranes were worn, which explains leakage of larger components as such protein.

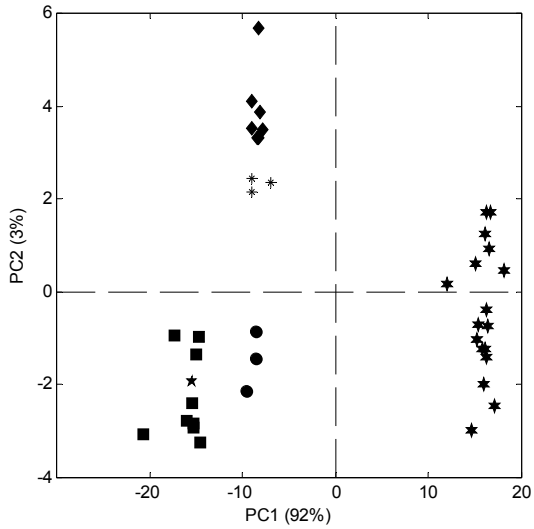

Figure 38. PCA scoreplot of IR spectra from 40 UF permeate samples. Symbols denote different origins (six factories) of permeate.

In order to examine if other factors than protein and total solid content were causing significant factory-to-factory variation these two factors were removed one after another from the spectra through orthogonalization. The essential principles of orthogonalization are described below, while a detailed mathematical treatment can be found in the appendix of **PAPER II**. Orthogonalization is the process of removing information from a data matrix X linearly related to an external factor (Equation 30)

Equation 30

$$\mathbf{X_o} = (\mathbf{I} - \mathbf{v}(\mathbf{v^T v})^{-1}\mathbf{v^T})\mathbf{X}$$

Where X_o is data orthogonalized towards the external vector v, X is the data matrix and I is the identity matrix. Orthogonalization of a data set can be employed to focus subsequent data analysis steps on that variation in data not related to the external factor (v). In case of several *independent* external factors (v_1, v_2 … v_k; $v_i \cdot v_j = 0$ for all combinations of $i \neq j$) data can be corrected for one factor and analyzed with respect to the others. In e.g. observational data or if outliers are removed the external factors may become dependent i.e. correlated ($v_i \cdot v_j \neq 0$ for combinations of $i \neq j$). In this case orthogonalization with one external factor *i* will result in removal of information related to another external factor *j*. In order to only remove information related to one factor and retain the full degree of information related to another factor, the data is only orthogonalized with that part

of factor *i* which is orthogonal to factor *j*. This can be exemplified through Equation 2, where factor one (v_i) is the external vector we wish to remove which is orthogonalized towards factor two (v_j), which we wish to retain. Then v_{ioj} is used for orthogonalization of X as described in Equation 30, substituting v by v_{ioj} (Equation 31)

Equation 31

$$\mathbf{v_{ioj}} = (\mathbf{I} - \mathbf{v_j}(\mathbf{v_j^T v_j})^{-1}\mathbf{v_j^T})\mathbf{v_i}$$

In the remainder of this thesis I will refer to the two orthogonalization approaches as *conventional orthogonalization* in the case external factor is uncorrected and *compensated orthogonalization* in the case where the external factor is corrected, prior to orthogonalization of X.
IR spectra of permeat samples (from Figure 38) were subjected to conventional and compensated orthogonalization towards *protein* content determined by a reference analysis. The result of PCA on orthogonalized spectra is given in Figure 39.

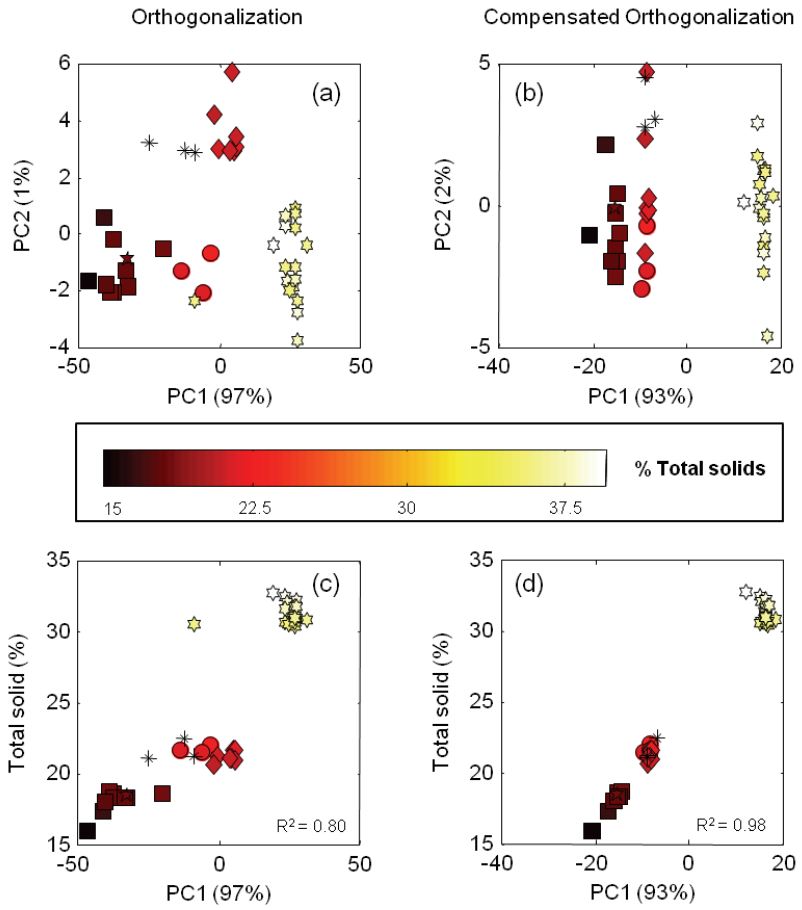

Figure 39. Effect of (a, c) *orthogonalization* and (b, d) *compensated orthogonalization* of IR spectra towards total protein content; (a, b) PCA score-plots after orthogonalization, (c, d) total solid content versus PC1 score values. Symbols denote the origin (six factories) of permeate.

Notice that when protein variation is removed by conventional orthogonalization, total solid variation is also removed (Figure 39a vs. b). This is because protein and total solid content is partially confounded (R^2 = 0.39), which means you cannot remove information from one without removing information from the other. In compensated orthogonalization (Figure 39b) only the part of protein variation is removed which is not linearly related to total solid variation. Subplots (d) and (c) in Figure 39 show that after removal of protein variation the PC1 scores explain most of the variation in total solid content.

Figure 40 show IR spectra of permeat samples subjected to conventional and compensated orthogonalization towards *total solid* content determined by reference analysis.

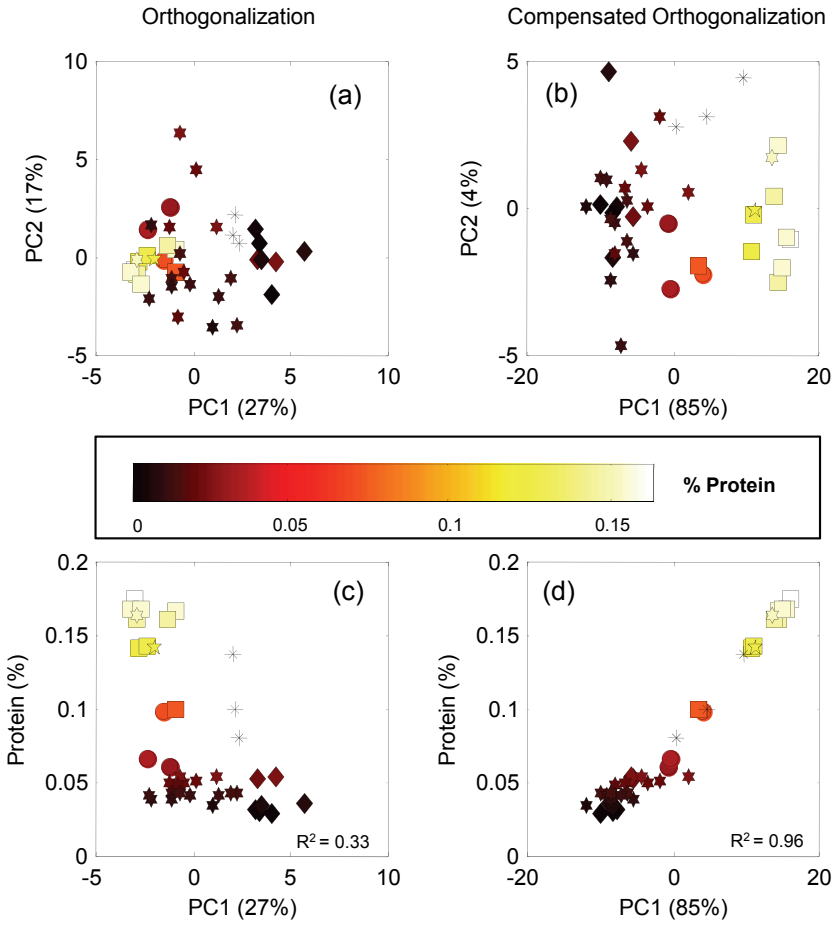

Figure 40. Effect of (a, c) *orthogonalization* and (b, d) *compensated orthogonalization* of IR spectra towards total solid content; (a, b) PCA score-plots after orthogonalization, (c, d) protein content versus PC1 score values. Symbols denote the origin (six factories) of permeate.

5.7 Summary

This chapter describes standard and advanced chemometric methods used in this thesis. Models PCA, PLS and ECVA are briefly explained. The PARAFAC model is described with special emphasis on the PARAFAC solution diagnostics core consistency. Core consistency quantifies model appropriateness by comparing a Tucker3 core calculated from PARAFAC loadings to the identity core I.

Analyzing TD-NMR data is considered in detail. Especially the estimation of the actual number of real components in relaxation curves as opposed to random instrumental noise. The curve resolution method DOUBLESLICING is introduced. DOUBLESLICING upgrades the individual relaxation curve into three-way data by systematically slicing the curve. Subsequently, three-way data can be modeled by multi-way models, which are advantageous in having many diagnostics of validating the appropriate number of components. These validation diagnostics include residual shape inspection, split-half analysis and core consistency.

External factor orthogonalization (EFO) is the process of removing information from a data matrix X linearly related to an external factor. EFO is exemplified through **PAPER II**. In this study protein and total solid variations were removed from IR spectra of UF permeate by orthogonalization.

CHAPTER 6
CONCLUSIONS AND PERSPECTIVES

The scope of this thesis has been to evaluate the use of spectroscopic methods to analyze and optimize the dairy processes: *milk coagulation*, *curd syneresis* and *ultrafiltration* of milk. The introduction part of the thesis has described the complexity of dairy processes as well as the spectroscopic and chemometric methods used. The appended papers have each contributed with new knowledge about the processes and the application of spectroscopic and chemometric methods:

PAPER I: The objective of this study was to investigate (TD-NMR) as a method for quantification of syneresis. The results shows that curd syneresis can be quantified non-invasively during the process using TD-NMR. This finding is novel and interesting for two main reasons: 1) it is very difficult to quantify syneresis in an unbiased way using classical methods; 2) whereas most methods measure syneresis *after* the process, the approach of PAPER I could monitor syneresis continuously *during* the process. Furthermore, the study is the first to demonstrate the use of DOUBLESLICING on real TD-NMR data. The technique was found highly advantageous for automatic analysis of TD-NMR, due to the many validation possibilities and high computation speed. Thus, an automated algorithm was constructed, that selected the optimal number of proton components, based on a number of diagnostic criteria.

PAPER II: Ultrafiltration of milk yields a by-product UF permeate, which is extensively re-used in the other dairy processes. Factory-to-factory variation in permeate composition can be a potential problem when permeate from multiple UF factories are used as ingredient in one product. The objective of PAPER II was to survey UF permeate compositional variation between six dairy factories using infrared spectroscopy. PCA of IR spectra revealed two continuous sources of variation (protein and total solid content) and qualitative source (production site). In other words, results showed that permeate samples had a unique infrared signature based on the factory of origin and that variations in total solid and protein were the major difference between factories. To further investigate if other factory dependent variations existed protein and total solids information were removed from the IR spectra by orthogonalization. After orthogonalization, neither PCA nor ECVA could classify the factory origin based on IR spectra. These results indirectly indicated that total solids and protein content were the

only factors different between factories. The study has demonstrated the application of external factor orthogonalization to remove information from data.

PAPER III: The objective was to investigate rapid NIR analysis in the cheese vat (in-line) as a method for monitoring milk coagulation. A two-stage model was formulated, which captured the kinetic information in the time profile of NIR measurements of coagulating milk. An algorithmic procedure for extracting coagulation kinetic parameters in real-time was constructed. The developed methodology is interesting for two reasons 1) it captures the process dynamics from NIR measurements to a greater extent than previous studies 2) it opens up for coagulum cutting time prediction based on kinetic parameters. **PAPER IV** focuses on understanding the NIR light scattering properties of milk. The main observation was that scatter changes are highly wavelength dependent in the beginning of coagulation and less in the later stages.. The observations are discussed in relation to particle size and geometry changes occurring during milk coagulation.

PAPER V: In this paper the performance of DOUBLESLICING for determining the appropriate number of components was tested on a dataset of TD-NMR relaxation curves of 210 potatoes. It was found that DOUBLESLICING could determine the right number of components. PLS regression between NMR parameters T_2 and M_0 and dry matter content resulted in models with low errors (RMSEP = 0.60 and CV = 2.6%) and high correlation (r_{test} = 0.98).

PAPER VI: This paper describes the concept of DOUBLESLICING and the use of core consistency as a diagnostic tool for finding the optimal number of components in TD-NMR data.

Overall, this thesis has shown some advantages of spectroscopic and chemometric methods for analyzing three dairy processes. The combination of these two disciplines provides insight and process control possibilities that classical analytical techniques cannot offer.

REFERENCES

Andrade, L., Micklander, E., Farhat, I., Bro, R. and Engelsen, S.B. (2007): DOUBLESLICING: A non-iterative single profile multi-exponential curve resolution procedure - Application to time-domain NMR transverse relaxation data. Journal of Magnetic Resonance, 189, 286-292.

Bechmann, I.E., Pedersen, H.T., Nørgaard, L. and Engelsen, S.B. (1999): Comparative chemometric analysis of transverse low-field 1H NMR relaxation data. *In:* Advances in Magnetic Resonance in Food Science. Ed.: Belton, P. S., Hills, B. P., Webb, G. A., The Royal Society of Chemistry, Cambridge, UK, 217-225.

Belloque, J., and Ramos, M. (1999): Application of NMR spectroscopy to milk and dairy products. Trends in Food Science and Technology, 10, 313-320.

Berridge, N.J., (1952): An improved method of observing the clotting of milk containing rennin. Journal of Dairy Research, 19, 328-229.

Bloch, F., Hansen, W.W., Packard, M. (1946): Nuclear Induction, Physical Review, 69, 127–127.

Bohr, N. (1913): On the Constitution of Atoms and Molecules, Philosophical Magazine, 26, 1-24.

Bonanno, A.S., Ollinger, J. M. and Griffiths, P.R. (1992): The origin of band positions and widths in near-infrared spectroscopy. *In:* Near-infrared Spectroscopy, Bridging the Gap between Data Analysis and NIR Applications. Ed.: Hildrum, K.I., Isaksson, T., Naes, T. and Tandberg, A. Ellis-Horwood, New York, USA, 19-28.

Bro, R. (1996): Håndbog i multivariable kalibrering. DSR tryk, Copenhagen, Denmark.

Bro, R. and Kiers, H.A.L. (2003): A new efficient method for determining the number of components in PARAFAC models. Journal of Chemometrics, 17, 274-286.

Carlson, A., Hill, C.G. and Olson, N.F. (1987a): Kinetics of milk coagulation: I. The kinetics of kappa casein hydrolysis in the presence of enzyme deactivation. Biotechnology and Bioengineering, 29 (5), 582-589.

Carlson, A., Hill, C.G. and Olson N.F. (1987b): Kinetics of milk coagulation: II. Kinetics of the secondary phase: micelle flocculation. Biotechnology and Bioengineering, 29 (5), 590-600.

Carlson, A., Hill, C.G. and Olson, N.F. (1987c) The Kinetics of milk coagulation: IV. The kinetics of the gel-firming process. Biotechnology and Bioengineering 29 (5), 612-624.

Carr, H.Y. and Purcell E.M. (1954): Effect of diffusion on free precession in nuclear magnetic resonance experiments. Physical Review, 94, 630-638.

Castillo, M., Gonzáles, R., Payne, F.A., Laencina, J., López, M.B. (2005): Optical Monitoring of Milk Coagulation and In-line Cutting Time Prediction in Murcian Al Vino Cheese. Applied Engineering in Agriculture, 21 (3), 465-471.

Castillo, M., Lucey, J.A., and Payne, F.A. (2006): The effect of temperature and inoculum concentration on rheological and light scatter properties of milk coagulated by a combination of bacterial fermentation and chymosin. Cottage cheese-type gels. International Dairy Journal, 16, 131-146.

Castillo, M., Payne, F.A., Hicks, C.L., Laencina, J., and Lopez, M.B. (2002): Effect of calcium and enzyme in cutting time prediction of coagulating goats' milk using a light scattering sensor. International Dairy Journal, 12, 1019-1023.

Castillo, M., Payne, F.A., Hicks, C.L., Laencina, J. and López, M.B. (2003): Effect of protein and temperature on cutting time prediction in goat's milk using an optical reflectance sensor. Journal of Dairy Research, 70, 205-215.

Castillo, M., Payne, F.A., Hicks, C.L. and López, M.B. (2000): Predicting cutting and clotting time of coagulating goat's milk using diffuse reflectance: effect of pH, temperature and enzyme concentration. International Dairy Journal, 10, 551-562.

Cevallos-Cevallos, J.M., Reyes-De-Corcuera, J.I., Etxeberria, E., Danyluk, M.D. and Rodrick, G.E. (2009): Metabolomic analysis in food science: a review. Trends in Food Science & Technology, 20 (11-12), 557-566.

Chatterjee, A. (2000): An introduction to the proper orthogonal decomposition. Computational Science, 78 (7), 808-817.

Crofcheck, C.L., Payne, F.A. and Nokes, S.E. (1999): Predicting the cutting time of cottage cheese using light backscatter measurements. Transactions of the ASAE, 42 (4), 1039-1045.

Dahm, D.J. and Dahm, K.D. (2001): The Physics of Near-Infrared Scattering. Chapter 1 *In:* Near-Infrared Technology in the Agricultural and Food Industries, second edition, Ed.: Williams, P. and Norris, K., AACC Inc., Minnesota, USA.

Dalgleish, D.G. (1979): Proteolysis and aggregation of casein micelles treated with immobilized or soluble chymosin. Journal of Dairy Research, 46, 653-661.

Dalgleish, D.G. (1993). The enzymatic coagulation of milk. *In*: Cheese Chemistry, Physics and Microbiology, vol. 1, pp. 69-100, Ed. Fox, P.F., Chapman & Hall, London,UK.

Dejmek, P., Walstra, P. (2004) The Syneresis of Rennet-coagulated Curd, *In*: Cheese: Chemistry, Physics and Microbiology 3rd Ed. Eds:Fox, P.F., McSweeney, P.L.H, Cogan, T.M, Guinee, T.P. Elsevier academic press, Oxford, UK.

Dufour, E. (2009): Principles of infrared spectroscopy. Chapter 1 *In:* Infrared spectroscopy for food quality analysis and control. First edition. Ed.: Sun, Da-Wen. Elsevier Inc., New York, USA.

Ellen, G. and Tudos, A.J. (2003): On-line measurement of product quality in dairy processing. Chapter 13. *In:* Dairy Processing Improving Quality. Ed.: Smit, G., CRC Press, Florida, USA.

Everard, C.D., Fagan, C.C., O'Donnell, C.P., O'Callaghan, D.J., Castillo, M. and Payne, F.A. (2007): Computer vision and colour measurement techniques for inline monitoring of cheese curd syneresis. Journal of Dairy Science, 90, 3162-3170.

Fagan, C.C, O'Donnell, C.P., Rudzik, L. and Wüst, E. (2009): Milk and Dairy Products, Chapter 10 *In:* Infrared Spectroscopy for Food Quality Analysis and Control. First edition, Ed.: Sun, Da-Wen, Elsevier Inc., New York, USA.

FDA: United States Food and Drug Administration (2004): Guidance for industry PAT – a framework for innovative pharmaceutical development, manufacturing and quality assurance, U.S. Department of Health and Human Services, Rockville, USA.

Foss (2010). Webpage: www.foss.dk, 15th August 2010.

Fox, P.F., McSweeney, P.L.H. (1998): Dairy Chemistry and Biochemistry, Kluwer Academic Publicers Group, MA, USA.

Geladi, P. and Kowalski, B.R. (1986): Partial least-squares regression: a tutorial. Analytica Chimica Acta, 186, 1-17.

Griffiths, P.R. (2002): Introduction to Vibrational Spectroscopy. *In*: Handbook of Vibrational Spectroscopy. Vol. 1, Eds: Chalmers, J.M., Griffiths, P.R. John Wiley & Sons, Ltd., West Succex, UK.

Gunasekaran, S., Ak, M.M. (2003):Cheese Rheology and Texture. CRC Press, Florida, US.

Hahn, E.L. (1950): Spin echos, Physical Reviews, 80, 580-594.

Heino, A., Uusi-Rauva, J., Outinen, M. (2009): Microfiltration of milk III: Impact of milk modification on milk coagulation kinetics, Milchwissenschaft, 64 (2), 128-131.

Herschel, W. (1800): Investigation of the powers of the prismatic colours to heat and illuminate objects; with remarks, that prove the different refrangibility radient heat. To which is added, an inquiry into the method of viewing the sun advantageously, with

telescopes or large apertures and high magnifying powers. Philosophical Transactions of the Royal Society of London, 90, 255-283.

Hills, B.P., Takacs, S.F. and Belton, P.S. (1990): A new interpretation of proton NMR relaxation time measurements of water in food. Food Chemistry, 37 (2), 95-111.

Hinrichs, R., Bulca, S. and Kulozik, U. (2007): Water mobility during renneting and acid coagulation of casein solutions: a differentiated low-resolution nuclear magnetic resonance analysis. International Journal of Dairy Technology, 60 (1), 37-43.

Holroyd, S. (2002): 'In-line analysis', presented at the Symposium Laboratories in Transition, IDF/ISO/AOAC Analytical Week, Toledo, Spain.

Holzgrabe, U. (2010): Quantitative NMR spectroscopy in pharmaceutical applications. Progress in Nuclear Magnetic Resonance Spectroscopy, 57 (2), 229-240.

Hori, T. (1985): Objective measurements of the process of curd formation during rennet treatment of milks by the hot wire method. Journal of Food Science, 50, 911–917.

IDF (1992): *Bovine rennets*. Determination of Total Milk-clotting activity, Provisional Standard 157, International Dairy Federation, Brussels, Belgium.

IDF (1993): Determination of Water Content, Standard s6A, International Dairy Federation, Brussels, Belgium.

Juan, A. and Taulor, R. (2003): Multivariate Curve Resolution (MCR) from 2000: Progress in Conceps and Applications. Critical Reviews in Analytical Chemistry, 36, 163-176.

Kawamura, S., Tsukahara, M., Natsuga, M. and Itoh, K. (2007): On-line Near Infrared Spectroscopic Sensing Technique for Assessing Milk Quality during Milking. ASAE Annual International Meeting.

Koch, M.V. (2006): Optimizing the impact of developments in micro-instrumentation on process analytical technology: a consortium approach, Analytical Bioanalytical Chemistry, 384, 1049-1053.

Kubelka, P. and Munk, F. (1931): Ein beitag zur optic der farbanstriche. Z. Tech. Phys., 12, 593-601.

Lelievre, J. and Creamer, L.K. (1978): NMR-Study of Formation and Syneresis of Renneted Milk Gels. Milchwissenschaft, 33 (2), 73-76.

Lu, C., Xiang, B., Hao, G., Xu, J., Wang, Z. and Chen, C. (2009): Rapid detection of melamine in milk powder by near infrared spectroscopy. Journal of Near Infrared Spectroscopy, 17, 59-67.

Laporte, M.F., Martel, R. and Paquin, P. (1998): The near infrared optic probe for monitoring rennet coagulation in cow's milk. International Dairy Journal, 8, 659-666.

Lucey, J.A. (2002): Formation and physical properties of milk protein gels. Journal of Dairy Science, 85, 281-294.

Lucey, J.A., Johnson, M.E., & Horne, D.S. (2003): Perspectives on the Basis of the Rheology and Texture Properties of Cheese, Journal of Dairy Science, 86, 2725-2743.

Marquardt, D.W. (1963): An Algorithm for Least-Squares Estimation of Nonlinear Parameters. Journal of the Society for Industrial and Applied Mathematics, 11 (2), 431-441.

McMahon, D.J., Brown, R.J. and Ernstrom, C.A. (1984): Enzymic coagulation of milk casein micelles. Journal of Dairy Science, 67, 745-748.

McMahon, T. and Wright, E.L. (1996): Analytical Instrumentation: A Practical Guide for Measurement and Control. Ed.: Sherman, R.E. and Rhodes, L.J., Instrument Society of America: Research Triangle Park, NC, USA.

Miller, C.E. (2001): Chemical Principles of Near-Infrared Technology. Chapter 2. *In:* Near-Infrared Technology in the Agricultural and Food Industries, second edition, Ed.: Williams, P. and Norris, K., AACC Inc., Minnesota, USA.

Miller, C.E. (2005): Chemometrics in Process Analytical Chemistry. Chapter 8. *In:* Process Analytical Technology, Ed. Bakeev, K.A., Blackwell Publishing Ltd, Oxford, UK.

Meiboom, S. and Gill, D. (1958): Modified spin-echo method for measuring the nuclear relaxation time. The Review of Scientific Instruments, 29, 688-691.

Mertens, B.J.A., O'Donnell, C.P. and O'Callaghan, D.J. (2002): Modelling near-infrared signals for on-line monitoring in cheese manufacturing, Journal of chemometrics, 16, 89-98.

Niki, R. (1994): Rheological Study on the Rennet-Induced Gelation of Casein Micelles with Different Sizes. Polymer Gels and Network, 2, 105-118.

Nørgaard, L., Saudland, A., Wagner, J., Nielsen, J.P., Munck, L., and Engelsen, S.B. (2000): Interval partial least-squares regression (iPLS): A comparative chemometric study with an example from near-infrared spectroscopy. Applied Spectroscopy, 54 (3), 413-419.

Nørgaard, L., Bro, R., Westad, F. and Engelsen, S.B. (2006): A modification of canonical variates analysis to handle highly collinear multivariate data. Journal of Chemometrics, 20 (8-10), 425–435.

Nørgaard, L., Soletormos, G., Harrit, N., Albrechtsen, M., Olsen, O., Nielsen, D., Kampmann, K. and Bro, R. (2007): Fluorescence spectroscopy and chemometrics for classification of breast cancer samples – A feasibility study using extended canonical variates analysis. Journal of Chemometrics, 21 (10-11), 451-458.

O'Callaghan, D.J., O'Donnell, C.P. and Payne F.A. (1999): A comparison of on-line techniques for determination of curd setting time using cheesemilk under different rates of coagulation. Journal of Food Science, 41, 43-54.

O'Callaghan, D.J., O'Donnell, C.P. and Payne, F.A. (2002): On-line sensing techniques for coagulum setting in renneted milks. Journal of Food Engineering 43, 155-165.

O'Callaghan, D.J., O'Donnell, C.P. and Payne, F.A. (2002): Review of systems for monitoring curd setting during cheesemaking. International Journal of Dairy Technology, 55 (2), 65-74.

Ouellette, R.J. (1998): Organic chemistry: a brief introduction. Second edition, Prentice-Hall, Inc. New Jersey, USA.

Ozilgen, M. and Kauten, R.J. (1994): NMR Analysis and Modeling of Shrinkage and Whey Expulsion in Rennet Curd. Process Biochemistry, 29 (5), 373-379.

Pearse, M.J. and Mackinlay, A.G. (1989): Biochemical Aspects of Syneresis: A Review. Journal of Dairy Science, 72, 1401-1407.

Payne, F.A., Hicks, C.L. and Shen P.S. (1993): Predicting optimal cutting time of coagulating milk using diffuse reflectance. Journal of Dairy Science, 76, 48-61.

Payne, F.A., Freels, R.C., Nokes, S.E. and Gates, R.S. (1998): Diffuse reflectance changes during the culture of cottage cheese. Transactions of the ASAE, 41 (3), 709-713.

Provencher, S.W. (1982): Contin - A General-Purpose Constrained Regularization Program for Inverting Noisy Linear Algebraic and Integral-Equations. Computer Physics Communications, 27 (3), 229-242.

Purcell, E.M., Torrey, H.C. and Pound, R.V. (1946): Resonance Absorption by Nuclear Magnetic Moments in a Solid. Physical Reviews, 69, 37-38.

Ruettiman, K.W. and Ladisch, M.R. (1987): Casein micelles: structure, properties and enzymatic coagulation, Enzyme Microbiological Technology, 9, 578-589.

Rutledge, D.N. (2001): Characterisation of water in agro-food products by time domain NMR. Food Control, 7, 437-445.

Savorani, F., Picone, G., Badiani, A., Fagioli, P., Capozzi, F. and Engelsen, S.B. (2010): Metabolic profiling and aquaculture differentiation of gilthead sea bream by 1H NMR metabonomics, Food Chemistry, 120, 907-914.

Scher, J. and Hardy, J. (1993): Study of the variations in particle size distribution after renneting by means of quasi-elastic light scattering. Australian Journal of Dairy Technology, 48, 62-65.

Scott Blair, G.W. (1971): A simple model to describe the kinetics of coagulation of casein (milk) and fibrin (blood). Rheologica Acta, 10 (3), 316-318.

Sheppard, N. (2002): Introduction to the Theory and Practice of Vibrational Spectroscopy. *In:* Vibrational Spectroscopy. Vol.1. First edition. Ed.: Chalmers, J.M. and Griffiths, P.R., John Wiley & Sons Ltd, Chichester, UK, 1-33.

Storry, J.E. and Ford, G.D. (1982): Development of coagulum firmness in renneted milk – a two-phase process. Journal of Dairy Research, 49, 343-346.

Talens, C., O'Callaghan, D.J., Everard, C.D., Fagan, C.C., Castillo, M. and Payne, O'Donnel (2009): Evaluation of an improved tracer method to monitor cheese curd syneresis at varying milk fat levels in a cheese vat. Milchwissenschaft, 64 (2), 161-164.

Tellier, C., Mariette, F., Guillement, J.P. and Marchal, P. (1993): Evolution of Water Proton Nuclear Magnetic-Relaxation during Milk Coagulation and Syneresis - Structural Implications. Journal of Agricultural and Food Chemistry, 41 (2), 2259-2266.

TEN GROTENHUIS E. (1999): Prediction of cutting time during cheese production, European Dairy Magazine, 11, 40-41.

Tsenkova, R., Atanassova, S., Kawano, S. and Toyoda, K. (2001): Somatic cell count determination in cow's milk by near-infrared spectroscopy: A new diagnostic tool. Journal of Animal Science, 79, 2550-2557.

van Hooydonk, A.C.M. and van den Berg, G. (1988): Control and Determination of the Curd-Setting During Cheesemaking. IDF Bulletin No 225. Brussels: International Dairy Federation.

Walstra, P. and Jenness, R. (1984): Dairy Chemistry and Physics. John Wiley & Sons Inc, New York, USA.

Walstra, P. (2003): Chapter 4: Reaction kinetics. *In:* Physical Chemistry of Foods Dairy. Ed.: Walstra, P., Marcek Dekker Inc., New York, USA.

Walstra, P., Wouters, J.T.M. and Geurts, T.J. (2006): Dairy Science and Technology. Second edition, CRC Press, Florida, USA.

Wold, S., Esbensen, K.H. and Geladi, P. (1987): Principal component analysis. Chemometrics and Intelligent Laboratory Systems, 2, 37-52.

Wold, S. (1992): Nonlinear PLS modelling II: Spline inner relation. Chemometrics and Intelligent Laboratory Systems, 14 (1-3), 71-84.

Wold, S., Sjöström, M. and Eriksson, L. (2001): PLS-regression: a basic tool of chemometrics. Chemometrics and Intelligent Laboratory Systems, 58, 109-130.

Workman Jr., J., Koch, M., Lavine, B. and Chrisman, R. (2009): Process Analytical Chemistry. Analytical Chemistry, 81, 4623-4643.

Paper I

Effect of Gel Firmness at Cutting Time, pH, and Temperature on Rennet Coagulation and Syneresis: An *in situ* ^{1}H NMR Relaxation Study.

Reprint from Journal of Agricultural and Food Chemistry, 58 (1), 513-519.

JOURNAL OF AGRICULTURAL AND FOOD CHEMISTRY
ARTICLE

J. Agric. Food Chem. 2010, 58, 513–519 513
DOI:10.1021/jf902264y

Effect of Gel Firmness at Cutting Time, pH, and Temperature on Rennet Coagulation and Syneresis: An in situ ^{1}H NMR Relaxation Study

Christian Lyndgaard Hansen,*,† Åsmund Rinnan,† Søren Balling Engelsen,† Thomas Janhøj,‡ Elisabeth Micklander,† Ulf Andersen,§ and Frans van den Berg†

†Quality and Technology Group, and ‡Dairy Technology Group, Department of Food Science, Faculty of Life Sciences, University of Copenhagen, Rolighedsvej 30, 1958 Frederiksberg, Denmark, and §Arla Foods Innovation, Rørdrumvej 2, 8220 Brabrand, Denmark

The objective of this study was to monitor rennet-induced milk gel formation and mechanically induced gel syneresis in situ by low-field NMR. pH, temperature, and gel firmness at cutting time were varied in a factorial design. The new curve-fitting method Doubleslicing revealed that during coagulation two proton populations with distinct transverse relaxation times ($T_{2,1}$ = 181, $T_{2,2}$ = 465 ms) were present in fractions (f_1 = 98.9%, f_2 = 1.1%). Mechanical cutting of the gel in the NMR tube induced macrosyneresis, which led to the appearance of an additional proton population ($T_{2,3}$ = 1500−2200 ms) identified as whey. On the basis of NMR quantification of whey water the syneresis rate was calculated and found to be significantly dependent on pH and temperature.

KEYWORDS: In situ monitoring; NMR; rennet coagulation; syneresis; casein; slicing

INTRODUCTION

During cheese manufacture rennet is added to milk, where it breaks the bond between the amino acids Phe_{105} and Met_{106} in κ-casein. Subsequently, the casein starts to aggregate and form a gel. This gel retains all of the constituents of the milk including the aqueous phase. An important step in cheese manufacture is the separation of the main part of the water phase from the casein-gel, which is achieved through a process called syneresis (*1*). Syneresis occurs as a result of local stresses in the gel network, leading to rearrangements and local expulsion of whey, a phenomenon termed endogenous syneresis or microsyneresis. Physical separation of whey from the rennet gel (i.e., macrosyneresis) is normally dependent on cutting of the gel (*2*, *3*). Furthermore, the firmness of the gel at the cutting influences the moisture content of the final cheese. If the gel is cut at a too low firmness (cutting too early), the final cheese yield is reduced due to loss of fat and curd fines to the whey. If the gel is cut at a too high firmness (cutting too late), the syneresis is retarded, which results in cheese with high moisture content and undesirable textural properties (*4*, *5*). The process parameters pH and temperature have a major impact on syneresis. Lowering the pH of the gel during syneresis has been found to increase the rate of syneresis (*6*, *7*); increasing the temperature accelerates the rate of syneresis. The kinetics of syneresis is commonly considered to be of first order over the time scale used in cheese production (*2*, *8*). Thus, pH, temperature, and gel firmness at cutting are crucial for the water content and the texture of the final cheese product.

Traditional methodologies for studying syneresis can be divided into physical separation methods and tracer methods. In the physical separation methods the whey and/or gel is weighed to determine the extent of syneresis. The problem with physical separation methods is that the gel expels additional whey when being handled, which results in a biased measurement. The tracer methods measure dilution of an added compound such as Blue Dextran 2000 (*9*, *10*). A difficulty with tracer methods, however, is finding a tracer compound that does not adsorb to or diffuses into the gel (*11*).

Time domain proton (^{1}H) low-field nuclear magnetic resonance (LF-NMR) represents a particularly attractive alternative method for characterizing and quantifying water in food and dynamic food systems such as gel formation and syneresis. The major advantage of LF-NMR in this context is that the method is both nondestructive and noninvasive (*12*). The NMR relaxation of water protons in high water content biological systems is met by different restrictions that increase the rate of relaxation. In this manner different relaxation rates can give selective information about the surrounding environment of different water *pools* or *populations* within biological matter. Restrictions to relaxation are due to water protons being present in different states or sites in the system in a time scale compatible with the NMR experiment: (1) restriction due to chemical exchange between the water protons and the biopolymer protons and (2) restriction of proton relaxation due to physical compartmentalization in the sample. The latter restriction cause is related to diffusion of water protons because water protons will experience fast relaxation in the

*Address correspondence to this author at the Quality and Technology Group, Department of Food Science, Faculty of Life Sciences, University of Copenhagen, Rolighedsvej 30, 1958 Frederiksberg, Denmark (telephone +45 35 33 25 65; fax +45 35 33 32 45; e-mail chha@life.ku.dk).

Published on Web 11/16/2009

proximity of a physical barrier. Naturally, fast relaxation will only occur if the diffusion time for protons to reach the barrier is shorter than the intrinsic relaxation time of the protons and the time scale of the NMR experiment (*13*).

Several NMR relaxation studies have been reported on milk gel formation (*14*−*17*) and syneresis (*3*, *15*, *17*). The effect of milk gel syneresis on water proton relaxation has so far been studied on undisturbed gels that exhibit only endogenous syneresis (i.e., syneresis caused by pressure being built up by network formation within the gel). This is, however, not representative for actual cheese manufacturing, in which mechanical cutting of the gel into dices is an essential process step. Two inconsistencies exist in the interpretation of the water proton relaxation during to milk gel formation and syneresis: (1) the development (or lack) of the transverse relaxation time constant, T_2, and its corresponding proton population size during gel formation and (2) the number of proton populations necessary to describe water proton relaxation during cheese gel formation. Two studies have found no change in the relaxation time constant, T_2, during milk gel formation (*15*, *17*). On the other hand Hinrichs et al. (*14*) found small changes in T_2 relaxation time during the gel formation. The latter study found (without providing explicit proof) that three populations of water protons were required to describe the relaxation during milk gel formation, whereas the former studies found that one proton population was sufficient to describe the proton relaxation. There is a general agreement that the onset of milk gel syneresis is associated with the appearance of an additional water population with slower relaxation, which are the protons in the whey water (*14*, *15*, *17*). In these studies, however, the syneresis happened spontaneously, and the actual onset of syneresis was not controlled by cutting, which speed up the syneresis.

One of the reasons for the discrepancy in number of proton components is related to the data analytical methods chosen for studying and deconvoluting the NMR relaxation data. Proton relaxation occurs exponentially with time. If multiple proton populations exist in the samples, the relaxation decay curve is a sum of multiple exponential terms. The major challenge in the analysis of relaxation decay curves of LF-NMR experiments using multiexponential curve fitting is to decide the appropriate number of exponential terms that describe the actual water populations present in a sample. A new exponential curve-fitting method called *Doubleslicing* was introduced by Micklander et al. (*12*) to assist in the determination of water populations. Andrade et al. (*18*) tested the performance of Doubleslicing against existing methods and found that it was accurate in estimating relaxation times and that it outperformed exponential fitting by a factor of 4 with regard to computation time.

The primary objective of this study was to investigate the effect of milk gel formation and in situ mechanically (by cutting) induced gel syneresis by LF-NMR. The secondary objective was to demonstrate Doubleslicing as a method for determining the appropriate number of components in a semiautomated way. For these purposes the effect of milk gel formation and syneresis was studied using an experimental design with three factors: (1) pH, (2) temperature, and (3) gel firmness at cutting time. Time domain LF-NMR measurements were carried out in parallel with rheological measurements. The rheological measurements were done only during gel formation (and not syneresis) to evaluate the gel firmness.

MATERIALS AND METHODS

Experimental Approach. In this study we investigate rennet-induced gel formation of skim milk and the subsequent syneresis process after gel cutting by time domain LF-NMR. Rennet was added to skim milk, and this volume was split into two fractions: one was transferred to an NMR tube with an inner diameter of 17 mm. This tube was immediately inserted in the LF-NMR spectrometer and continuously measured without interruption during milk coagulation, cutting, and syneresis. The other fraction was injected into a rheological instrument that continuously measured gel firmness during gel formation. The role of the rheological measurements was to ensure that the gels formed in the NMR tube for repeated experiments had the same, wanted firmness when being cut. A *knife*, consisting of a thin polycarbonate blade tightly matching the tube diameter, was used to cut the gel manually and straight once over the entire inner diameter of the NMR tube. This was done when the firmness of the gel in the *twin* sample in the rheometer had reached a predefined level. To avoid interruption of the NMR measurements, the gel cutting was done inside the spectrometer in a 4 s delay between consecutive measurements. The delay did not always occur simultaneously with the predefined level of gel firmness, which therefore gave rise to slight variations in gel firmness at cutting.

Experimental Design. During the gel formation and syneresis three experimental factors were investigated on two levels (2^3 factorial design): pH (6.3 and 6.5), temperature (32 and 35 °C), and gel firmness at cutting time (low and high; defined later). The eight combinations of the three design factors were replicated twice, resulting in 16 ($= 2 \times 2^3$) gel and syneresis experiments. A center point with pH 6.4, gel firmness at cutting (middle level), and 35 °C was replicated four times. Unfortunately, a middle temperature level (33.5 °C) could not be tested due to experimental limitations. Overall, this resulted in 20 ($= 16 + 4$) gel and syneresis experiments performed in random order in the NMR spectrometer.

Materials. Arla Foods Ingredients (Denmark) kindly donated low-heat skim milk powder (SMP; Milex 240). The composition of SMP as reported by the manufacturer was 34−39% protein, <1.25% fat, 48−56% lactose, 7−9% ash, and <4% moisture. Chy-Max Plus rennet with 220 international milk clotting units (IMCU) mL^{-1} was obtained from Chr. Hansen A/S (Hørsholm, Denmark). Calcium chloride dihydrate ($CaCl_2 \cdot H_2O$) from Merck A/S (Darmstadt, Germany) and HCl from Acros Organic (Morris Plains, NJ) were used for preparation of the reconstituted milk samples.

Preparation of Milk and Renneting. Reconstituted skim milk samples were prepared by dissolving 100.0 g of SMP in 1000 mL of deionized water. The reconstituted skim milk was left overnight at 5°C to allow the proteins to fully dissolve. The protein concentration of the reconstituted milk was 3.4−3.9% (calculated from manufacturer's data). A 10% $CaCl_2 \cdot H_2O$ stock solution (1.50 mL) was added, resulting in a final concentration of 0.015% (~1.2 mM) $CaCl_2 \cdot H_2O$ in the milk. The pH was adjusted according to the experimental design with weak HCl (0.5 M). The reconstituted milk samples were conditioned to the temperatures of the experimental design for approximately 10 min in a water bath.

A diluted rennet solution of 6.60 IMCU mL^{-1} was made within 3 min before initialization of the experiment by mixing 300 μL of Chy-Max Plus (220 IMCU mL^{-1}) with 10 mL of deionized water. Renneting was initialized by adding 1.000 mL of diluted rennet solution to 150 mL of preheated milk placed in a water bath with magnet stirring, resulting in a final concentration of 0.044 IMCU mL^{-1} of milk. Thirty seconds after rennet addition, the stirring was stopped and 1.000 mL of milk was transferred to each of four sample cups in the rheometer. Sixty seconds after rennet addition, 7.000 mL of milk was transferred to a temperature-conditioned NMR tube, and LF-NMR measurements were immediately started.

Rheological Measurements. Firmness of the milk gel at cutting time was regulated by cutting at one of three levels according to the experimental design (low, medium, or high). The viscoelastic properties of the gel were monitored during gel formation by free oscillation rheometry (FOR) by using a ReoRox4 instrument from MediRox (Nyköping, Sweden) using disposable polypropylene sample cups and the accompanying software (ReoRox4 v2.00 and ReoRox Viewer v2.11). In free oscillation rheometry the measurement geometry is released into free oscillations at a frequency of around 10 Hz, and the amplitude and period time are measured by optical sensing. The frequency implies that the method is noninvasive toward the rennet gel system and hence does not disturb the gel during formation (*19*). The gel was cut inside the NMR tube when the elastic modulus G' (10 Hz) reached 90, 125, or 160 Pa, corresponding to the gel firmness defined as low, middle, or high in the experimental design.

This resulted in a cutting-time range for the 20 experiments in the design of 17−61 min. Note that the elastic modulus, G', as well as strain is appreciably higher in FOR than in conventional small-amplitude oscillation rheometry (SAOR) due to the higher oscillation frequency.

NMR Acquisitions. Time domain LF-NMR analysis was done on a benchtop 23.2 MHz Maran pulsed ^{1}H NMR spectrometer (Oxford Instrument, U.K.) equipped with a 17 mm inner diameter variable-temperature probe head. The temperature of the probe was set according to the experimental design. The Carr−Purcell−Meiboom−Gill (CPMG) pulse sequence was used to determine the relaxation behavior. This sequence was chosen because it minimizes the influence of magnetic field inhomogeneities, diffusion, and chemical exchange (*13*). A total of 8100 data points/echo times were acquired, with a 90−180 pulse spacing (τ) value of 500 μs. Only the even-numbered data points were used in the data analysis, resulting in 4050 data acquisition points per measurement. By using every second echo only (even echoes), inaccuracies in the 180° pulse setting are corrected. Prior to the first measurement, the frequency of the instrument was adjusted on a 10 mM $CuSO_4$ standard sample. During gel formation four scans were accumulated with a relaxation delay between consecutive scans of 14 s. Prior to the four scans, each measurement was preceded by two dummy scans, leading to a total measurement time of 2 min and 12 s. Measurements were carried out continuously until a maximum of 100 min after cutting.

NMR Data Analysis by Doubleslicing. Time domain LF-NMR data are most frequently analyzed using multiexponential fitting using, for example, the Levenberg−Marquardt algorithm, which applies nonlinear iterative curve-fitting algorithms to extract and characterize the underlying pure exponentials from random noise in the data (eq 1):

$$M(t) = \sum_{n=1}^{N} M_{0,n} \exp\left(\frac{-t}{T_{2,n}}\right) + e(t) \quad (1)$$

$M(t)$ is the reduced magnetization at time t, $M_{0,n}$ is the concentration or magnitude parameter of the n^{th} exponential, $T_{2,n}$ is the corresponding transverse relaxation time constant, and $e(t)$ is the residual error. After the relaxation curve has been deconvoluted into n exponential components, inspection of residuals can reveal whether the curve has been modeled into too few, too many, or the correct number of components. If the relaxation curve has been resolved into fewer exponential components than actually present, the residuals will show a systematic pattern. If the right number of exponential components is used, the residual will be randomly distributed. If too many exponential components are used, the residuals will also be randomly distributed, but instrumental noise will be incorporated in the fit. With large data sets (e.g., ~800 curves in the present study), this procedure including the inspection of the residual plots can become very time-consuming.

Micklander et al. (*12*) introduced an alternative noniterative and rapid technique for curve resolution called Doubleslicing. The technique utilizes the fact that in every part of a multiexponential decay curve each of the monoexponentials is present, but in different amounts. The technique pseudo-upgrades the single relaxation curve to become trilinear data, by cutting the relaxation curve into slices. By selectively removing parts of the signal curve (slicing) and using the remaining curve, the relaxation curve can be transformed from a one-dimensional signal (a vector **x**) into two-dimensional data (a matrix X). By repeating this procedure on the matrix, the data are transformed to three-dimensional data (a cube $\underline{X}$). This procedure of converting the relaxation curve into three-way data may appear to be pointless at first glance, but it enables the use of three-way mathematical methods such as direct trilinear decomposition [DTLD (*20*)], which has some very attractive features. Andrade et al. (*18*) tested the performance of Doubleslicing against existing methods and found that it was accurate in estimating relaxation times and that it outperformed exponential fitting by a factor of 4 with regard to computation time. The speed advantage is desirable when large data sets are analyzed. Besides drastic improvement in speed, Doubleslicing also improves modeling and method diagnostic.

In the present study Doubleslicing was performed similar to the method of Andrade et al. (*18*). To validate that the relaxation curves were resolved into the actual number of exponentials and not under- or overfitting, an extensive range of diagnostic criteria had to be fulfilled. This set of diagnostic criteria enabled the construction of an automated algorithm, which could successively determine the relaxation times and the appropriate number of exponentials in the approximately 800 relaxation curves analyzed in the present study without manual intervention. Doubleslicing with diagnostic criteria was compared with the classical approach discrete exponential fitting using visual inspection of residuals. The implementation of diagnostic criteria and comparison with discrete exponential fitting are described in the Supporting Information.

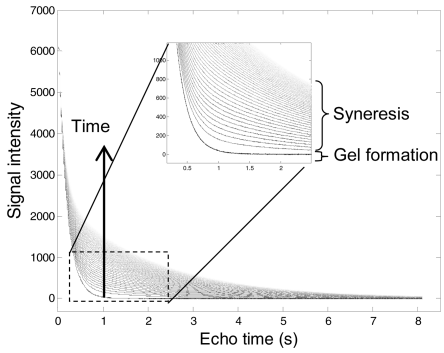

Figure 1. NMR CPMG relaxation curves during gel formation and syneresis in one gel formation and syneresis experiment. Notice that the overall relaxation becomes systematically slower with experiment time.

Syneresis Rate. The expected rate at which water leaves a milk gel when cut (i.e., syneresis) has been found to follow first-order reaction kinetics (*2*), which implies that the rate is dependent on the concentration of water in the gel. First-order reaction kinetics for syneresis can be expressed as (eq 2)

$$W_{\text{gel}} \rightarrow W_{\text{whey}}$$

$$-\frac{\mathrm{d}[W_{\text{gel}}]}{\mathrm{d}t} = k[W_{\text{gel}}] \quad (2)$$

where W_{gel} is the concentration of water in the gel, t is time, and k is the first-order rate constant. Integration and variable separation of eq 2 yields eqs 3 and 4:

$$\ln \frac{[W_{\text{gel}}]}{[W_{\text{gel},0}]} = -kt \quad (3)$$

$$[W_{\text{gel}}] = [W_{\text{gel},0}]\, \mathrm{e}^{-kt} \quad (4)$$

For a first-order reaction, therefore, a plot of natural logarithm versus t is linear and the first-order rate constant is obtained from the slope (*21*). In this study the proton population sizes of the whey water protons are assumed to represent the concentration of water outside the gel.

Statistical Analysis. On the syneresis rate constant k, obtained in the 2^3 factorial design, a three-way analysis of variance (ANOVA) was performed (omitting the partial center point) using the following main-effects model (eq 5)

$$k = \mu + \alpha \times \mathrm{pH} + \beta T + \gamma \times \mathrm{GF} + e \quad (5)$$

where μ is the common mean, α is the coefficient characterizing the pH effect, β is the temperature effect, and γ is the gel firmness effects. Interaction terms were not included, that is, evaluated as insignificant ($p < 0.05$) by iterative testing.

All data analysis steps (data exploration, trilinear modeling, ANOVA, etc.) were performed with Matlab version 7.6 (MathWorks Inc., Natick, MA) and an in-house algorithm.

RESULTS AND DISCUSSION

Development in T_2 Relaxation Time Constants and Population Sizes. Figure 1 shows CPMG relaxation curves recorded in one

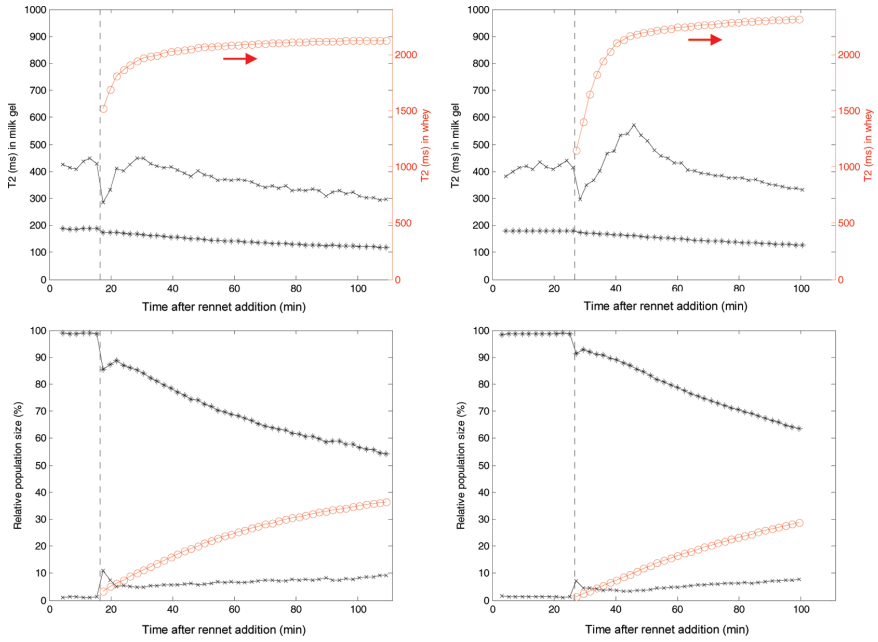

Figure 2. Development in transverse relaxation time constants $T_{2,1}$, $T_{2,2}$, and $T_{2,3}$ (upper row) and the corresponding relative population sizes f_1, f_2, and f_3 (lower row) during gel formation and syneresis of two experiments with different experimental settings. The left-column graphs show the development in an experiment with conditions pH 6.3, 34.9 °C, and low firmness at cutting. The right-column graphs show the development in an experiment with conditions pH 6.5, 34.9 °C, and low firmness at cutting. The vertical broken line indicates the time when the milk gel was cut.

Table 1. Average T_2 and Relative Population Size during Gel Formation and Syneresis for the 20 Experiments

	transverse relaxation time constant (ms)			relative population size (%)		
phase	$T_{2,1}$	$T_{2,2}$	$T_{2,3}$	f_1	f_2	f_3
gel formation	180.7 (5.1)[a]	465.3 (69.0)		98.9 (0.2)	1.1 (0.2)	
gel syneresis	151.1 (5.9)	425.9 (35.1)	1849.2 (125.2)	79.0 (5.7)	5.3 (1.1)	11.8 (5.2)

[a] Standard deviation in parentheses.

batch during gel formation and subsequent syneresis induced by cutting the milk gel at predetermined degrees of gel firmness [i.e., size of the viscous module G'' (10 Hz)]. By visual inspection of the relaxation curves in **Figure 1** it is not possible to observe any changes prior to cutting of the gel. However, overall relaxation becomes systematically slower after cutting of the milk gel, implying that the proton population(s) progressively changes as a result of the syneresis process, when water (i.e., whey) is expelled from the gel network. The trend in **Figure 1** is representative for all experiments in the design.

The development in T_2 and population sizes calculated from the relaxation curves using the correct number of exponential terms for each LF-NMR measurement are shown for two representative experiments (**Figure 2**). Notice that the trend lines through the 50 time points in **Figure 2** are added for interpretational purposes only after DTLD component determination. The abrupt change at the cutting point and the otherwise smooth curves give rise to high confidence in both the modeling approach and the automated method of model rank determination. **Figure 2** displays some key trends that are representative for all 20 batches.

During gel formation and prior to cutting, two components are present, which correspond to two distinguishable populations of protons with characteristic relaxation times $T_{2,1}$ and $T_{2,2}$. Within the gel formation phase the relaxation times $T_{2,1}$ and $T_{2,2}$ and population sizes are relatively constant compared to the syneresis phase (**Figure 2** and **Table 1**). The main part of the (water) protons (relative contribution in total signal of 98.8%, SD = 0.2%) prior to cutting of the gel originates from a population that is characterized by an average $T_{2,1}$ of 180.7 ms (SD = 5.1 ms).

Changes in T_2 and Population Size during Gel Formation. During gel formation and syneresis two proton populations with the characteristic transverse relaxation times $T_{2,1}$ and $T_{2,2}$ are present within the gel (**Figure 2**). The sizes of $T_{2,1}$ and $T_{2,2}$ show that the proton population originates from water associated with different parts/constituents of the gel. Data analysis clearly showed that biexponential behavior characterizes the system during gel formation, prior to cutting. The second component characterized by $T_{2,2}$ has not been previously described in the literature, to the authors' knowledge. The $T_{2,2}$ component represents only ~1% of the water protons during gel formation, but cutting caused it to increase to ~5% of the water. Cutting induced an immediate decrease in $T_{2,2}$ followed by an increase simultaneously with an increase in $T_{2,3}$, suggesting that the events are related. More experiments should be done to further elucidate what $T_{2,2}$ represents, but this is beyond the scope of the present study.

Le Dean et al. (*22*) studied the origin of proton populations in milk and milk protein mixtures using a factorial design of various

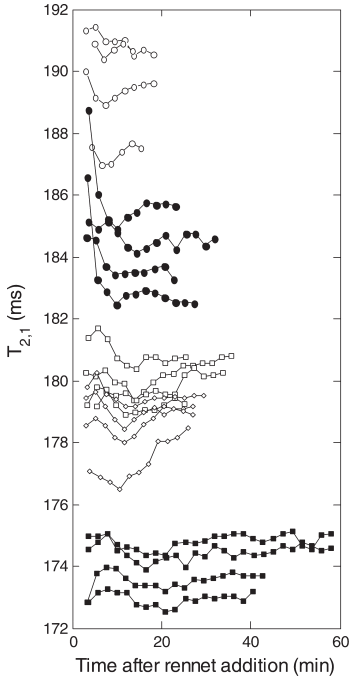

Figure 3. Development of $T_{2,1}$ with time after rennet addition, before cutting, in 20 coagulation experiments: (circles) pH 6.3; (diamonds) pH 6.4; (squares) pH 6.5; (open symbols) 32 °C; (solid symbols) 35 °C. Notice the V-like shape present in the graphs, that is, an initial decrease followed by an increase.

levels of milk components (i.e., caseinates, whey protein, $CaCl_2$, and lactose). They found that a bulk proton component having a T_2 = 163−205 ms was present in both milk and milk protein mixtures and that caseinate concentration explained most of the variation in relaxation time T_2. This finding was a confirmation of previously observed variations in T_2 due to casein concentration (*23*). It has also been shown that addition of lactose and whey protein slightly decreased the relaxation time T_2 of milk protein mixtures (*22*). According to Le Dean et al. (*22*) and Davenel et al. (*23*), the bulk proton component ($T_{2,1}$ = 180.7 ms, **Table 1**) found in the present study could correspond to water protons strongly associated with casein. During gel formation and prior to cutting, the bulk water protons represented by $T_{2,1}$ make up ∼99% of the water protons (**Figure 2**). **Figure 3** shows the development in $T_{2,1}$ before cutting for all 20 experiments in the factorial design. The effect of pH on $T_{2,1}$ is that a reduction in pH from 6.5 to 6.3 slightly increases $T_{2,1}$ (**Figure 3**). Assuming that $T_{2,1}$ represents a proton fraction strongly associated with casein, an increase in $T_{2,1}$ can be interpreted as an enrichment of water to the protein hydration layer. This effect of pH is consistent with the previous NMR findings (*22*, *24*), but in contrast with other studies concluding that lowering the pH reduces hydration of casein micelles (*25*, *26*). In the present study the effect of temperature on $T_{2,1}$ during gel formation is small but significant. $T_{2,1}$ in gels formed at 32 °C (**Figure 3**, open symbols) is lower than $T_{2,1}$ in gels formed at 35 °C (**Figure 3**, solid symbols). T_2 of protons is in general sensitive to temperature due to differences in molecular diffusion and the Boltzmann distribution of protons, which could explain the $T_{2,1}$ variation due to temperature.

Close inspection of $T_{2,1}$ development (**Figure 3**) shows a small trend over the experiments. The trend in the majority of the 20 experimental runs is that $T_{2,1}$ initially decreases and then increases in a V-like shape. This shape development could be some sort of NMR artifact or coincidental. Further studies should be done to validate the V-like shape. Assuming it is a real sample phenomenon, it could be interesting to determine if it is related to proteolysis of κ-casein and aggregation steps taking place during coagulation.

Changes in T_2 and Population Size during Syneresis. The most noticeable trend during syneresis is the rise of a new population of slowly relaxing water protons just after cutting, which is clearly the whey phase. Moreover, we observe that the average $T_{2,3}$ of the water protons in the whey grew asymptotically toward a near steady state, showing that the whey water is being progressively diluted until a certain limit. That the initial water leaving the gel has a lower $T_{2,3}$ than the water leaving later (**Figure 2**, upper row) suggests that the initial water contains more substances (i.e., whey, lactose, and minerals) that restrict relaxation. The population size of the whey water protons increase simultaneously (**Figure 2**, lower row), also toward an expected steady state, which is, however, not reached in the time span of the experiment.

During syneresis the bulk proton population characterized by $T_{2,1}$ steadily decreases to a level of ∼50−70% of the water protons after 100 min. If we assume this proton population is primarily associated with casein micelles as previously suggested (*22*), then the decrease in population size initiated by cutting suggests that the casein micelles are being steadily dehydrated. The simultaneous increase in proton populations characterized by $T_{2,2}$ and $T_{2,3}$ (primarily $T_{2,3}$, the whey) indicates that during syneresis the protons are transferred from the population characterized by $T_{2,1}$ to the populations characterized by $T_{2,2}$ and $T_{2,3}$. A steady decrease is also observed in $T_{2,1}$ during syneresis (**Figure 2**), which presumably is related to the up-concentration of solutes in the gel after expulsion of whey. A more concentrated solution of, for example, lactose and minerals in this water population would generally cause the water protons to relax more quickly. Another possible explanation for the steady decrease in $T_{2,1}$ during syneresis is that the simultaneous loss of water from the gel means that protons have less space for self-diffusion, which in turn will affect relaxation time.

Experimental Repeatability. To investigate the reproducibility of the cheese-making process as well as the data analytical approach, examples of repeated run are superimposed in **Figure 4**. The process in **Figure 4A** shows excellent repeatability, but the process in **Figure 4B** displays reduced repeatability. Especially the syneresis process is sensitive, as evidenced by **Figure 4B** showing the development in relative population sizes, where one of the gels exhibits faster syneresis. Because pH, temperature, and gel firmness are controlled by the design, a possible source for the reduced repeatability could lie in differences in the action of cutting. Indeed, Mateo et al. (*27*) studied the effect of cutting intensity on syneresis and found that gel moisture significantly depends on cutting intensity. It is thus possible that the not fully standardized, manual cutting intensity used in the present study may explain (modest) duplicate differences in syneresis rates.

Effect of Temperature, pH, and Gel Firmness at Cutting on Syneresis Rate. The relative population sizes determined during modeling quantitatively show how much water (protons) with different T_2 values is present at a given time during syneresis. The primary development can be summarized as follows: fast-relaxing water ($T_{2,1}$ ∼ 180 ms) within the gel is mainly converted to slow-relaxing water ($T_{2,3}$ ∼ 2000−2200 ms) situated outside the gel. A small fraction of the fast-relaxing water protons is seemingly converted into water present within the gel with an intermediate relaxation rate ($T_{2,2}$ ∼ 400−500 ms). The rate by

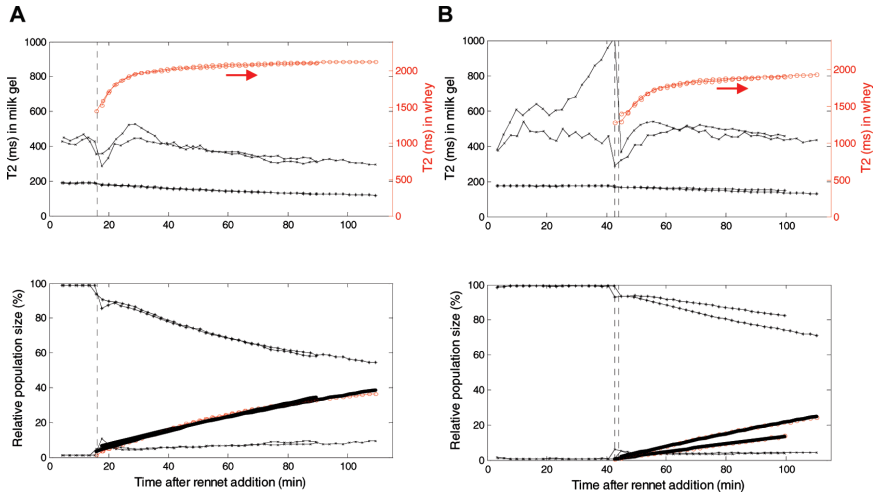

Figure 4. Development in two duplicated experiments of $T_{2,1}$, $T_{2,2}$, and $T_{2,3}$ (upper row) and the corresponding relative population sizes f_1, f_2, and f_3 (lower row): (**A**) duplicates at pH 6.3, 35 °C, and low firmness at cut; (**B**) duplicates at pH 6.5, 32 °C, and low firmness at cut. Broken lines show when the gel was cut. The thick lines are trend lines based on first-order reaction rate constants calculated from natural logarithmic transformed population size values.

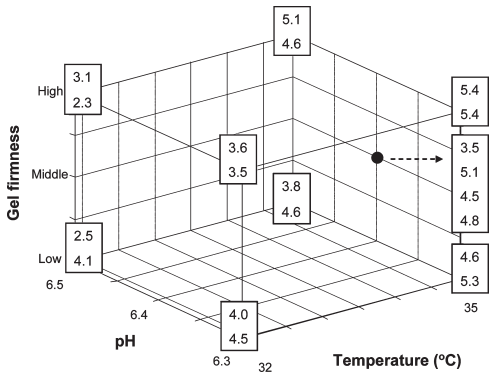

Figure 5. 2^3 factorial design with partial centerpoint used in the present milk coagulation and syneresis study. In the squares are given the first-order reaction rate constants k ($\times$ 10^{-3}) of whey syneresis estimated using LF-NMR. k is given for all design combinations and replicates.

Table 2. Analysis of Variance: Effects Temperature, pH and Gel Firmness at Cutting on the First-Order Water Proton Syneresis Rates k during Milk Gel Syneresis

	k ($\times$ 10^{-3})	
	P value	av
temperature (°C)		
32	< 0.001	3.4 (0.5)[a]
35		4.8 (0.3)
pH		
6.3	0.036	4.4 (0.3)
6.5		3.8 (0.5)
gel firmness at cutting		
low	0.65	4.2 (0.5)
high		4.0 (0.3)

[a] Parentheses show standard deviation.

which the water leaves a cut milk gel (i.e., syneresis) can be described as a reaction of first order, meaning that the rate of water expulsion is dependent on the concentration of water present at a given time (*2*). The evolution in population size of the whey water in **Figure 4** indicates first-order reaction behavior, seen as an initial rapid increase that asymptotically flattens out. The model of a first-order reaction was fitted to the evolution in population size of the whey water, and a nice fit with small randomly distributed residuals confirmed that whey water expulsion in the present study followed first-order reaction kinetics.

Figure 5 shows the first-order reaction rate constant k from eqs 2 and 3 for how water is arriving to the (water) proton population, making up the whey water for all 20 gel formation and syneresis experiments inside the factorial design. **Table 2** shows the corresponding results from an analysis of variance (ANOVA) evaluation on whether or not the first-order reaction rate constant k significantly depends on the design factors temperature, pH, and/or gel firmness at cutting.

A noticeable trend is that k is higher at pH 6.3 than at pH 6.5, which is consistent with previous findings showing that lowering the pH increases the rate of syneresis (*6*, *7*). Another trend is that k is highly temperature dependent; thus, the rate of syneresis accelerates as temperature increases, which is known from previous studies as well (*2*, *8*).

No significant dependence of the syneresis rate constants on gel firmness at cutting was found within the experimental design (**Figure 5**; **Table 2**), which is consistent with previous findings (*28*, *29*). This result presents a paradox because one could expect that a firmer gel with high endogenous pressure should expel whey more quickly than a less firm gel. Within the experimental design the temperature showed a major influence on the syneresis rate constant and is thus of great importance for process control.

To summarize, LF-NMR was used to characterize skim milk gel formation and syneresis qualitatively and quantitatively. A new automated algorithm based on Doubleslicing proved to be precise in finding the appropriate number of underlying exponential components (i.e., proton populations) in single relaxation curves measured during gel formation and syneresis. All 20 batches showed the same tendency that two underlying components of water protons were present during gel formation,

whereas the syneresis initiated by cutting produced an extra proton population with slow relaxation, identified as whey water. Quantitatively, we demonstrated that LF-NMR could monitor the relative amount of water present in each of the populations by the signal magnitude. In this way the first-order syneresis rates of whey being separated from the gel was derived. ANOVA showed that the syneresis rate constant is dependent on pH in the range from 6.3 to 6.5 and on temperature in the range from 32 to 35 °C; gel firmness at cutting did not show any significant effect on syneresis rate. The present approach enables the quantification of macrosyneresis on a rational basis and could be useful in, among other things, studying the relationship between the kinetics of rennet coagulation and syneresis.

Supporting Information Available: NMR data analysis by Doubleslicing, solution diagnostics, exemplification of solution diagnostics, and comparison with discrete exponential fitting. This material is available free of charge via the Internet at http://pubs.acs.org.

LITERATURE CITED

(1) Gunasekaran, S.; Ak, M. M. *Cheese Rheology and Texture*; CRC Press: Boca Raton, FL, 2003.

(2) Fox, P. F.; McSweeney, P. L. H. *Dairy Chemistry and Biochemistry*; Kluwer Academic/Plenum Publishers: New York, 1998.

(3) Ozilgen, M.; Kauten, R. J. NMR analysis and modeling of shrinkage and whey expulsion in rennet curd. *Process Biochem.* **1994**, 373–379.

(4) Payne, F. A.; Hicks, C. L.; Madangopal, S.; Shearer, S. A. Fiber optic sensor for predicting the cutting time of coagulating milk for cheese production. *Trans. ASAE* **1993**, 841–847.

(5) Johnson, M. E.; Chen, C. M.; Jaeggi, J. J. Effect of rennet coagulation time on composition, yield, and quality of reduced-fat cheddar cheese. *J. Dairy Sci.* **2001**, 1027–1033.

(6) Daviau, C.; Famelart, M. H.; Pierre, A.; Goudedranche, H.; Maubois, J. L. Rennet coagulation of skim milk and curd drainage: effect of pH, casein concentration, ionic strength and heat treatment. *Lait* **2000**, 397–415.

(7) Everard, C. D.; O'Callaghan, D. J.; Mateo, M. J.; O'Donnell, C. P.; Castillo, M.; Payne, F. A. Effects of cutting intensity and stirring speed on syneresis and curd losses during cheese manufacture. *J. Dairy Sci.* **2008**, 2575–2582.

(8) Fagan, C. C.; Castillo, M.; Payne, F. A.; O'Donnell, C. P.; O'Callaghan, D. J. Effect of cutting time, temperature, and calcium on curd moisture, whey fat losses, and curd yield by response surface methodology. *J. Dairy Sci.* **2007**, 4499–4512.

(9) Grundelius, A. U.; Lodaite, K.; Ostergren, K.; Paulsson, M.; Dejmek, P. Syneresis of submerged single curd grains and curd rheology. *Int. Dairy J.* **2000**, 489–496.

(10) Bueler, T.; Jakob, E.; Puhan, Z. Method for determining the syneresis of rennet coagulum. *Milchwissenschaft* **1997**, 131–134.

(11) Pearse, M. J.; Mackinlay, A. G. Biochemical aspects of syneresis − a review. *J. Dairy Sci.* **1989**, 1401–1407.

(12) Micklander, E.; Thygesen, L. G.; Pedersen, H. T.; Berg, F. v. d.; Bro, R.; Rutledge, D. N.; Engelsen, S. B. Multivariate analysis of time domain NMR signals in relation to food quality. In *Magnetic Resonance in Food Science: Latest Developments*; Belton, P. S., Gil, A. M., Webb, G. A., Rutledge, D., Eds.; Royal Society of Chemistry: Colchester, U.K., 2003; pp 239−254.

(13) Hills, B. P.; Takacs, S. F.; Belton, P. S. A new interpretation of proton NMR relaxation time measurements of water in food. *Food Chem.* **1990**, 95–111.

(14) Hinrichs, R.; Bulca, S.; Kulozik, U. Water mobility during renneting and acid coagulation of casein solutions: a differentiated low-resolution nuclear magnetic resonance analysis. *Int. J. Dairy Techol.* **2007**, 37–43.

(15) Lelievre, J.; Creamer, L. K. NMR-study of formation and syneresis of renneted milk gels. *Milchwissenschaft* **1978**, 73–76.

(16) Mariette, F.; Maignan, P.; Marchal, P. NMR relaxometry: a sensor for monitoring acidification of milk. *Analusis* **1997**, M24–M27.

(17) Tellier, C.; Mariette, F.; Guillement, J. P.; Marchal, P. Evolution of water proton nuclear magnetic-relaxation during milk coagulation and syneresis − structural implications. *J. Agric. Food Chem.* **1993**, 2259–2266.

(18) Andrade, L.; Micklander, E.; Farhat, I.; Bro, R.; Engelsen, S. B. Doubleslicing: a non-iterative single profile multi-exponential curve resolution procedure − application to time-domain NMR transverse relaxation data. *J. Magn. Reson.* **2007**, 286–292.

(19) Ranby, M.; Ramstrom, S.; Svensson, P. O.; Lindahl, T. L. Clotting time by free oscillation rheometry and visual inspection and a viscoelastic description of the clotting phenomenon. *Scand. J. Clin. Lab. Invest.* **2003**, 397–406.

(20) Bro, R. PARAFAC. Tutorial and applications. *Chemom. Intell. Lab. Syst.* **1997**, 149–171.

(21) Connors, K. A. *Chemical Kinetics − The Study of Reaction Rates in Solution*; VHC: New York, 1990.

(22) Le Dean, A.; Mariette, F.; Marin, M. ^{1}H nuclear magnetic resonance relaxometry study of water state in milk protein mixtures. *J. Agric. Food Chem.* **2004**, 5449–5455.

(23) Davenel, A.; Schuck, P.; Marchal, P. A NMR relaxometry method for determining the reconstitutability and the water-holding capacity of protein-rich milk powders. *Milchwissenschaft* **1997**, 35–39.

(24) Mariette, F.; Tellier, C.; Brule, G.; Marchal, P. Multinuclear NMR-study of the pH dependent water state in skim milk and caseinate solutions. *J. Dairy Res.* **1993**, 175–188.

(25) Snoeren, T. H. M.; Klok, H. J.; Vanhooydonk, A. C. M.; Damman, A. J. The voluminosity of casein micelles. *Milchwissenschaft* **1984**, 461–463.

(26) Dalgleish, D. G.; Law, A. J. R. pH-induced dissociation of bovine casein micelles. 2. Mineral solubilization and its relation to casein release. *J. Dairy Res.* **1989**, 727–735.

(27) Mateo, M. J.; O'Callaghan, D. J.; Everard, C. D.; Fagan, C. C.; Castillo, M.; Payne, F. A.; O'Donnell, C. P. Influence of curd cutting programme and stirring speed on the prediction of syneresis indices in cheese-making using NIR light backscatter. *Lebensm. Wiss. Technol.* **2009**, 950–955.

(28) Pearse, M. J.; Mackinlay, A. G.; Hall, R. J.; Linklater, P. M. A microassay for the syneresis of cheese curd. *J. Dairy Res.* **1984**, 131–139.

(29) Storry, J. E.; Ford, G. D. Development of coagulum firmness in renneted milk − a 2-phase process. *J. Dairy Res.* **1982**, 343–346.

Received for review July 1, 2009. Revised manuscript received October 27, 2009. Accepted October 31, 2009. We thank the Danish Dairy Foundation (MFF) for generous financial support of this work, which is part of the research projects "PAT in the Dairy Industry" and "Syneresis in Rennet Gels − Understanding and Quantification".

Paper II

Detecting variation in ultrafiltrated milk permeates – Infrared spectroscopy signatures and external factor orthogonalization

Reprint from Chemometrics and Intelligent Laboratory Systems, *In Press*

Chemometrics and Intelligent Laboratory Systems xxx (2010) xxx–xxx

Contents lists available at ScienceDirect

Chemometrics and Intelligent Laboratory Systems

journal homepage: www.elsevier.com/locate/chemolab

Detecting variation in ultrafiltrated milk permeates — Infrared spectroscopy signatures and external factor orthogonalization

Christian Lyndgaard Hansen [a,*], Frans van den Berg [a], Morten Arendt Rasmussen [a], Søren Balling Engelsen [a], Steve Holroyd [b]

[a] University of Copenhagen, Faculty of Life Sciences, Department of Food Science, Quality and Technology Group, Rolighedsvej 30, 1958 Frederiksberg, Denmark
[b] Fonterra Research Center, Private Bag 11029, Palmerston North, New Zealand

ARTICLE INFO

Article history:
Received 5 January 2010
Received in revised form 22 August 2010
Accepted 31 August 2010
Available online xxxx

Keywords:
Orthogonalization
Extended canonical variate analysis
Infrared spectroscopy
Ultrafiltration
Milk

ABSTRACT

Ultrafiltration (UF) of milk in the dairy industry generates significant quantities of UF permeate as a by-product. In the past decade UF permeate has been utilized as a mixing ingredient in the standardization of milk. Due to the role of permeate as an ingredient, it is important that the variation in composition is known and controlled in order to ensure uniform quality of the standardized milk. In this investigation we evaluate if the composition of permeate from the ultrafiltration of milk varies between different ultrafiltration plants as assessed by infrared spectroscopy. A total of 40 permeate samples from six production sites at different geographical locations were analyzed by infrared spectroscopy. Principal component analysis of the infrared spectra showed that it was possible to classify the plant manufacturer of permeates with great accuracy. Loading spectra revealed that total solids (mainly lactose) and protein were the main sources of compositional variation between the different sites. Through an orthogonalization procedure of the infrared spectra the spectral variation due to total solid and protein content was removed. Neither the unsupervised principal component analysis nor the supervised extended canonical variate analysis could classify the permeate plant origin after orthogonalization of the infrared spectra. The result shows that, besides total solids and protein variation, permeate from the six ultrafiltration sources does not contain plant specific composition in their infrared signature. The study demonstrates how multiple external factors can be removed from the spectral data by orthogonalization.

1. Introduction

The process of concentrating the fat and protein content in milk through ultrafiltration (UF) generates significant amounts of milk UF permeate in the dairy industry [1]. Milk permeate is composed of water and low molecular weight solutes from milk: minerals, vitamins, whey proteins and lactose. Lactose constitutes the majority of the total solids in milk permeate. The enormous volumes of milk permeate produced in the dairy industry have gone from being a major waste problem to being utilized in different ways to add value to the industry. Permeate is utilized as animal feed, fertilizer spread over land and in the production of lactose powder. However, since Codex Alimentarius Commission in 1999 approved standardization of the protein content of milk, an important utilization of permeate has been as a mixing ingredient in the protein standardization of milk [1,2]. Several scientific studies on milk permeate have focused on the effect of mixing permeate with milk on the technological and sensory properties of the out coming milk and milk products [3–5]. Collectively these findings emphasize that milk permeate used as an ingredient in standardized milk can have an impact on the quality of the final products.

The focus of the present study is to characterize the milk permeate itself and demonstrate how it varies in a real production environment. Since permeate has been shown to have an effect on technological and sensory properties of milk [3–5], there is a reason to believe that variation in permeate due to process variation will affect the final product quality. The incentive for investigating permeate variation is that an increased knowledge about "raw material variation" can be used to reduce end-product variation. Permeate can vary due to "normal" changes in raw milk composition as well as variation due to the UF process itself. *Uncontrolled* "disturbances" such as leaks due to worn membranes or *controlled process factors* such as membrane pore size, flow pressure, pH regulation and the simultaneous use of reverse osmosis (RO) for water removal all have the potential to impact permeate variation.

Infrared (IR) spectroscopy is a powerful analytical tool used in routine laboratory analysis in the dairy industry. IR spectra contain multiple absorbance bands from molecular vibrations where many of the bands are overlapping. As a consequence multivariate data analysis is frequently used for analyzing the spectra. Principal component analysis (PCA) is one of the most often used methods for finding the main features in IR spectra [6]. One general property of PCA is that each of the principal components represents orthogonal (uncorrelated) variations in the data.

Abbreviations: ECVA, extended canonical variate analysis; EPO-PLS, external parameter orthogonalization PLS; RO, reverse osmosis; TS, total solids; UF, ultrafiltration.

* Corresponding author. Tel.: +45 35 33 25 65; fax: +45 35 33 32 45.
E-mail address: chha@life.ku.dk (C.L. Hansen).

0169-7439/$ – see front matter © 2010 Elsevier B.V. All rights reserved.
doi:10.1016/j.chemolab.2010.08.014

Pre-treatment of IR spectra can be used to remove various effects from the measurements that subsequently enhance the use of the model. One group of pre-treatment methods is orthogonalization. Orthogonalization of a matrix can be performed in the *row space* by a vector or a matrix with individual sample information (design matrix, continuous variable, etc.) with length equal to number of samples or in the *column space* by a vector or a matrix with the signature of a feature with length equal to number of variables. Orthogonal signal correct (OSC) [7] is an example of row space orthogonalization. Here the so-called OSC components are effects orthogonal to the response y, which are removed from the data, and hence do not depend on an external feature, but a direction in the null space of y. External parameter orthogonalization PLS (EPO-PLS) as presented by Roger et al. [8] provides an example of a method that involves column space orthogonalization. In EPO-PLS the effect or signature, of an external factor (e.g. temperature) is estimated on a data set consisting spectra (or other measurements) of n samples each measured at k levels of the external factor. Subsequently an *influence matrix* D is defined as the mean spectra of samples at each factor level ($k \times p$). D is also mean-centered according to the mean of mean spectra. Subsequent PCA on D provides a loading matrix G, which can be used to correct new spectra for external factor effects by column space orthogonalization: $x_{newcorr} = x_{new}(I - GG')$. Both pre-treatment methods attempt to remove unwanted disturbing effects in order to improve calibration performance. In the present study, we use row space orthogonalization in another way, to remove multiple effects from data and analyze the residual information to investigate how it affects classification performance. In this way it is a variant of backward feature elimination.

In this paper we present a case study in which six dairy plants transfer their UF permeate to one site for further processing. The dairy plant receiving permeate uses it to mix in with standardized milk and timely knowledge of the variation in the imported permeate is therefore essential. The main expected effects of process variations between UF plants are differences in the protein composition and in the total solid concentration. The objective of this study is to investigate the plant-to-plant variation in UF permeate from the six locations. To pursue this objectives the permeate samples were analyzed by Fourier transform infrared spectroscopy (FT-IR) used as site or permeate "signature". The FT-IR spectra were analyzed by multivariate data analysis. In order to investigate if other factors than protein and total solid content are causing significant plant-to-plant variation in the FT-IR signature, these two factors are mathematically removed from the spectra through orthogonalization.

2. Material and methods

2.1. Experimentals

Forty ultrafiltration (UF) milk permeate samples of 100 mL were collected over a two week period from a milk powder producing dairy plant in New Zealand. The samples were taken from trucks arriving from five different dairy plants utilizing UF, and one dairy plant utilizing UF and reverse osmosis in combination. Each sample was analyzed in duplicate using a Foss MilkoScan FT2 (Hillerød, Denmark) which takes up 15 mL sample for a single measurement. Absorbance spectra were acquired in the range 5009–925 cm^{-1} in transmission mode over a path length of 50 μm. The total solid content in the samples was determined via a build-in calibration made for analyzing UF permeate. For reference analyses 1 mL of each permeate sample was centrifuged at 13,000 rpm for 5 min. The supernatant was analyzed for protein content by reverse phase high performance liquid chromatography (RP-HPLC) according to the method described by Elgar et al. [9].

2.2. Data analysis

Overall the IR spectra of milk permeates contained three sources of known variation: total solids and proteins (continuous) and production site (qualitative). The spectra were evaluated using unsupervised grouping by PCA and supervised grouping by extended canonical variate analysis (ECVA); all multivariate models were made on mean-centered or auto-scaled data using the spectral region from 1800 to 925 cm^{-1}. Autoscaling of spectral data is uncommon, because it up-weights regions of low variance. We applied it because the protein variance in the sample set is low, but might explain production site variation. External factors protein and total solid were removed from the IR spectra by orthogonalization.

2.2.1. PCA

PCA decomposes a data matrix **X** into a few significant bilinear components, in terms of the outer product of two sets of vectors: scores in the sample direction (plants/sites in this study) and loadings in the variable direction (wavenumbers in this study). These components capture the essential information in **X**, and are called principal components (PC). One problem when using PCA is that the components calculated describe the direction of major variance which might not be relevant for discrimination between different groups of samples [6].

2.2.2. ECVA

ECVA is a supervised method for the estimation of directions in space that maximizes the differences between the groups and at the same time minimizes the differences within the known groups. ECVA is an extension of the standard canonical variate analysis which uses partial least square regression in order to be able to deal with highly collinear data such as spectroscopic signals [10].

2.2.3. Orthogonalization

In order to examine if other factors than protein and total solid content are causing significant plant-to-plant variation in the FT-IR spectra, these two factors were removed one after another from the spectra through orthogonalization. The essential principles of orthogonalization are described below, while a detailed mathematical treatment can be found in Appendix A. Orthogonalization is the process of removing information from a data matrix **X** linearly related to an external factor

$$\mathbf{X}_o = \left(\mathbf{I} - \mathbf{v}\left(\mathbf{v}^T\mathbf{v}\right)^{-1}\mathbf{v}^T\right)\mathbf{X} \tag{1}$$

where $\mathbf{X}_o$ is the data orthogonalized towards the external vector **v**; **X** is the data matrix and **I** is the identity matrix. Orthogonalization of a data set can be used for focusing subsequent data analysis on that variation in data not related to the external factor (**v**). In the case of several *independent* external factors ($\mathbf{v}_1, \mathbf{v}_2 \ldots \mathbf{v}_k$; $\mathbf{v}_i \cdot \mathbf{v}_j = 0$ for all combinations of $i \neq j$) data can be corrected for one factor and analyzed with respect to the other. In e.g. observational data or if outliers are removed the external factors may become dependent i.e. correlated ($\mathbf{v}_i \cdot \mathbf{v}_j \neq 0$ for combinations of $i \neq j$). In this case orthogonalization with one external factor i will result in removal of information related to another external factor j. In order to only remove information related to one factor and retain the full degree of information related to another factor, the data is only orthogonalized with that part of factor i which is orthogonal to factor j. This can be exemplified through Eq. (2), where factor one ($\mathbf{v}_i$) is the external vector we wish to remove which is orthogonalized towards factor two ($\mathbf{v}_j$), which we wish to retain. Then $\mathbf{v}_{ioj}$ is used for orthogonalization of **X** as described in Eq. (1), substituting **v** by $\mathbf{v}_{ioj}$

$$\mathbf{v}_{ioj} = \left(\mathbf{I} - \mathbf{v}_j\left(\mathbf{v}_j^T\mathbf{v}_j\right)^{-1}\mathbf{v}_j^T\right)\mathbf{v}_i. \tag{2}$$

Please cite this article as: C.L. Hansen, et al., Detecting variation in ultrafiltrated milk permeates — Infrared spectroscopy signatures and external factor orthogonalization, Chemometr. Intell. Lab. Syst. (2010), doi:10.1016/j.chemolab.2010.08.014

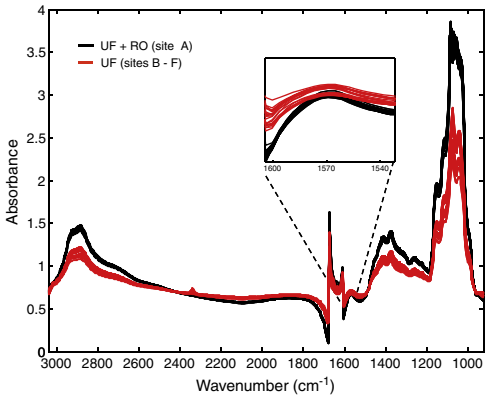

Fig. 1. An infrared spectrum of ultrafiltrated (UF) milk permeates from six different plants (site A–F). Permeate from plant A (dark spectra) has also been subjected to reverse osmosis (RO) which concentrates the total solids; zoom-in shows absorbance band from the amide II (protein) vibrations. Note: only 1800–925 cm^{-1} is used in PCA/ECVA. (For interpretation of the references to color in this figure legend, the reader is referred to the web version of this article.)

In the remainder of this paper we will refer to the two orthogonalization approaches as *orthogonalization* in the case the external factor is uncorrected and *compensated orthogonalization* in the case where the external factor is corrected, prior to orthogonalization of **X**.

2.3. Software

All multivariate data analysis was carried out using Matlab version 7.6 (MathWorks Inc. Natick, MA, USA). PCA was performed using the PLS toolbox (Eigenvector Research, WA, USA). ECVA and orthogonalization were done using in-house scripts freely available at www.models.kvl.dk.

3. Results and discussion

Fig. 1 shows the spectra of 40 permeate samples that are shown colored according to treatment (UF or UF plus reverse osmosis, RO). The red spectra are especially different from the remaining spectra in the range 1480–950 cm^{-1}. The main part of this spectrum is the so-called fingerprint region (1400–900 cm^{-1}), where complex molecular vibrations rather than group vibrations absorb the infrared radiation. For that reason absorbance in the fingerprint region is by approximation proportional to the sum of solutes in the sample. The black spectra are the permeate samples which come from UF of milk followed by RO of the UF permeate. Because RO only removes water, the UF permeates are up-concentrated. For that reason the black spectra show an increase absorbance in the fingerprint region. If fat is present in the sample it will cause a major absorbance from the strong carbonyl stretching vibrations at 1745 cm^{-1}. The absence of a peak at this position in the FT-IR permeate spectra (Fig. 1) validates that the UF membranes at all sites have withheld fat well. Protein presence in a sample is seen as absorbance bands at 1640 cm^{-1} (amid I vibrations) and 1550 cm^{-1} (amid II vibrations). The weak band at 1550 cm^{-1} (Fig. 1) shows the presence of proteins in small concentrations. The amide I band is hidden under the strong OH bending vibrations at 1640 cm^{-1} from water, which absorb so heavily that no light is passing the transmission cell. The strong absorbance in the fingerprint region and CH vibrations seen from 2700 to 3000 cm^{-1} confirm the presence of carbohydrates. Since permeate is nearly fat free, these CH vibrations can almost only come from carbohydrates primarily lactose.

Further scrutinizing of the spectra (Fig. 1) shows that permeates from UF plants B–F (red spectra) have the highest absorbance in the amide II mode, suggesting that these sites let more of the protein sieve to the permeate. Overall, the spectra suggest that FT-IR is able to fingerprint the manufacturer of permeate samples. Fig. 2 shows a PCA score- and loading-plot of the 40 FT-IR spectra of UF milk permeates. From the score-plot (Fig. 2a) it is observed that the permeate samples are clustered according to the individual site where it was produced. The samples from plant A are particularly separated in the score-plot. The loading-plot of PC1 (Fig. 2b) shows that the fingerprint region is the main contributor, which suggests that PC1 primarily describes variation in total solids between the samples; in permeate the vast majority of solids is lactose. The loading of PC1 is surprisingly flat in the fingerprint region. This flat shape of the loading is explainable because the PCA is performed on auto-scaled data, and in the fingerprint region the spectra have almost the same relative absorbance. The zoom-in of the region reveals that the loading is not completely flat. In the loading-plot of PC2 (Fig. 2b) a large peak can be observed in the region 1580–1530 cm^{-1}. This infrared region can be assigned to protein content through amide II vibrations. Collectively, PCA shows that protein and total

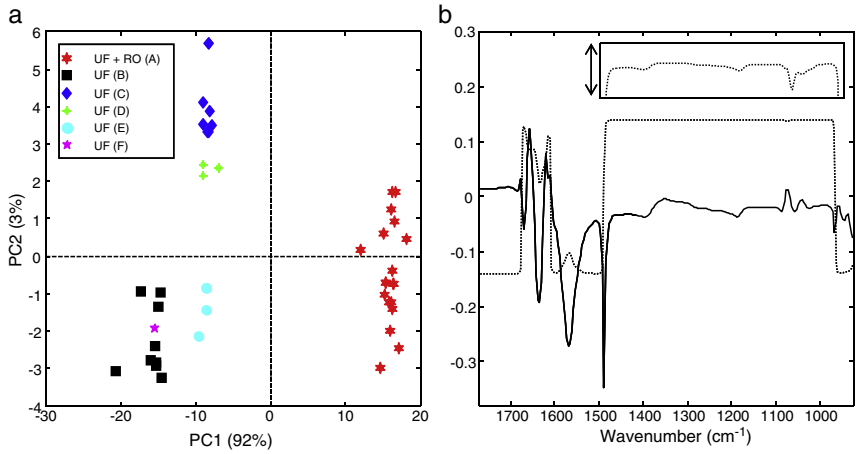

Fig. 2. Principal component analysis of auto-scaled infra spectra of ultrafiltrated milk permeates: (a) score-plot PC1 versus PC2 and (b) loading spectra PC1 (broken line) and PC2 (solid line).

Please cite this article as: C.L. Hansen, et al., Detecting variation in ultrafiltrated milk permeates — Infrared spectroscopy signatures and external factor orthogonalization, Chemometr. Intell. Lab. Syst. (2010), doi:10.1016/j.chemolab.2010.08.014

solid content explains the main part of the variation (~95%) and the concentration of these constituents are highly plant dependent. One could speculate that other factors could influence the variation in permeate originating from different sites e.g. process pH or storage time of permeate. In the following section we will investigate if other factors than protein and total solids (TS) affect the differences in the permeate composition, which is present between the six factories, as seen from the FT-IR signatures. The approach for this investigation is to successively remove variation from the FT-IR spectra caused by protein and TS through *compensated orthogonalization*. Subsequently PCA and ECVA of spectra orthogonalized towards protein and TS will show whether the permeate samples still cluster according to the plant of origin.

The total solid and protein content of the permeate samples as determined by reference methods proved to be somewhat correlated ($R^2 = 0.39$) i.e. conventional *orthogonalization* of the spectra to one of the factors will thus also remove information related to the other factor. Using *compensated orthogonalization* of the spectra against one factor will only remove the information related to this factor and retain the variation caused by other external factors. Fig. 3a shows the PCA score-plot of spectra after *orthogonalization* against TS, while Fig. 3b shows the PCA score-plot of spectra after *compensated orthogonalization* against TS retaining variation due to protein. It is observed that the samples in the score-plot of *orthogonalization* (Fig. 3a) to some degree are grouped according to protein content, but the score-plot of the *compensated orthogonalization* (Fig. 3b) shows a much more systematic pattern according to protein content along PC1. To further investigate this observation the protein concentration is plotted against PC1 scores after *orthogonalization* (Fig. 3c) and *compensated orthogonalization* (Fig. 3d). The low correlation observed in Fig. 3c shows that relevant information about protein content in the spectra has been removed, while the protein information is kept by the *compensated orthogonalization* approach (Fig. 3d). This is worth noting because *compensated orthogonalization* only removes information in the TS variation that is not correlated to protein variation, the corrected spectra will still contain the TS variation which is correlated to protein variation. Fig. 4 shows the effect of *orthogonalization* on the raw spectra (Fig. 4a and b) in the protein band

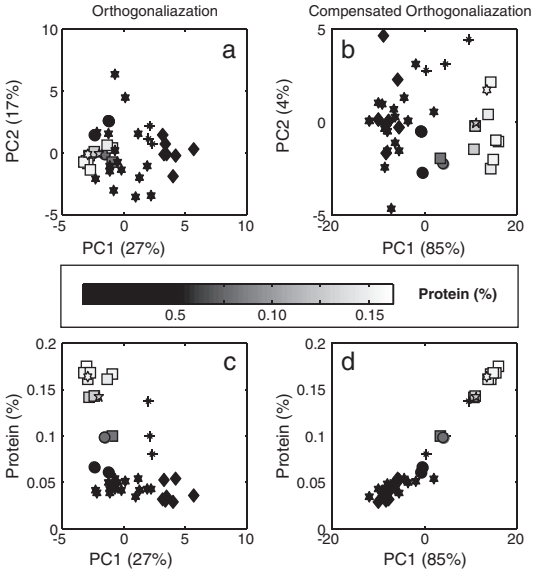

Fig. 3. Effect of (a, c) *orthogonalization* and (b, d) *compensated orthogonalization* of FT-IR spectra towards the total solid content; (a, b) PCA score-plots after orthogonalization, and (c, d) protein content versus PC1 score values; symbols: see Fig. 2.

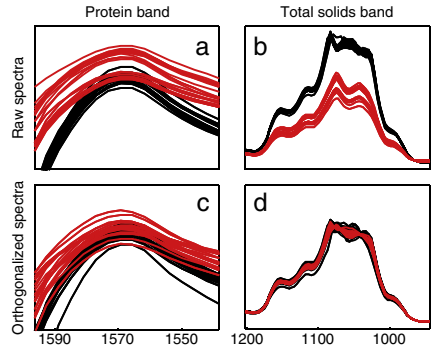

Fig. 4. The effect of orthogonalization on FT-IR spectra of permeate from ultrafiltration of milk. Raw spectra in the (a) protein and (b) total solid bands and spectra *orthogonalized* towards (c) protein content and (d) total solids.

(Fig. 4c) and the total solid band (Fig. 4d). It is observed that the variation between spectra is reduced by orthogonalization especially for the total solid band, where the variation is large in the raw spectra. Fig. 5 shows a PCA score-plot (PC1 versus PC2) of *compensated orthogonalized* spectra against both TS and protein. When TS and protein variation is removed from the spectra, no obvious clustering of the permeate samples according to production site is observed. The lack of clustering suggests that permeate from different plants only differs with respect to TS and protein and not any other characteristics as recorded by the FT-IR signature.

In order to verify whether the permeate spectra contain other plant specific characteristics, the supervised classification method extended canonical variate analysis (ECVA) is applied on the *compensated orthogonalized* spectra. Fig. 6 shows an ECVA scatterplot (ECV1 versus ECV2) of raw spectra (Fig. 6a) and corrected spectra (Fig. 6b). No sensible clustering according to plant can be observed in the *compensated orthogonalized* spectra, again suggesting that permeate samples only differ in total solid and protein content.

4. Conclusion

In this case study we have mapped the variation in permeate composition from six different ultrafiltration plants. We conclude that

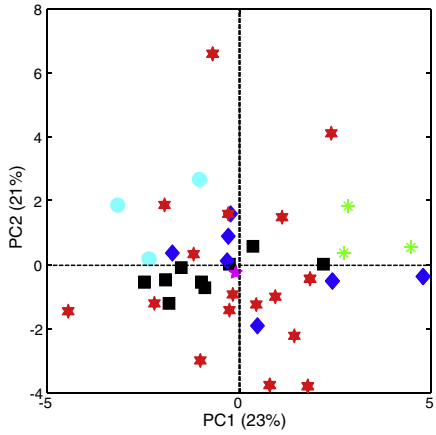

Fig. 5. Effect of orthogonalization on classification performance of PCA: score-plot after successive *compensated orthogonalization* of spectra towards protein and total solid content; symbols: see Fig. 2.

Please cite this article as: C.L. Hansen, et al., Detecting variation in ultrafiltrated milk permeates — Infrared spectroscopy signatures and external factor orthogonalization, Chemometr. Intell. Lab. Syst. (2010), doi:10.1016/j.chemolab.2010.08.014

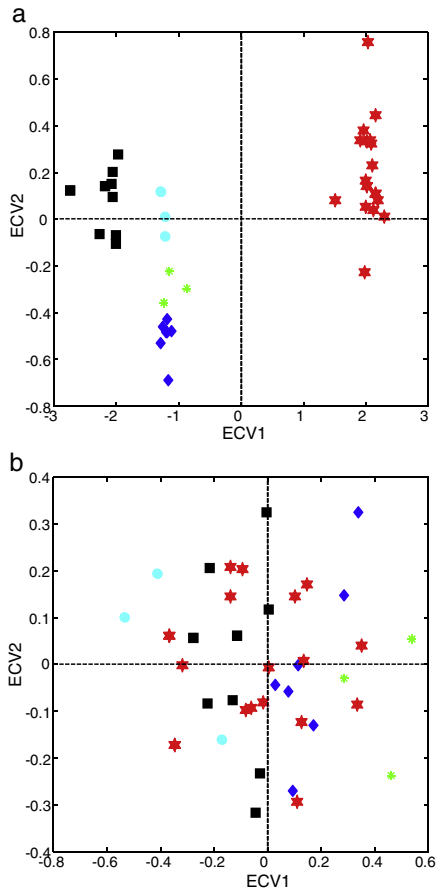

Fig. 6. Effect of orthogonalization on classification performance of ECVA: score-plot (a) before and (b) after successive *compensated orthogonalization* of spectra towards protein and total solid content; symbols: see Fig. 2. Note that factory F – pertaining to only one sample – has been removed because the ECVA algorithm cannot handle classes with less than two objects.

FT-IR analyses of permeate samples and PCA could completely distinguish which of the six UF production sites permeate originates from, and that it was the relative protein and the total solid concentrations that made the differences apparent. The study demonstrated that factors protein and total solid (determined by reference analysis) could be removed from the FT-IR spectra by orthogonalization. Subsequently, neither unsupervised PCA nor supervised ECVA of orthogonalized spectra could classify which of the six UF plants the permeate samples originated from. On this basis it can be concluded that FT-IR could find no other variation between the plants than protein and total solids and that FT-IR could be considered as near a "real-time" tool in quality assurance and process/product optimization.

Acknowledgements

CLH would like to thank the Danish Dairy Board for the financial support and the Fonterra Research Center, New Zealand, for hosting a research stay.

Appendix A

Orthogonalization is the process of removing information from a data matrix **X** linearly related to an external factor (**v**) (Eq. (A1)):

$$\mathbf{X}_o = \left(\mathbf{I} - \mathbf{v}\left(\mathbf{v}^T\mathbf{v}\right)^{-1}\mathbf{v}^T\right)\mathbf{X} \tag{A1}$$

where $\mathbf{X}_o$ is the orthogonalized data matrix and **I** is the identity matrix.

The regression vector **b** between the external factor vector **v** and **X** is found by multiple linear regression according to Eq. (A2):

$$\mathbf{v} = \mathbf{X}\mathbf{b} \Leftrightarrow \mathbf{b} = \left(\mathbf{X}^T\mathbf{X}\right)^{-1}\mathbf{X}^T\mathbf{v} \approx \mathbf{X}^+\mathbf{v} \tag{A2}$$

where $\mathbf{X}^+$ is the Moore–Penrose pseudo-inverse of **X**. In case **X** is full rank $\left(\mathbf{X}^T\mathbf{X}\right)^{-1}\mathbf{X}^T = \mathbf{X}^+$.

An estimate of **X**, **Xhat** using *b* is given by Eq. (A3):

$$\hat{\mathbf{X}} = \mathbf{v}\mathbf{b}^T\left(\mathbf{b}\mathbf{b}^T\right)^{-1} = \mathbf{v}\mathbf{b}^+. \tag{A3}$$

The orthogonalized data $\mathbf{X}_o$ is the difference (residual) between the observe and estimate data (Eq. (A4))

$$\begin{aligned}\mathbf{X}_o &= \mathbf{X} - \hat{\mathbf{X}} \\ &= \mathbf{X} - \mathbf{v}(\mathbf{X}^+\mathbf{v})^+ \\ &= \mathbf{X} - \mathbf{v}\mathbf{X}\mathbf{v}^+ \\ &= (\mathbf{I} - \mathbf{v}\mathbf{v}^+)\mathbf{X} \\ &= \left(\mathbf{I} - \mathbf{v}\left(\mathbf{v}^T\mathbf{v}\right)^{-1}\mathbf{v}^T\right)\mathbf{X}\end{aligned} \tag{A4}$$

Compensated orthogonalization is used to remove information related to one factor and retain the full degree of information related to another factor, the data is orthogonalized with that part of e.g. factor i which is orthogonal to factor j. This is shown in Eq. (A5), where factor i ($\mathbf{v}_i$) is the part which we wish to remove orthogonalized towards factor j ($\mathbf{v}_j$), which we wish to retain. Next, $\mathbf{v}_{ioj}$ is used for orthogonalization of **X** as described in Eq. (A1), substituting **v**

$$\mathbf{v}_{ioj} = \left(\mathbf{I} - \mathbf{v}_j\left(\mathbf{v}_j^T\mathbf{v}_j\right)^{-1}\mathbf{v}_j^T\right)\mathbf{v}_i \tag{A5}$$

The regression vector **b** between the external factors $\mathbf{v}_i$ and $\mathbf{v}_j$ is found by Eq. (A6):

$$\mathbf{v}_i = \mathbf{v}_j\mathbf{b} \tag{A6}$$

The mathematical operations in Eqs. (A2)–(A4) are performed in the same way where $\mathbf{v}_i$ replaces **v** and $\mathbf{v}_j$ replaces **X**.

Reference

[1] R.J. Durham, J.A. Hourigan, Waste management and co-product recovery in dairy processing, in: K. Waldron (Ed.), Handbook of Waste Management and Co-product Recovery in Food Processing (Volume 1), Woodhead Publishing Limited, Cambridge, UK, 2007, pp. 332–387.
[2] W. Rattray, P. Jelen, Protein standardization of milk and dairy products, Trends Food Sci. Technol. 7 (1996) 227–234.
[3] W. Rattray, P. Jelen, Freezing point and sensory quality of skim milk as affected by addition of ultrafiltration permeates for protein standardization, Int. Dairy J. 6 (1996) 569–579.
[4] W. Rattray, P. Jelen, Thermal stability of skim milk with protein content standardized by the addition of ultrafiltration permeates, Int. Dairy J. 6 (1996) 157–170.
[5] A.K. Shrestha, T. Howes, B.P. Adhikari, B.R. Bhandari, Spray drying of skim milk mixed with milk permeate: effect on drying behavior, physicochemical properties, and storage stability of powder, Dry technol. 26 (2008) 239–247.
[6] S. Wold, K. Esbensen, P. Geladi, Principal component analysis, Chemom. Intell. Lab. Syst. 2 (1987) 37–52.
[7] S. Wold, H. Antti, F. Lindgren, J. Öhman, Orthogonal signal correction of near infrared spectra, Chemom. Intell. Lab. Syst. 44 (1998) 175–185.

Please cite this article as: C.L. Hansen, et al., Detecting variation in ultrafiltrated milk permeates — Infrared spectroscopy signatures and external factor orthogonalization, Chemometr. Intell. Lab. Syst. (2010), doi:10.1016/j.chemolab.2010.08.014

[8] J.M. Roger, F. Chauchard, V. Bellon-Maurel, EPO-PLS external parameter orthogonalisation of PLS application to temperature-independent measurement of suger content of intact fruits, Chemom. Intell. Lab. Syst. 66 (2003) 191–204.
[9] D.F. Elgar, C.S. Norris, J.S. Ayers, M. Pritchard, D.E. Otter, K.P. Palmano, Simultaneous separation and quantitation of the major bovine whey proteins including proteose peptone and caseinomacropeptide by reversed-phase high-performance liquid chromatography on polystyrene–divinylbenzene, J. Chromatogr. A 878 (2000) 183–196.
[10] L. Norgaard, R. Bro, F. Westad, S.B. Engelsen, A modification of canonical variates analysis to handle highly collinear multivariate data, J. Chemom. 20 (2006) 425–435.

Please cite this article as: C.L. Hansen, et al., Detecting variation in ultrafiltrated milk permeates — Infrared spectroscopy signatures and external factor orthogonalization, Chemometr. Intell. Lab. Syst. (2010), doi:10.1016/j.chemolab.2010.08.014

Paper III

Real-time modeling of milk coagulation

Submitted for publication in Journal of Food Engineering

Real-time modeling of milk coagulation

Christian Lyndgaard Hansen*, Søren Balling Engelsen, and Frans W.J. van den Berg

University of Copenhagen, Faculty of Life Sciences, Department of Food Science, Quality & Technology Group, Rolighedsvej 30, 1958 Frederiksberg, Denmark.

*Corresponding author. University of Copenhagen, Faculty of Life Sciences, Department of Food Science, Quality & Technology Group, Rolighedsvej 30, 1958 Frederiksberg, Denmark. Tel.: +45 35 33 25 65; fax: +45 35 33 32 45
E-mail address: chha@life.ku.dk (C. L. Hansen)

ABSTRACT

Coagulum cutting time is a critical production factor affecting cheese yield and quality. Previous studies have investigated the use of near infrared reflectance (NIR) to capture coagulation kinetics for the prediction of optimal cutting time. This paper considers aspects of modeling milk coagulation in real-time from NIR with the aim of being able to better predict optimal cutting time. NIR spectra during coagulation were compressed into a single variable (principal component) and the time profile of component scores clearly displayed kinetics of the multiple reaction phases: κ-casein proteolysis, micelle aggregation, and network formation by micelle strand cross-linking. Models for the entire time profile and models for individual phases were compared with the latter providing the best fit. The novelty of this study is the construction of an algorithmic procedure for real-time modeling during coagulation based on NIR data. The procedure involves real-time parameter estimation of individual phase models, determination of transition time between phases, and prediction forward in time, all describing kinetics of the milk coagulation process. The perspectives in using the designed produce for optimal cutting time prediction are discussed.

1. Introduction

In cheese manufacturing cutting time of the gel is a critical production factor affecting both cheese yield and quality, thus making optimization of great economic importance (Johnson *et al.*, 2001; Lucey, 2002; Payne *et al.*, 1993). If the gel is cut with too low firmness (cutting too early) the final cheese yield is reduced due to loss of gel fines to the separated whey. If the gel is cut with too high firmness (cutting too late) the subsequent syneresis is retarded which results in cheese with a high moisture content and undesirable sensory and textural properties (Johnson *et al.*, 2001; Payne *et al.*, 1993).

In this paper we consider *real-time* modeling and extrapolation of rennet induced milk coagulation as a way towards cutting time optimization in cheese production. The on-line predictor measurements are multivariate near-infrared (NIR) reflectance measurements acquired during coagulation, which are subsequently compressed into a single variable (principal component) time profile by principal component analysis (PCA; Fig. 1). The profile shown represents a typical development observed in studies of NIR reflectance during rennet induced milk coagulation (Payne *et al.*, 1993; Crofcheck *et al.*, 1999; Mertens *et al.*, 2002; Castillo *et al.*, 2003a; Fagan *et al.*, 2007). There seems to be consensus in literature that rennet induced milk coagulation is the result of three underlying stages with different mechanisms: (I) initial enzymatic proteolysis of κ-casein after which the altered casein micelles are referred to as para-casein; (II) a subsequent aggregation of para-casein, where the aggregation rate depends on the concentration of free para-casein sites, implying that this stage is dependent on rate and degree of κ-casein proteolysis; (III) gelation, formation of polymer networks where aggregated micelle strands are cross-linking, also referred to as gel firming (Storry & Ford, 1982; McMahon *et al.*, 1984; Carlson *et al.* 1987a; Castillo *et al.* 2003b). The transition between stages is not easy to detect, because *head-and-tail* of the successive stage overlap to some extend in the process.

In this paper we investigate real-time estimation of model parameters from NIR measurements during the coagulation process. We hope this approach can supplement the existing methodologies for cutting time prediction and optimization suggested in literature, with the ultimate goal of process automation.

We first present the experiments performed followed by a review of the previously suggested approaches for analyzing this type of data. We then apply models for the observed NIR time profiles and propose a real-time/on-line modeling method with continuous uncertainty estimation. It is beyond the scope of this paper to evaluate the proposed profile modeling method as input for a cutting time prediction, but potential strategies are briefly discussed.

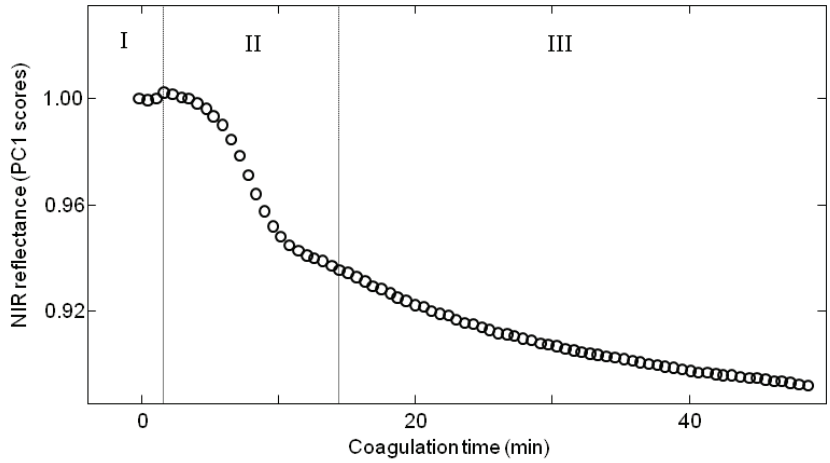

Fig. 1. Principal component scores from near-infrared reflectance measurement during milk coagulation time (experiment 1, Table 1). Marking of stages (I) – (III) is based on qualitative assessment: (I) κ-casein proteolysis, (II) paracasein aggregation and (III) gel network formation.

2. Experimentation

To mimic production in an industrial setting twelve milk coagulation experiments (with similar parameter settings) were performed simulating Normal Operating Condition (NOC) batches. It is well known that different process parameters change the gel formation profile and cheese yields (Lucey, 2002). Industrial cheese production is however - like most industrial food manufacturing – a generally well-controlled process, often involving milk standardization. However, occasionally *gross-errors* occur such as recipe miss-formulations, equipment malfunctioning or biological contamination of the starter cultures, but normal fluctuations are of a statistical nature or gradually sneaking into the production

chain over time (e.g. equipment *wear-and-tear*, seasonal changes in milk metabolites or strain deterioration). Under such normal fluctuations, improvements in productivity are to be achieved by better statistical process control from accumulation of (small) increased yields over time. In this paper we present a tool that can assist in such a statistical process optimization.

Preparation of reconstituted milk from skim milk powder followed the procedure of Hansen *et al.* (2010). 5 L of reconstituted milk was transferred to a 6 L cheese vat, which was inserted in a water bath for pre-conditioning to 32.0^{o}C, approximately 10 minutes before rennet addition. Chy-Max Plus rennet with 190 international milk clotting units IMCU·mL^{-1} was used (Chr. Hansen A/S, Hørsholm, Denmark). A diluted rennet solution made within 3 min before experiment initialization was added to the milk resulting in a final concentration of 0.066 IMCU·mL^{-1} of milk. The milk was stirred (18 rpm) for thirty seconds after rennet addition to ensure homogenous distribution.

NIR measurements were carried out using the Antaris MX FT-NIR Process Analyzer from Thermo Scientific (MA, USA) with a reflectance probe with SMA fiber connection. The spectrometer is self-referenced, so stability is ensured by collecting background spectra simultaneously with the sample measurements using an internal integrating sphere. To account for optical changes in the fibers cables connecting the probe to the spectrometer, a background spectrum was taken approximately 10 minutes prior to each batch run using a built-in reflectance standard (99% reflectance) in the instrument. In the NIR range 10001 – 4000 cm^{-1} (corresponding to 1000-2500 nm) 1557 frequencies (v) were measured equidistant with Δv = 3.8569 cm^{-1}. A total of 32 averaged scans were found to provide an adequate *signal-to-noise* ratio. This resulted in an acquisition time of 36 seconds. Spectra were recorded as expressed in Eq. 1:

$$log_{10}\left(\frac{1}{R}\right) = -log_{10}\left(\frac{I}{I_0}\right) \quad (1)$$

Where I is intensity of the light beam striking the detector after being reflected from the sample and I_0 is the intensity of the light beam after being reflected from the built-in 99% reflectance standard. In this way, I/I_0 is the fraction of light being

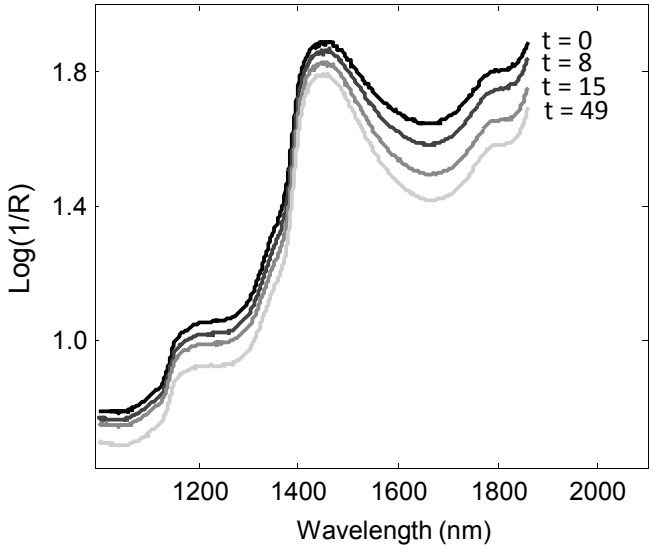

Fig. 2. Near-infrared reflectance spectra (1000 – 1850 nm) acquired during milk coagulation, *t* is batch-time in minutes (experiment 1, Table 1).

reflected by the coagulating milk. During modeling we will use the spectral range 1000 - 1850 nm, with a total of 1200 variables. Representative sample spectra from a coagulation batch are shown in Fig. 2, where the main changes over time are an increase in scatter as a result of the gel (particle) formation and a narrowing of the water band around 1400-1500 nm.

3. Previous approaches of coagulation profile analysis

Rheological analytical methods can determine physical cheese gel characteristics, e.g. storage modulus G' (Lucey, 2003), that cutting time is directly dependent on. These types of measurements are, however, not easily implemented as on-line, real-time process measurements. There is no direct dependency between cutting time and optical properties such as acquired by NIR reflectance. The fundamental idea of predicting cutting time using NIR is that the shape of the time profile (i.e. the kinetics) somehow contains information that the optimal cutting time is dependent on. A prerequisite for this idea to work is that the variability of production factors which cutting time depends on (e.g. temperature and milk composition) are accounted for by variability in the shape of the time profile of the NIR measurements. This idea has been pursued previously

by extracting a collection of numerical features that are characteristic for the time profile such as maxima or points of inflection and subsequently investigating if cutting time depends on these descriptors. Two main approaches have been used to summarize the profile shape into a collection of descriptors: (1) purely observational and (2) modeling with a set of parameters.

The majority of studies have summarized the time profiles as observed time-based or response-based numbers and the feature extraction is done by identifying time or response at maxima or minima of the first or second derivative of the profile. Particularly, the process time at the maximum of the first derivative, referred to as the inflection-point, has been used. A cutting time prediction model (Eq. (2)) is then made by linear regression:

$$t_{cut} = a + bt_f \tag{2}$$

Where t_f is the inflection-point and *a* and *b* are parameters estimated by least squares based on a set of inflection-points and their corresponding optimal cutting times t_{cut} (Payne *et al.*, 1993; Crofcheck *et al.*, 1999; Castillo *et al.*, 2003a). This prediction model has however proven to be too simplistic when protein content varies, because the profile variability at the inflection-point does not entirely account for the variability in cutting time that protein variations infer (Mertens *et al.*, 2002). An improved cutting time model was then proposed with the addition of a protein term (Castillo *et al.*, 2003a). It is however perhaps too difficult to implement a registration of milk protein content for every new batch in a production environment.

Another approach of summarizing the NIR coagulation time profile is to parameterize the observed shape using an appropriate model. Exploration of such coagulation model parameters has revealed that an offset parameter (β_1) is curvilinear related to protein content. With this finding, β_1 can be used to augment the cutting time prediction model to Eq. 3 that also accounts for protein variation:

$$t_{cut} = a + b_f t_f + b_1\beta_1 + b_2\beta_1^2 \tag{3}$$

Where a, b_f, b_1 and b_2 are parameters estimated by least squares based on a set of inflection-points t_f, β_1's and their corresponding cutting times t_{cut} (Mertens *et al.*, 2002).

4. Coagulation profile modeling

The modeling approaches as described in the previous paragraph have shown that profile variability does contain information related to the cutting time, and real-time profile modeling will thus be a precursor for using profile model parameters in cutting time predictor models. The main spectral development during coagulation is baseline changes (Fig. 2). We will not further evaluate band specific changes due to coagulation here, but Hansen *et al.* (2010b) provides details on this topic. Instead we apply principal component analysis (PCA; Wold, 1987) to transform the multivariate response into a single variable referred to as the first principal component (PC1) which account for of the main variability in the spectra (> 95% explained variance). The values (scores) of PC1 as a function of time after rennet addition represents the coagulation time profile (Fig. 1) used for further analysis. The advantage of using the time profile of PC-scores opposed to the profile of single wavelength NIR variables is due to the first order advantage which utilizes the covariation between spectral variables to provide robust estimates of spectral features and to strongly improve the signal to-noise-ratio (Bro, 2003).

We apply a model (Eq. (4)) with seven parameters fitted by non-linear least squares using a Gauss-Newton algorithm with Levenberg-Marquardt regularization (Seber & Wild, 2003) to approximate the observed score-values coagulation profile *x(t)*. This model is a slight modification of the model proposed by Merten *et al.* (2002):

$$x(t) = \frac{\alpha_1}{1+exp(-k_{aggre}(t_{max}-t))} + \alpha_2 exp\big(-k_{network}(t_{network}-t)\big) + \alpha_3 \qquad (4)$$

This model is composed of three terms: the logistic equation (also known from autocatalytic processes), an exponential term (also known from first order reactions) and an offset term. The logistic equation, is a model of the initial s-shaped part of the profile were micelle aggregation occur. The exponential term

is a model of the later stage where micelle network formation takes place. Parameters α_1, α_2, and α_3 are related to the magnitudes in the profile; parameters k_{aggre} and $k_{network}$ are rate constants related to the speed of micelle aggregation and network formation, respectively. Parameters t_{max} and $t_{network}$ are concerned with the location of the s-shape and the exponential along the time-axis. More specifically, t_{max} is the time of maximum slope in the s-shape, which is the modeling counterpart for inflection point as determined by the maximum of first derivative (see Eq. 2 and 3); $t_{network}$ is likewise the time of maximum slope in the exponential shape, which in this time profile is the located at the onset of the exponential and thereby related to the onset of network formation.

Fig. 3 shows a plot of the observed profile and the model (Eq. 4) fitted by non-linear regression. The model clearly fits the observed profile well, which holds for all twelve experiment profiles with a range for the coefficient of determination, R^2, of 0.9985 to 0.9994. Note that here we neglect stage (I) in Fig. 1 - κ-casein proteolysis before aggregation- because this stage represents a deviation from the s-shape and has too few observations to justify an additional modeling term. Our objective is to investigate how coagulation profile parameters can be derived in a real-time monitoring strategy. This would potentially provide a basis for a cutting time-point prediction model.

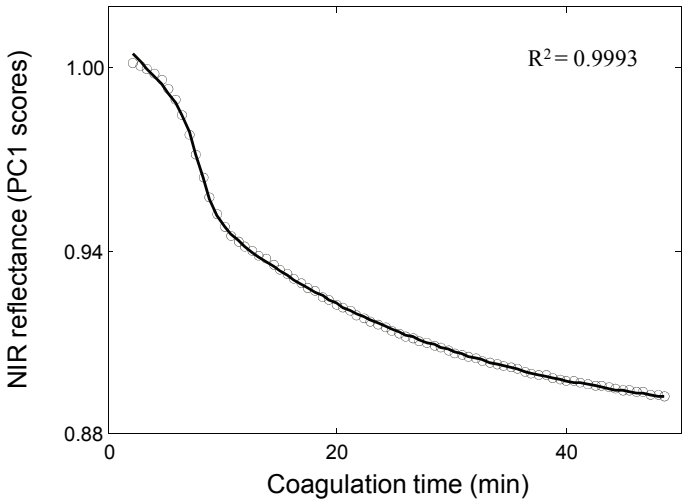

Fig. 3. Observed near-infrared reflectance PCA-scores (o) and fitted model (—) for a sample during rennet induced milk coagulation (experiment 1, Table 1).

However, non-linear regression by the all inclusive solution Eq. (4) leads, despite the close fit, to an ill-conditioned Jacobian matrix, which is an indication that we cannot trust all parameter estimates. An ill-conditioned solution means that small variations in the numbers making up the profile will cause large variation in some parameter estimates (Seber & Wild, 2003). This was confirmed by calculation of confidence intervals of model parameters, which were extremely large for some parameters (α_2 and $t_{network}$). This situation will obviously be critical during the first half of the coagulation reaction where the exponential part is underrepresented or even not present in the data. This observation led to the conclusion that a model for the entire profile is not feasible or desirable in an industrial setting for the aim of on-line model parameter estimation.

In order to make real-time modeling feasible, we apply an individual model strategy using Eq. 5 to approximate, in two segments, the profile *x(t)*:

Segmented model

$$\begin{cases} x(t) = \frac{\alpha_1}{1+exp(-k_{aggre}(t_{max}-t))} + \alpha_2 & t < t_{transition} \quad (5a) \\ x(t) = \alpha_3 exp(-k_{network}t) + \alpha_4 & t > t_{transition} \quad (5b) \end{cases}$$

This two segments profile model focus on each coagulation stage, the s-shape and the exponential phase, individually. We define the segments as strictly separate before and after the time of transition $t_{transition}$ which is estimated algorithmically as described below. Parameters α_1, α_2, α_3, and α_4 relate to the magnitudes of the two profiles, k_{aggre} and $k_{network}$ are rate constants and t_{max} is time of maximum slope of the s-shape. Note that in comparison to the full profile model (Eq. (4)), $t_{network}$ is excluded because it is implicitly included in the parameter $t_{transition}$. Fig. 4 shows a plot of the observed profile and the segmented profile model (Eq. (5)) fitted by non-linear regression. Like the full profile model (Eq. (4)) this model fits the observed profile very well, which is consistent for all twelve experiments with R^2 ranging from 0.9887 to 0.9995 for the s-shaped segment and 0.9960 to 0.9998 for the exponential segment.

Non-linear regression of the segmented profile model (Eq. (5)) led to a well-conditioned solution with well defined parameter estimates and acceptable small confidence intervals, Table 1.

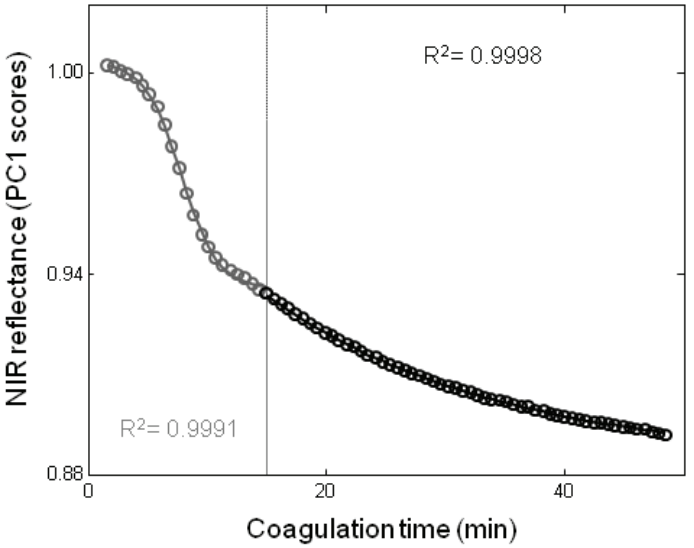

Fig. 4. Observed near-infrared reflectance PCA-scores (o) and fitted *segmented* model (—) for a sample during rennet induced milk coagulation (experiment 1, Table 1).

These results lead to the conclusion that a segmented profile model (Eq. (5)) provides a better summary of profile variability than the full profile model (Eq. (4)), and is thus a better suited candidate for a real-time cutting time determination.

5. Real-time coagulation modeling

While the segmented model gives a better summary of profile variability than the full profile model, it requires that the transition time $t_{transition}$, is determined in real-time as well. We propose an algorithmic procedure for locating $t_{transition}$ composed of three steps:

(1) For every new NIR measurement, the profile is augmented by one point using PCA on the new data matrix and the segmented model (Eq. (5)) is fitted to the available data points (score values) multiple times at all possible locations of $t_{transition}$ along the time axis.

(2) For each possible location of $t_{transition}$ the mean square error of fit (MSE) is calculated as the sum of the MSE for the two segments (MSE_{sum}). In this way MSE_{sum} is a measure of how the available data points are best modeled

between the s-shape and the exponential shape with $t_{transition}$ being the border point.

(3) $t_{transition}$ is defined as the time where the MSE_{sum} has a minimum.

Fig. 5 illustrates the concept of the algorithmic procedure and compares it with the best estimate for the analog parameter $t_{network}$ from the full profile model (Eq. (4)). Before the actual $t_{transition}$ is reached (Fig. 5, top row [a]) the estimate of $t_{transition}$ will of course be lower. Notice also that $t_{transition}$ estimation cannot commence until a sufficient number of data points are available for the segmented model. The algorithmic approach is clearly more stable at estimating the transition time, quickly converging to an acceptable value as soon as enough *evidence* is collected in the form of NIR measurements. As discussed previously the micelle aggregation and network formation stages are in reality overlapping phenomena. Through inspection of the NIR spectral profiles and the fitting performance of the model it appeared however that the transition period between stages is relatively short, which make our definition of $t_{transition}$ combined with the two-stage model (Eq. (5)) an acceptable and workable approximation. We also note that the $t_{transition}$ estimate will become more exact with a higher NIR measurement frequency.

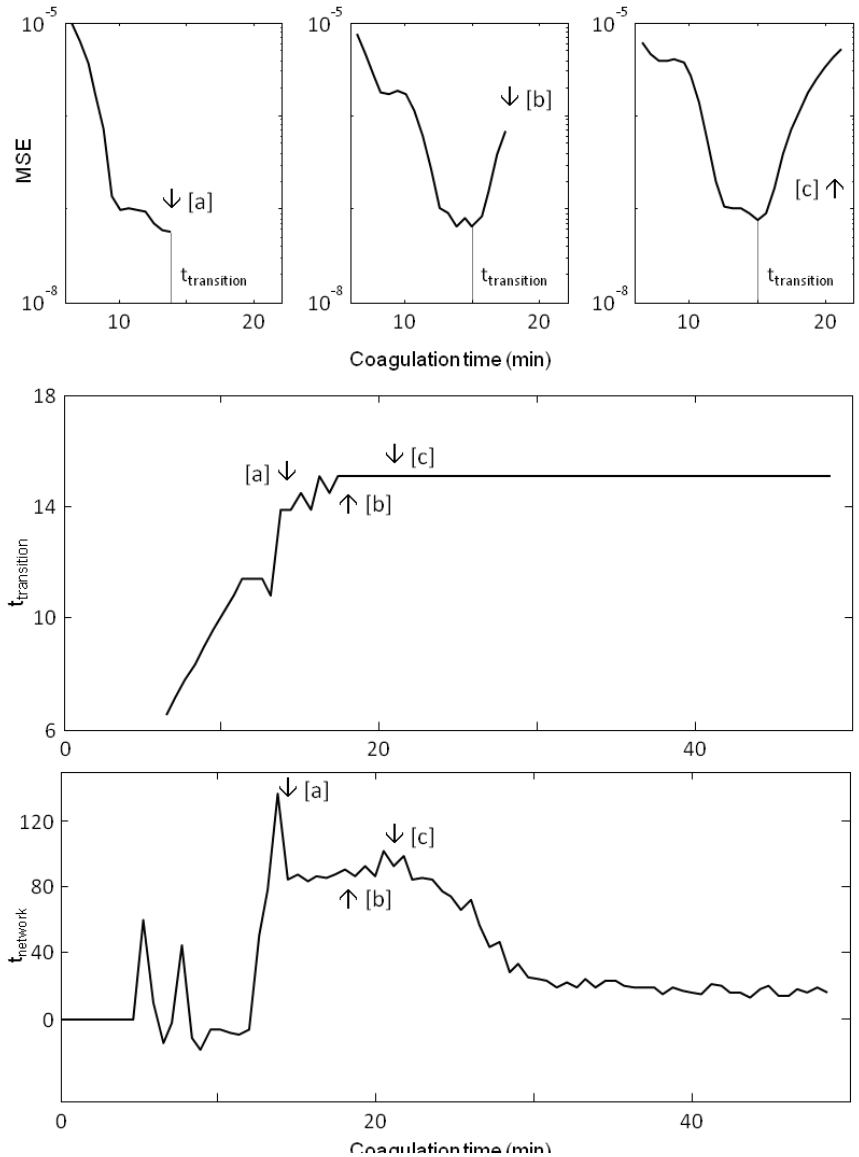

Fig. 5. Top and middle plots: example of how the proposed algorithm estimates transition time $t_{transition}$ between s-shape and exponential part in coagulation profile (see Eq. (5)). Bottom plot: estimation of network onset time $t_{network}$ by full profile model (Eq. (4), experiment 1, Table 1).

The strongest point of real-time modeling based on *first principle models* (also called mechanistic models) is that it allows for Model Predictive Control or decision making. First principle *modeling* (e.g. Eq. (5)), rooted in knowledge of

chemical, physical or biological insight is often more robust than *black box* modeling such as neural networks which are often applied in process monitoring (Roupas, 2008). However, in first principle models, parameters (e.g. the *k*-values in Eq. (5)) have to be determined from data, in our case real-time using on-line NIR measurements. This is illustrated by prediction of the remaining the network formation profile including confidence intervals on these predictions (Fig. 6a).

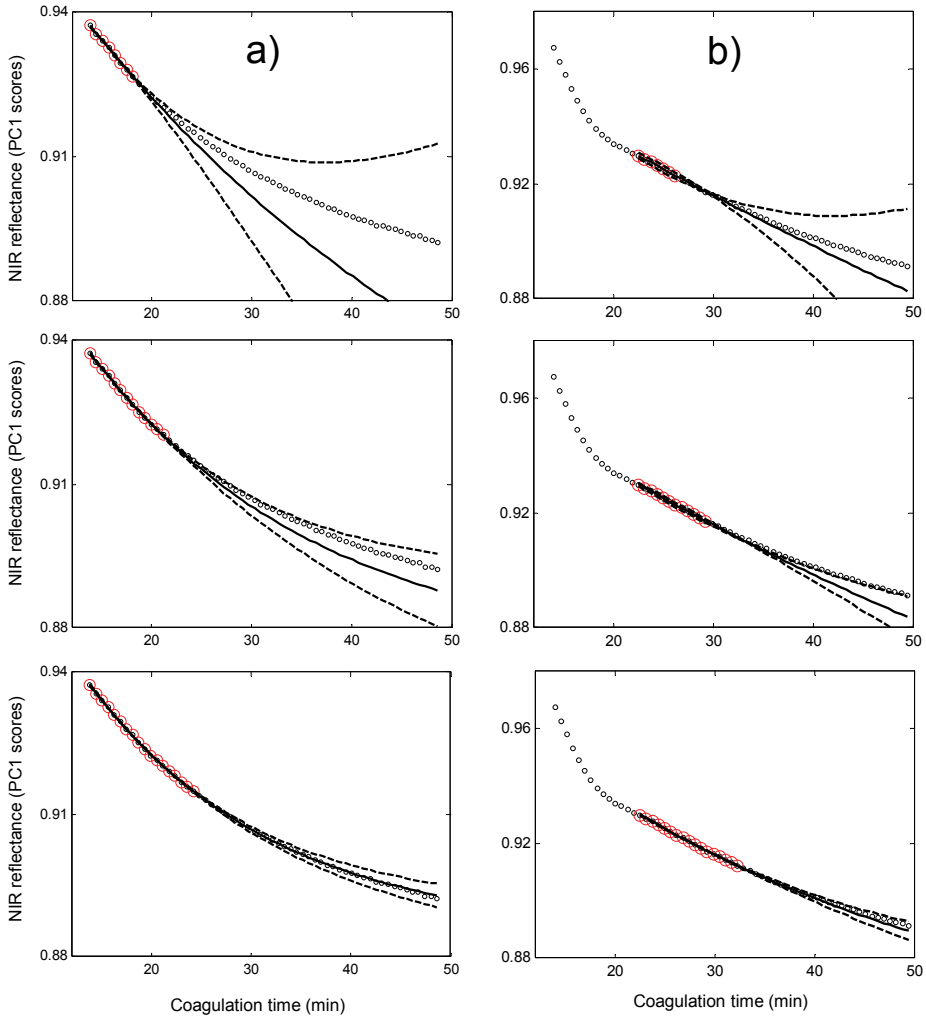

Fig. 6. Real-time modeling and prediction of the remaining milk coagulation. (o) actual PC1 score, (O) measurements included in model parameter estimation, (—) predicted progress, (---) 95% confidence interval; (a) experiment 1 and (b) experiment 8, Table 1.

Using the covariance matrix of the updated parameters and the model residuals, a symmetric 95% confidence interval on the prediction was made based on error propagation as described in detail in Seber and Wild (2003). It clearly shows that the reaction rate of gel network formation stabilizes as soon as enough evidence has been collected. At this stage in the batch process the plant operator can start anticipating the next action, which could lead to improved overall batch scheduling. It is also possible that a better estimate of optimal cutting time-point can be determined based on all or some of the frequently updated parameters found from Eq. (5), but this is beyond the scope of the present study. A flowchart detailing all steps involved for a potential coagulation process monitoring and control scheme is given in the appendix. It summarizes how real-time cutting time-point prediction could be performed using NIR on-line monitoring and automated decision making. Despite the apparent complexity, it is possible to perform all operations well within one minute time on a modern process computer, even for the last time points where most measurements have been collected leading to the highest computational work load. This could easily be optimized but it will not be further pursued in this paper.

7. Discussion and conclusion

In this paper we discuss real-time parameter estimation for monitoring and control in rennet induced milk coagulation. NIR spectra collected with a high sample frequency during processing are used as on-line data collection, and a two segmented first principle model is demonstrated to fit these data well. To discuss applications further Fig. 5b shows three progress prediction *snapshots* in the exponential phase of a second batch run (experiment eight in Table 1). Despite efforts to generate twelve NOC coagulation batches it appears that number eight was slightly retarded in the casein micelle aggregation phase or that the transition-point was less sharp for this experiment. Despite the deviating behavior of this batch, the suggested algorithm is still capable of identifying and modeling the network formation phase, providing the operator with valuable information (albeit later in the process). Table 1 indicates another strong benefit of detailed process modeling based on reliable in-process measurements like NIR: some or all model parameters could be used in Multivariate Statistical Process Control and Optimization using historical data. This might provide the

food engineer with tools to identify expected (e.g. seasonal changes) and unexpected (e.g. suboptimal equipment) trends or differences (e.g. in parallel production lines) by comparing every-day/NOC variations with observed tendencies, while plant managers could use the same information for a long-term economic maximization.

Acknowledgements

We thank the Danish Dairy Foundation (MFF) for generous financial support of this work, which is part of the research project “PAT in the Dairy Industry”. We would also like to thank Thermo Scientific for lending us the Antaris MX FT-NIR Process Analyzer.

9. References

Bro, R. (2003). Multivariate calibration – What is in chemometrics for the analytical chemist? *Analytica Chimica Acta*, 500, 185–194.

Carlson, A., Hill, C.G., & Olson, N.F. (1987). Kinetics of milk coagulation: I. The kinetics of kappa casein hydrolysis in the presence of enzyme deactivation*, Biotechnology and Bioengineering*, 29(5), 582–589.

Castillo, M., Payne, F.A., Hicks, C.L., Laencina, J. & Lopez, M.B. Effect of protein and temperature on cutting time prediction in goats' milk using an optical reflectance sensor, *Journal of Dairy Research*, 70(2), 205–215.

Castillo, M.Z., Payne, F.A., Hicks, C.L., Laencina, J.S., & Lopez, M.B.M. (2003). Modelling casein aggregation and curd firming in goats' milk from backscatter of infrared light. *Journal of Dairy Research*, 70, 335–348.

Crofcheck, C.L., Payne, F.A., & Nokes, S.E. (1999). Predicting the cutting time of cottage cheese using light backscatter measurements, *Transactions of the ASAE*, 42(4), 1039–1045.

Fagan, C.C., Leedy, M., Castillo, M., Payne, F.A., O'Donnell, C.P. & O'Callaghan, D.J. (2007). Development of a light scattering sensor technology for on-line monitoring of milk coagulation and whey separation. *Journal of Food Engineering*, 83(1), 61-67.

Hansen, C.L., Rinnan, Å., Engelsen, S.B., Micklander, E., Andersen, U. & van den Berg, F. (2010) Effect of Gel Firmness at Cutting Time, pH, and Temperature on Rennet Coagulation and Syneresis: an in situ ^{1}H NMR Relaxation Study, *Journal of Agricultural and Food Chemistry*, 58(1), 513-519.

Hansen, C.L., van den Berg, F., Rinnan, Å. & Engelsen, S.B. (2010). Near infrared scatter and absorbance properties of coagulating milk. *Unpublished results*.

Johnson, M.E., Chen, C.M. & Jaeggi, J.J. (2001). Effect of rennet coagulation time on composition, yield, and quality of reduced-fat cheddar cheese. *Journal of Dairy Science*, 84, 1027-1033.

Lucey, J.A. (2002). Formation and physical properties of milk protein gels. *Journal of Dairy Science*, 85, 281–294.

Lucey, J.A., Johnson, M.E., & Horne, D.S. (2003). Perspectives on the Basis of the Rheology and Texture Properties of Cheese, *Journal of Dairy Science*, 86 2725-2743.

McMahon, D.J., Brown, R.J., & Ernstrom, C.A. (1984). Enzymic coagulation of milk casein micelles, *Journal of Dairy Science*, 67, 745–748.

Mertens, B.J.A., O'Donnell, C.P., & O'Callaghan, D.J. (2002). Modelling near-infrared signals for on-line monitoring in cheese manufacture. *Journal of Chemometrics*, 16 (2) 89-98.

Payne, F.A., Hicks, C.L., Madangopal, S. & Shearer, S.A. (1993). Fiber Optic Sensor for Predicting the Cutting Time of Coagulating Milk for Cheese Production. *Transactions of the ASAE*, 36(3), 841-847.

Roupas, P. (2008). Review - Predictive modelling of dairy manufacturing processes, *International Dairy Journal*, 18(7), 741-753.

Seber, G.A.F. & Wild, C.J. (2003). Chapter 14: Computational Methods for Nonlinear Least Squares, In G. A. F. Seber, C. J. Wild (Eds.), *Non-linear Regression* (pp. 619-660). John Wiley & Sons Inc., New Jersey.

Storry, J.E. & Ford, G.D. (1982). Development of coagulum firmness in renneted milk – a two-phase process, *Journal of Dairy Research*, 49, 343–346.

Wold, S., Esbensen, K., Geladi, P. (1987). Principal component analysis. *Chemometrics and Intelligent Laboratory Systems*, 2(1), 37-52.

9. Appendix – Process flowchart of real-time cutting time prediction

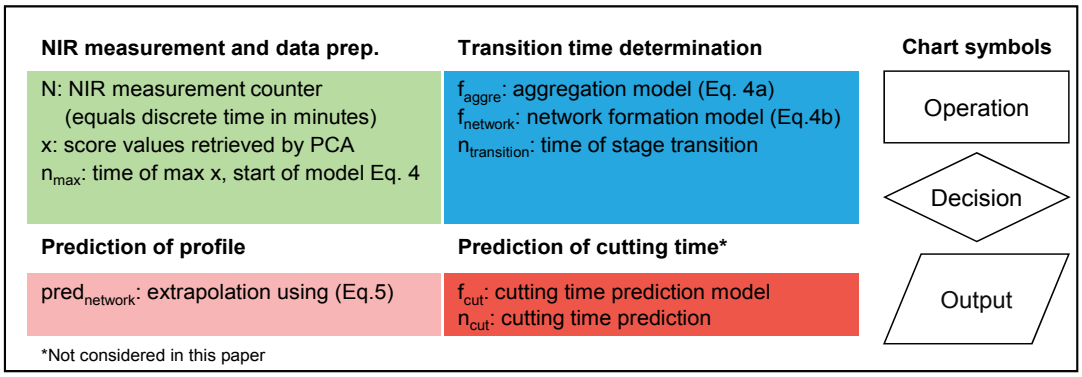

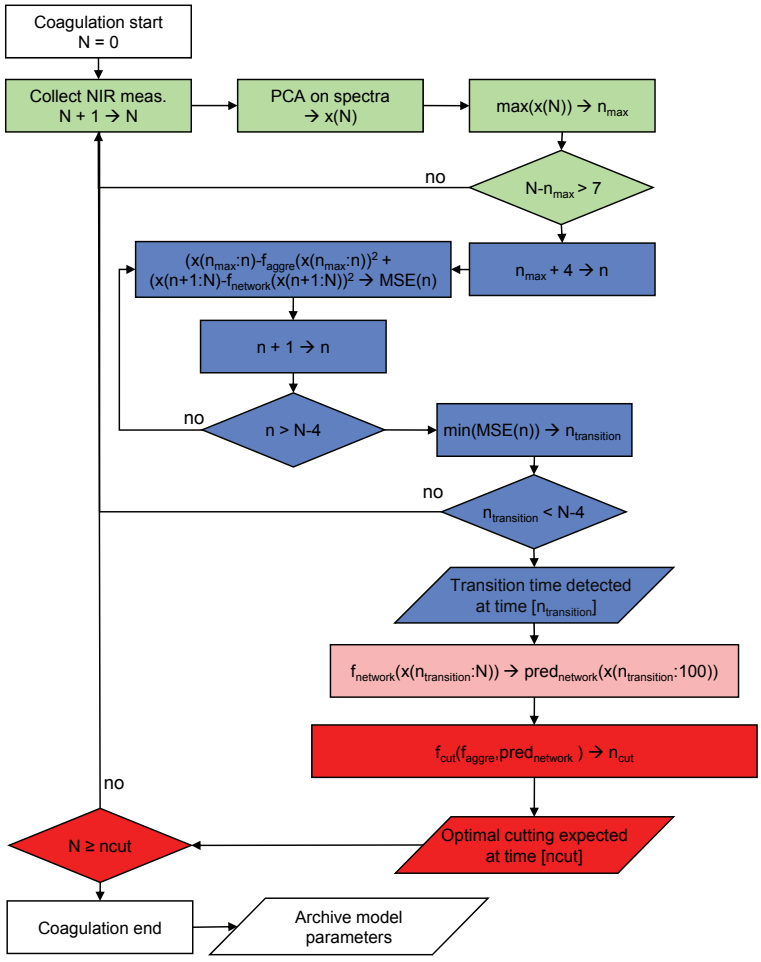

Table 1. Segmented profile model parameters (± 95 % confidence interval) estimated from the observed profile of NIR reflectance measurements during coagulation.

	Casein micelle aggregation parameters								**Network formation parameters**						
Exp.	α_1		k_{aggre}		t_{max} (min)		α_2		α_3		$k_{network}$		α_4		$t_{transition}$
1	0.068	±0.002	0.66	±0.04	7.9	±0.1	0.94	±0.001	0.11	±0.001	0.052	±0.001	0.88	±0.0004	15
2	0.069	±0.003	0.67	±0.06	7.6	±0.1	0.94	±0.001	0.12	±0.001	0.053	±0.001	0.88	±0.0008	15
3	0.051	±0.007	0.65	±0.16	7.2	±0.5	0.96	±0.002	0.10	±0.002	0.049	±0.001	0.91	±0.0005	17
4	0.070	±0.002	0.62	±0.04	8.5	±0.1	0.93	±0.001	0.12	±0.001	0.053	±0.001	0.88	±0.0008	16
5	0.071	±0.002	0.59	±0.03	9.1	±0.1	0.93	±0.001	0.11	±0.001	0.043	±0.001	0.88	±0.0005	17
6	0.068	±0.007	0.74	±0.16	6.7	±0.3	0.94	±0.003	0.12	±0.002	0.050	±0.002	0.88	±0.0007	13
7	0.067	±0.002	0.62	±0.04	8.9	±0.1	0.94	±0.001	0.13	±0.001	0.048	±0.001	0.88	±0.0006	16
8	0.076	±0.002	0.39	±0.02	14.3	±0.1	0.93	±0.001	0.14	±0.001	0.028	±0.002	0.86	±0.0030	22
9	0.069	±0.004	0.68	±0.09	7.4	±0.2	0.94	±0.002	0.14	±0.001	0.054	±0.001	0.87	±0.0010	15
10	0.072	±0.003	0.57	±0.06	9.0	±0.2	0.93	±0.002	0.14	±0.004	0.057	±0.002	0.88	±0.0006	18
11	0.072	±0.004	0.67	±0.09	6.9	±0.2	0.94	±0.002	0.12	±0.003	0.047	±0.003	0.87	±0.0019	14
12	0.066	±0.003	0.74	±0.07	7.3	±0.1	0.94	±0.001	0.13	±0.006	0.060	±0.006	0.88	±0.0030	14
Mean	0.068		0.63		8.4		0.94		0.12		0.050		0.88		16
SD	0.006		0.09		2.0		0.01		0.01		0.008		0.01		2

Paper IV

NIR discussion forum: analysis of coagulating milk

Reprint from NIR news, 21, issue 5, 16-17, (2010)

doi: 10.1255/nim.1195

NIR discussion forum: analysis of coagulating milk

Donald Dahm, with Christian Hansen, Dave Hopkins and Karl Norris

The NIR Discussion Forum is a useful vehicle for getting help and exchanging views on all aspects of NIR theory and practice. Very recently there has been a lot of activity which developed from a question asked by a PhD student. I felt that the ensuing exchange was so interesting that it merited summary and presentation to our readers, some of whom may not be regular visitors to the forum. I approached Don Dahm (one of the participants in the discussion) to summarise the key points; Don's summary is reproduced below.—Ed.

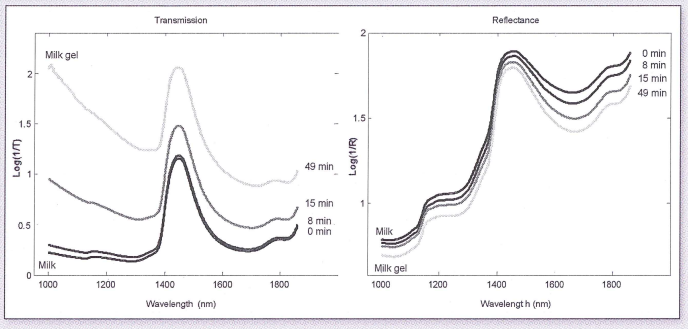

Figure 2. Log (1/*t*) and log (1/*t*) spectra as a function of time over the transition from milk to milk gel. Spectra were acquired using a multichannel spectrometer connected to fibre optic probes.

There is a thread on the NIR Discussion Forum[1] that especially attracted my attention. Christian Hansen, a PhD student at the University of Copenhagen, posted a series of four reflectance spectra taken at various times during a study of the rennet coagulation of milk as it turns into a gel, a step in the cheese making process. Christian asked for help in understanding the "scattering physics" involved.

There was a tendency on the part of the more experienced participants in the discussion to hold back on explanations of spectra based on vibrational changes in bonds which might be occurring during the gelation until the trends in the spectra were understood on the basis of trends in scatter and pathlength change. As is frequently the case, differences of opinion arose, which led to requests for more data. It turned out that Christian also had transmission data that was obtained simultaneously with the reflectance spectra. Christian was willing and able to post many requested transformations very rapidly. A graphical illustration of the experimental set-up is shown in Figure 1; some of the data posted are shown in Figures 2–4.

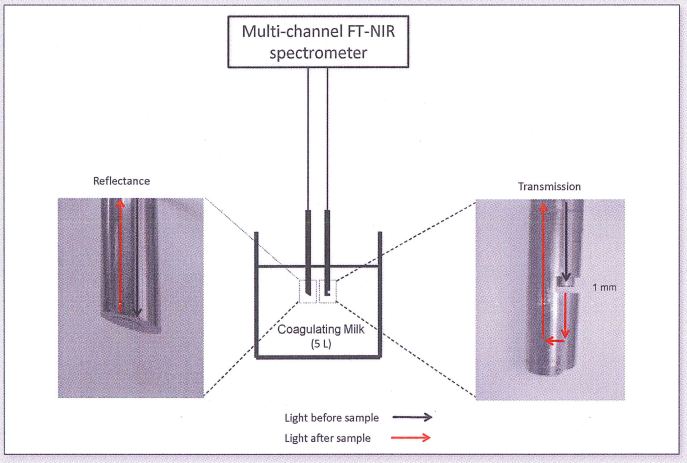

Figure 1. Experimental setup.

The following paragraph contains Christian's current interpretation. Bear in mind that this is an ongoing discussion and there is not necessarily total agreement among all of the contributors to the Forum. Furthermore, sometimes we change our minds as the discussion proceeds!

The log(1/*T*) plot in Figure 2 (left) shows spectra with a downward baseline slope, consistent with a decrease in scatter with increasing wavelength. This baseline slope decreases in severity as milk coagulates. There is also an increase in absorbance with coagulation time, consistent with an increase in scatter. The major change in both the reflection and transmission spectra over time is the change in baseline. Since the general slope in a log(1/*R*) plot (Figure 2, right) frequently tracks particle size, there was a request for a plot of the MSC coefficients ("slope" and "offset") for the dataset; these are displayed in Figure 3. Previous research using Dynamic Light Scatter has observed a decrease in average micelle size in the initial minutes of rennet coagulation attributing it to proteolytic removal of the hairy layer (κ-casein) surrounding casein micelles. This slight change in micelle size seems to be what is causing

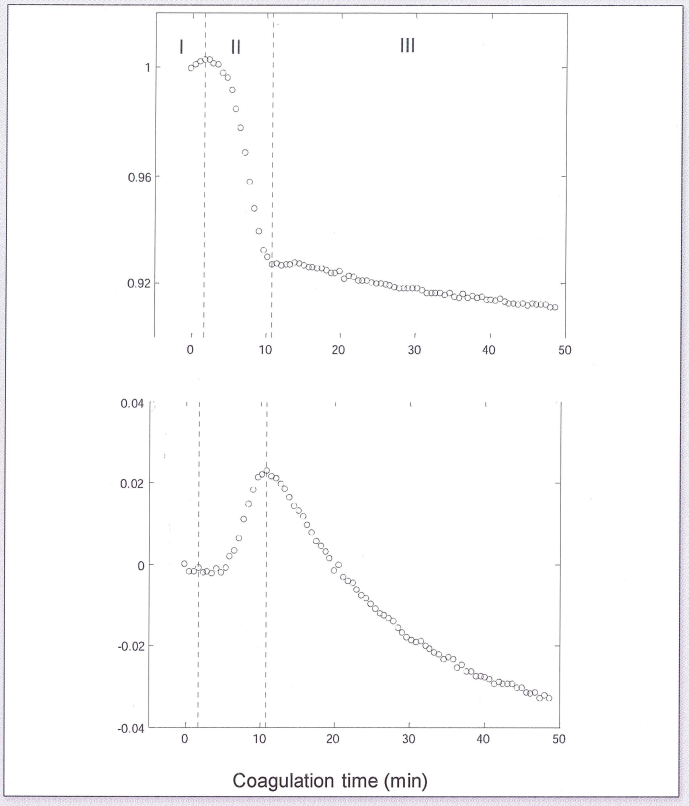

Figure 3. "Slope" and "Offset" from MSC corrections as a function of coagulation time (in minutes). Marking of coagulation stages (I)—(III) is based on qualitative assessment: (I) k-casein proteolytic removal, (II) micelle aggregation and (III) gel network formation.

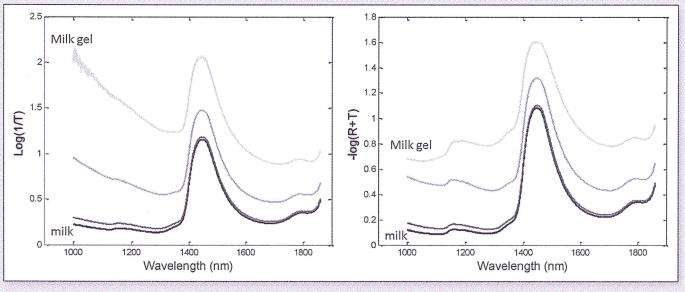

Figure 4. Illustration of effect of removing some scatter effects from transmission data for four spectra by adding remission data.

an increase in spectral "slope" very early in the process (Figure 3, stage I). This is followed by a rapid decrease in spectral "slope" (Figure 3, stage II), presumably attributable to an increase in particle size due to flocculation of micelles. The sharp decrease in slope is accompanied by an increase in "offset". In stage III, there is apparently a transition accompanied by a slow decrease in spectral "slope" and a decrease in "offset".

The normal observation is for spectral "slope" to be directly related to particle size[2,3] while here, at least in stages I and II, we observe the opposite. As discussed in a recent article on emulsions,[4] absorption due to components in the continuous aqueous phase decreases with drop size while absorption due to absorbers within the drop increases. Because the absorption is dominated by the water in the continuous phase, the slope decreases with increasing particle size. We believe the behaviour of the slope in stages I and II is explained by this.

Between stages II and III there may be an "inversion" in which the continuous phase becomes the non-aqueous portion of the gel. It would follow then that the decrease in slope in this stage would be due to a decrease in particle size of the water "droplets" which are now acting like normal "particles". No explanation for the behaviour of the slope has been offered in the discussions.

A collaborative process of sorts has arisen which seems to be addressing the hard work of figuring out what is happening with the bonding. This is involving derivatives and spectral subtraction. This process may be aided by the use of a little known technique of plotting $\{-\log(R+T)\}$. This procedure removes some of the scatter effects from the transmission spectra and highlights the effects of absorption. As illustrated in Figure 4, the spectra have less slope and show some absorption maxima far more clearly. This should enable better detection of peak shifts and changes in intensity that accompany network formation in the gel.

As noted above, the major change in both the reflection and transmission spectra over time is the change in baseline. The magnitude of the baseline change is much greater in transmission and the $-\log(R+T)$ really shows a large baseline shift with time. The reason for this may be an artifact of experimental arrangement but other speculation is being offered. Perhaps you'd like to check the Forum postings to see what progress is being made.

References

1. http://www.nirpublications.co.uk/cgi-bin/discus/show.cgi?5/6658
2. P. Frake, C.N. Luscombe, D.R. Rudd, I. Gill, J. Waterhouse and U.A. Jayasooriya, *Analyst* **123,** 2043–2046 (1998).
3. Å. Rinnan, F. van den Berg and S.B. Engelsen, *TrAC* **28,** 1201–1222 (2009).
4. D.J. Dahm, K.D. Dahm, A.M.K. Pedro and M.M.C. Ferreira, "Understanding confusing phenomena in remission spectra", *NIR news* **21(3),** 9–14 (2010).

Paper V

Determination of dry matter content in potato tubers by low-field NMR

Reprint from Journal of Agricultural and Food Chemistry, 58 (19), 10300-10304.

10300 J. Agric. Food Chem. 2010, 58, 10300–10304
DOI:10.1021/jf101319q

JOURNAL OF AGRICULTURAL AND FOOD CHEMISTRY
ARTICLE

Determination of Dry Matter Content in Potato Tubers by Low-Field Nuclear Magnetic Resonance (LF-NMR)

Christian Lyndgaard Hansen,*,† Anette Kistrup Thybo,‡ Hanne Christine Bertram,‡ Nanna Viereck,† Frans van den Berg,† and Søren Balling Engelsen†

†Quality and Technology, Department of Food Science, Faculty of Life Sciences, University of Copenhagen, DK-1958 Frederiksberg C, Denmark, and ‡Department of Food Science, Faculty of Agricultural Sciences, Aarhus University, Post Office Box 102, DK-5792 Aarslev, Denmark

The objective of this study was to develop a calibration model between time-domain low-field nuclear magnetic resonance (LF-NMR) measurements and dry matter (DM) content in single potatoes. An extensive sampling procedure was used to collect 210 potatoes from eight cultivars with a wide range in DM content, ranging from 16 to 28%. The exponential NMR relaxation curves were resolved into four mono-exponential components using a number of solution diagnostics. Partial least-squares (PLS) regression between NMR parameters (relaxation time constants $T_{2,1-4}$ and magnitudes $M_{0,1-4}$) and DM content resulted in a model with low error (RMSECV, 0.71; RMSEP, 0.60) and high correlation (r_{CV}, 0.97; r_{test}, 0.98) between predicted and actual DM content. Correlation between DM content and each of the proton populations revealed that $M_{0,1}$ ($T_{2,1}$, 3.6 ms; SD, 0.3 ms; r, 0.95) and $M_{0,4}$ ($T_{2,4}$, 508 ms; SD, 53 ms; r, −0.90) were the major contributors to the PLS regression model.

KEYWORDS: Low-field NMR; potato; PLS regression; dry matter content; DoubleSlicing; specific gravity; core consistency

INTRODUCTION

An increased consumer awareness of high-quality potato products increases the interest of the industry in high-technology-grading systems. If uniform good-quality products and high-end gourmet potatoes are to be produced, the industry requires a rapid instrumental method to grade the raw potatoes according to the final sensory and technological qualities. For potatoes, the texture is of great importance for the perception of quality by the consumer, and it is well-established that dry matter (DM) content, starch composition, and cell wall structures significantly affect the final texture of cooked potatoes (*1*−*6*). While starch composition and cell wall structure to a large extent are genetically determined, DM content mainly depends upon the maturity of the potato tuber, the composition of the soil, and fertilization and draft conditions (*7*, *8*). Specific gravity is a reliable measure of DM content, which is determined by weighing potatoes in air and water. This time-consuming and rather cumbersome method is the standard method used for quality control of potato samples in potato industries. Also, the brine grading method with various densities is used for industrial grading of potatoes according to DM content. A simplified, more automated online measurement of DM content could be the first target in obtaining better control on the postharvest potato quality. Two obvious rapid methods exist to determine the DM content of individual tubers: near-infrared spectroscopy (NIR) and low-field nuclear magnetic resonance (LF-NMR) relaxometry. In the case of NIR, the ideal transmission measurements are difficult, if not impossible, to obtain, because the combination of size and high water content of the tubers hinders the transmission of NIR light. The less advantageous NIR reflection measurements are easy to conduct and truly non-destructive but tend to vary strongly with the tuber surface morphology and the soil adhering to the surface. Perhaps most importantly, reflectance measurements will only provide information about the DM content in the outer shell of the tuber, which is likely non-representative for the quality question at hand. These are the main reasons why in the literature NIR assessments of DM content are performed in reflectance mode on a sliced potato (*9*−*11*). On the contrary, LF-NMR considers that the tubers have high water content and that the measurements give information on the entire volume measured. Unfortunately, most current benchtop LF-NMR instruments cannot accommodate a whole potato tuber in the sampling probe. The aim of this study is to characterize the performance and establish if LF-NMR is adequate for determining DM content of individual potato tubers.

LF-NMR as an analytical method is abundantly present in the food industry and food science research because of its unique capability to provide information about the mobility and distribution of water and fat protons in food products (*12*, *13*). These in turn are known to be critical to the perceived texture. Numerous studies have documented that LF-NMR is an excellent method for characterization of water mobility and water distribution in food items, such as meat, fish, cheese, cereals, fruits, and vegetables, including potatoes (*11*, *14*, *15*). Moreover, LF-NMR is capable of monitoring dynamic changes during processing, because

*To whom correspondence should be addressed. Telephone: +45-3024-0317. Fax: +45-3533-3245. E-mail: chha@life.ku.dk.

 Published on Web 09/20/2010

measurements can be performed non-destructively for example during cooking of potatoes with different levels of DM (*16*). In previous studies, LF-NMR has demonstrated a high correlation to DM content because of the inverse relationship between the water content in the raw potatoes with the starch and DM content. However, these studies were performed on limited sample sets with few different cultivars, using only a small range in DM content (*11*, *14*, *15*). One challenge when determining DM content in potatoes is the large biological variation between cultivars, within cultivars, and within each potato tuber.

To establish a rapid and reliable method for the determination of DM content by LF-NMR, we will use a large sample set using an extensive sampling procedure. The variation in DM content was obtained using eight different potato cultivars grown under different conditions and harvested at variable maturity to expand the natural biological variation and variation in DM content. The establishment of a general rapid method can have practical use in the potato industry for grading high-end gourmet potatoes.

MATERIALS AND METHODS

Potato Samples. Eight different potato cultivars ('Ballerina', 'Bintje', 'Inova', 'Fakse', 'Sava', 'Jutlandia', 'Estima', and 'Gunda') were selected to represent a large variation in DM content. The cultivars were received from the Danish Potato Breeding Station, the Danish Institute of Agricultural Sciences, and commercial growers. The potatoes were grown and harvested at different conditions to obtain a large variation in DM content. After harvest, the potatoes were stored at 4 °C and 95% relative humidity up until the day before analysis. All cultivars were subcategorized in 1−6 groups by a non-destructive grading using specific gravity (SG), which is highly correlated to DM content (eq 1)

$$\mathrm{SG} = \left(\frac{w}{w - w_w}\right) \quad (1)$$

where w is the weight in air and w_w is the weight in water, i.e., with the scale immerged in water. Using the SG value, DM estimates (DM_{est}) were calculated by the following equation (*17*, *18*):

$$\mathrm{DM_{est}} = (214\mathrm{SG}) - 211.44 \quad (2)$$

Accordingly, 21 cultivar/subcategories were obtained, each of which will be called DM bin in the remainder of the paper (**Table 1**). For each of the 21 DM bins, 10 potato tubers were collected, giving a total of 210 samples. This extensive sampling procedure ensured that the material represented a large and relevant variation in DM, cultivars, and texture quality of potatoes.

For determination of LF-NMR and DM content, a cylindrical sample (diameter, 11.5 mm; length, 45.0 mm) was taken from the storage parenchyma tissue in the bud end of the tuber with a cork borer, avoiding tissue from the center. The cylinder was first used for LF-NMR measurement and then for determination of DM content. The sample was placed in a glass tube with a plastic lid and placed in a measurement glass tube. The temperature of the sample was adjusted to 25 °C in a water bath for 10−15 min before LF-NMR measurements.

LF-NMR Relaxometry. The LF-NMR relaxation measurements were performed on a Maran benchtop pulsed NMR analyzer (Oxford Instruments, Witney, U.K.) with a magnetic field strength of 0.47 T corresponding to a resonance frequency for protons of 23.2 MHz. The NMR instrument was equipped with an 18 mm temperature-controlled probe; the temperature was set to 25 °C. The transverse relaxation time constant, T_2, was measured using the Carr−Purcell−Meiboom−Gill (CPMG) sequence (*19*, *20*). The T_2 measurements were performed with a τ value of 150 μs. The repetition time between two consecutive scans was 6 s. The dwell time was 0.5 μs, and the receiver gain was 5.0%. Data from 4096 echoes were acquired; they were obtained as a 16 scan repetition, with 1 dummy scan in front to ensure that a spin system is in a steady state before data are collected. Inaccuracy in the 180° pulse setting was compensated for using only even-numbered echo, resulting in 2048 data acquisition points per measurement.

Table 1. Overview of DM Grading Bins and Range and Mean DM Determined by Specific Gravity (DM_{SG}) on Intact Potatoes and Oven Drying on Sample Cylinders (DM_{oven})

DM grading bins	DM range (%)	mean DM_{SG} (%)	mean DM_{oven} (%)
Bintje_16.2	16.2−17.2	17.0	17.9
Bintje_18.5	18.5−20.5	19.0	19.5
Bintje_20.5	20.5−22.5	21.4	22.4
Bintje_22.5	22.5−23.5	23.0	23.9
Bintje_23.5	23.5−25.0	24.5	25.7
Bintje_25.0	25.0−28.0	26.2	27.8
Ballerina_16.4	16.4−17.4	16.9	16.6
Ballerina _17.4	17.4−18.4	17.7	18.8
Ballerina _18.4	18.4−19.4	18.9	19.7
Estima_19.0	19.0−21.0	20.3	19.9
Faxe_18.2	18.2−20.2	18.7	20.4
Faxe_20.2	20.2−22.2	21.8	23.5
Inova_16.0	16.0−17.5	16.6	17.7
Inova_17.5	17.5−18.5	18.1	19.1
Inova_18.5	18.5−20.0	19.6	19.6
Jutlandia_19.5	19.5−20.5	20.1	20.3
Jutlandia_20.5	20.5−21.5	20.9	20.0
Sava_18.0	18.0−19.5	18.3	17.7
Sava_19.5	19.5−20.5	19.9	19.6
Sava_20.5	20.5−22.2	22.0	22.4
Gunda_19.2	18.5−19.8	19.4	19.0

DM Content. The cylinder from the LF-NMR measurements was cut transversely and longitudinal and dried in an oven at 80−85 °C for 16−18 h, where after DM content, DM_{oven} was calculated.

Data Analysis. Regression analysis between LF-NMR data and the DM content was performed by partial least-squares (PLS) regression (*21*). To perform a comprehensive and comparative correlation analysis between the LF-NMR data and the DM content, a number of different data analytical models were applied to the LF-NMR data prior to PLS regression: (1) Raw relaxation data in the time domain. (2) Distributed exponential fitting analysis uses a regularization approach to the inverse Laplace transform, which results in a continuous distribution of relaxation time constants T_2 (*22*). Mathematically, the distributed exponential fitting problem is ill-defined, because it is very sensitive to the constraints used. (3) Discrete multi-exponential fitting by curve resolution of the relaxation curves into characteristic relaxation time constants $T_{2,n}$ and corresponding magnitudes $M_{0,n}$ (eq 3) (*23*, *24*)

$$M(t) = \sum_{n=1}^{N} M_{0,n} \exp\left(\frac{-t}{T_{2,n}}\right) + e(t) \quad (3)$$

where $M(t)$ is the residual magnetization at time t, $M_{0,n}$ is the concentration or magnitude parameter of the nth exponential, $T_{2,n}$ is the corresponding transverse relaxation time constant, and $e(t)$ is the residual error. After deconvolution of the relaxation curve into n exponential components, inspection of the residuals will reveal whether the curve has been modeled by too few, too many, or the correct number of components. Appropriate loss in fit and χ^2 misfit tests can also be used to validate if the right number of components have been used. (4) Multi-exponential fitting by "matrix fit" (*24*, *25*) of the relaxation curves into common characteristic relaxation time constants T_2 and corresponding magnitudes M_0. Matrix fit is the two-dimensional analogue to discrete exponential fitting and is generally less prone to overfitting compared to discrete exponential fitting. The disadvantage is that the T_2 values in samples might be more correctly described as a distribution of T_2 values. It should be emphasized that the matrix fit method represents the same underlying model as single Slicing (*25*) and PowerSlicing (*26*), which are not included in this paper. (5) Multiexponential fitting by "DoubleSlicing" (*27*) of the relaxation curves into transverse relaxation time constants T_2 and corresponding magnitudes M_0. The DoubleSlicing technique uses the fact that in every part of a multi-exponential decay curve each of the mono-exponentials are present but in different amounts. The technique pseudo-upgrades a single relaxation curve to become trilinear data, by cutting the relaxation curve into slices. When parts of the signal curve are selectively removed (slicing) and the remaining curve is used, the relaxation curve can be transformed from

a one-dimensional signal (a vector x) into two-dimensional data (a tensor X). When this procedure is repeated on the matrix, the data are transformed to three-dimensional data (a cube X) and three-way mathematical methods can now be used. The technique has been shown to be extremely rapid and have improved solution diagnostics. Andrade et al. (*27*) tested the performance of DoubleSlicing against existing methods and found that it was accurate in estimating relaxation times and that it outperformed exponential fitting by a factor of 4 with regards to computation time. These different data analytical approaches all have known advantages and disadvantages, but in this work, they are primarily applied to determine the correct rank of the data, i.e., the number of underlying exponential components extractable from the data. While the number of components in the PLS model under (1) is statistically validated, the approach adopted under (5) is accompanied by rigorous diagnostics of the number exponential components (*28*). The number of components in the curve fitting model under (3) and (4) can only be evaluated by the decrease in the residual error of the fit and visual inspection of residuals.

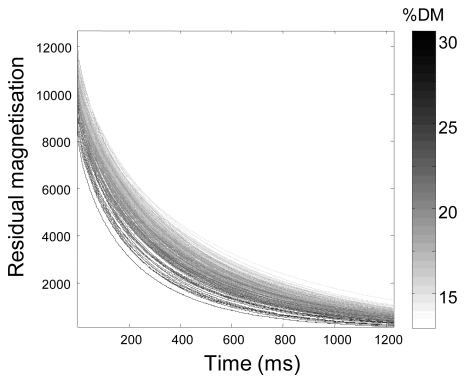

Figure 1. Raw LF-NMR relaxation data for 210 potato samples. The curves are gray-scale-colored according DM content.

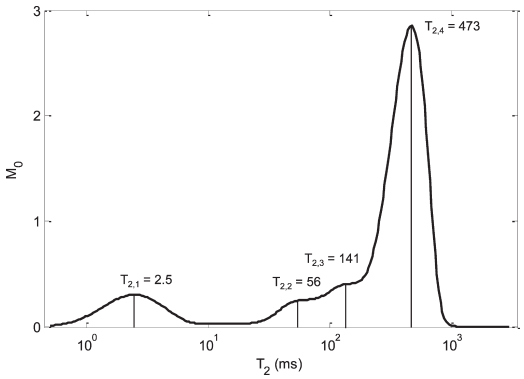

Figure 2. Mean distribution of T_2 relaxation times of 210 potatoes estimated by distributed exponential fitting of LF-NMR CPMG relaxation curves.

PLS Model Validation. For the PLS modeling, the sample set was divided into a calibration set and an independent test set. Of the 210 samples, 4 samples were chosen randomly from each of the 8 cultivars, giving a total of 32 samples in the independent test set. The test set was not used for PLS modeling but was only used to predict DM content from the generated PLS model. The PLS modeling was performed on the remaining 178 samples using segmented cross-validation, leaving out one cultivar at the time. The generated PLS models were compared by a correlation coefficient (r) and root-mean-square error of cross-validation (RMSECV) for the calibration set and root-mean-square error of prediction (RMSEP) for the independent test set.

All data analysis steps were performed by Matlab, version 7.6 (MathWorks, Inc., Natick, MA), using in-house algorithms (www.models.life.ku.dk).

RESULTS AND DISCUSSION

Table 1 shows the range of cultivars and DM grading bins used in the study, which ensures a large DM variation when modeling against LF-NMR relaxation data. DM content determination using SG data on a whole tuber and oven-drying data on cylinder samples gives similar results and is highly correlated (r = 0.96, albeit with a bias of ~1%). The small discrepancy between DM determinations by the two methods could be explained by sample heterogeneity because the SG method gives a DM estimate of the entire potato tube, while the oven-drying method was only carried out on a cylinder taken from a specific part of the tubers.

The LF-NMR CPMG relaxation curves are shown in **Figure 1**, gray-scaled colored according to DM content. It is observed that potatoes exhibiting slow relaxation have low DM content; i.e., an inverse relation is observed between T_2 and DM. **Figure 2** shows the mean distribution of T_2 relaxation times of 210 potatoes estimated by distributed exponential fitting of the relaxation data. The mean T_2 distributed curve shows the presence of four populations (**Figure 2**). Even though the three most slow-relaxing populations are overlapped, the distributed T_2 data indicate the presence of four proton components in the potato tubers. The development in residuals when using 1−5 components for discrete exponential fitting and DoubleSlicing is shown in the Supporting Information. It is observed that, after calculations using four components, both fitting approaches show residuals that are randomly distributed around zero and contain only noise. The minimal improvement in RMSE after 5 components contributes to the validation of a 4-component system. The determination of the correct number of components is a major challenge and often requires data inspection and subjective decision making; the main advantages for the DoubleSlicing method is calculation speed and improved solution diagnostics. The core consistency will drop dramatically from positive to negative values when the appropriate number of components is exceeded. This is shown on one representative NMR relaxation curve in the Supporting Information. By comparison, the drop in fit (e.g., RMSE) between consecutive components is more gradual and less obvious when an overfitted model is used.

Table 2. Effect of Different Modeling Approaches Resolving LF-NMR Relaxation Data Curves[a]

	T_2 (ms)				population size (%)			
fitting method	$T_{2,1}$	$T_{2,2}$	$T_{2,3}$	$T_{2,4}$	$M_{0,1}$	$M_{0,2}$	$M_{0,3}$	$M_{0,4}$
discrete	2.8 (0.2)	45 (2.7)	197 (18)	500 (53)	10 (2.0)	7.6 (1.3)	25 (3.7)	57 (6.1)
DoubleSlicing	3.6 (0.3)	53 (3.5)	213 (18)	508 (53)	9.4 (2.0)	8.4 (1.8)	27 (3.9)	56 (6.5)
distributed[b]	2.5	56	141	473	7.9	6.6	11	75
matrix fit	3.9	84	336	625	10 (1.9)	14 (4.4)	48 (10)	28 (13)

[a] Mean T_2 and population size for 210 potatoes are given with standard deviation in parentheses. [b] The population size for the distributed exponentials was calculated from the intensities of the peak maxima.

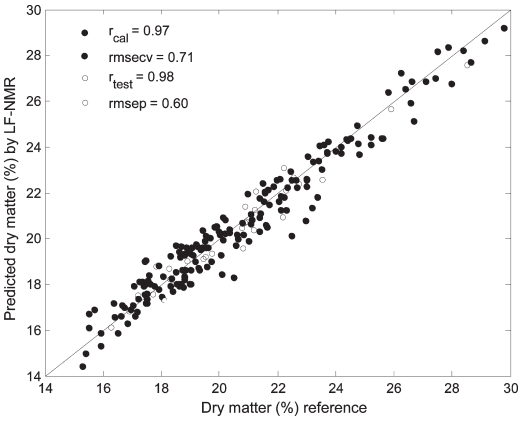

Figure 3. PLS regression (4 latent variables) of LF-NMR parameters (T_2 and M_0) resolved using DoubleSlicing and DM content as the response variable (●, calibration set; ○, test set).

Table 3. Prediction Error Performance for DM Content in Potatoes for Different Modeling Approaches Using LF-NMR Relaxation Curves

PLS modeling input	number of variables	number of LV	r_{cv}	RMSECV	R_{test}	RMSEP
raw NMR data	2048	5	0.96	0.89	0.97	0.65
$T_2 + M_0$ from discrete fitting	8	4	0.98	0.71	0.97	0.62
$T_2 + M_0$ from DoubleSlicing	8	4	0.97	0.71	0.98	0.60
M_0 from matrix fit	4	4	0.94	1.08	0.95	0.83

Table 2 describes the T_2 and M_0 distributions in the potato tubers as found by the four data analysis approaches: distributed exponential fitting, discrete exponential fitting, matrix fit, and DoubleSlicing. The four data analytical approaches give T_2 values that are in the same order of magnitude. It is observed that the classical discrete exponential fitting gives very similar T_2 relaxation time constants as DoubleSlicing, although the latter results in slightly higher values for all components. The magnitudes are also very similar for discrete exponential fitting and DoubleSlicing. The largest population $M_{0,4}$ represents more than half of the total proton population in the potato and is characterized by a $T_{2,4}$ of ~500 ms, representing the most mobile water in the sample. In previous studies, only two water components have been found, representing compartments with 20 and 80% water (*11*, *15*, *16*). The results of PLS regression of LF-NMR data and DM content are given in **Figure 3** and **Table 3**, which also include the model evaluation for LF-NMR data features from discrete exponential fitting, DoubleSlicing, and matrix fit. The table shows that the RMSECV and RMSEP are of similar size for all models, indicating that none of the models are overfitted. PLS regression using raw NMR data gives surprisingly good results with a high correlation ($r = 0.96$) and low error (RMSECV = 0.89) compared to previous observations in studies with less potato samples [r, 0.78 (*14*); *r*, 0.88 (*15*)]. Using the T_2 values and population sizes $M_{0,1-4}$ determined by exponential fitting (*r*, 0.98; RMSECV, 0.71) and DoubleSlicing (*r*, 0.97; RMSECV, 0.71) as variables in a PLS regression to DM content gives slightly better performance than using the raw NMR data. NMR parameter estimation from exponential fitting and DoubleSlicing gives nearly the same results for PLS model performance (**Table 3**).

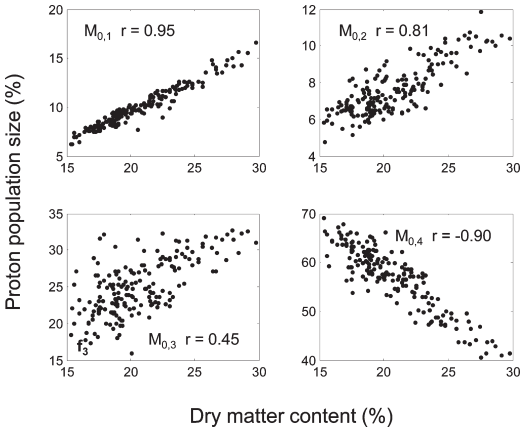

Figure 4. Scatter plot between the population concentration $M_{0,1-4}$ and DM. The correlation coefficients are given in each subplot. T_2 description of the relaxation components is given in **Table 2**.

Inspection of PLS loading and regression coefficients (not shown) revealed that the population sizes $M_{0,1-4}$ (not the T_2 values) were the dominating contributor to the PLS model. This is expected because the population size contains the quantitative information about the proton populations, which, in turn, are expected to be correlated to the DM content. To investigate why there is a high correlation between LF-NMR and DM, the population sizes ($M_{0,1-4}$) are plotted against the DM content (**Figure 4**). $M_{0,1}$ and $M_{0,4}$ are highly correlated to the DM content with $r = 0.95$ and -0.90, respectively. The strong positive correlation between $M_{0,1}$ and the DM content is in agreement with the fact that this population previously has been assigned to water on the surface or inside starch granules (*29*, *30*). The short T_2 relaxation time constant (~3 ms) of $M_{0,1}$ also indicates that this population of protons is strongly associated to potato constituents. In this context, the size of the $M_{0,1}$ proton population is an indirect marker for DM content. The negative correlation between $M_{0,4}$ and DM content is in agreement with the previous finding that this proton population represents extracellular water and water located in the cytoplasm (*29*). The negative correlation to DM content can be explained simply by the cytoplasmatic and extracellular water replacing DM. It is noteworthy that the PLS models in **Table 3** and shown in **Figure 3** give better correlation between predicted versus actual than each individual $M_{0,1-4}$. Thus, the exclusion of DM ($T_{2,4}$) and the proximity to DM ($T_{2,1}$) combined provide a better quantitative description of DM in potato.

With this study, we have confirmed a high correlation between LF-NMR data and DM content of single potatoes using a much larger sample material than previously investigated, including eight cultivars. A new decomposition method of the NMR relaxation curves into mono-exponentials unambiguously revealed that four components were required. The decomposition also revealed why LF-NMR data correlate well to DM. The proportion of the fastest relaxing proton population ($M_{0,1}$) is an indirect marker for DM content, because this population represent water on the surface or inside starch granules. The concentration of the most slowly relaxing protons ($M_{0,4}$) contributes information about DM because high amounts of cytoplasmatic and extracellular water are inversely related to DM content. When the two parameters describing the proportion of the two water pools are combined, $M_{0,1}$ and $M_{0,4}$, the correlation to DM content is further improved. The results show that LF-NMR is the most

precise and direct probe for DM content in potatoes. Because no online potato methods for grading potatoes according to DM content are available yet, there will be several advantages of using LF-NMR methods in the future. An online LF-NMR method can replace measurements of specific gravity of samples of potato bulks and gives more precise quality control data on the individual tuber level.

ABBREVIATIONS USED

LF-NMR, low-field nuclear magnetic resonance; DM, dry matter; UC, ultracentrifugation; NMR, nuclear magnetic resonance; PCA, principal component analysis; PLS, partial least squares; CPMG, Carr−Purcell−Meiboom−Gill; RMSECV, root-mean-square error of cross-validation.

Supporting Information Available: Residuals versus time for 1−5 components when using discrete exponential fitting and DoubleSlicing (Supplementary Figure 1) and solution diagnostic core consistency for 1−5 fitted exponentials using DoubleSlicing (Supplementary Figure 2). This material is available free of charge via the Internet at http://pubs.acs.org.

LITERATURE CITED

(1) Burton, W. G. Cooking and processing quality. In *The Potato*; Burton, W. G., Ed.; Longman Scientific and Technical: Harlow, U.K., 1989; pp 392−405.

(2) Freeman, M.; Jarvis, M. C.; Duncan, H. J. The textural analysis of cooked potato. 3. Simple methods for determining texture. *Potato Res.* **1992**, *35* (2), 103−109.

(3) Martens, H. J.; Thybo, A. K. An integrated microstructural, sensory and instrumental approach to describe potato texture. *LWT—Food Sci. Technol.* **2000**, *33* (7), 471−482.

(4) van Dijk, C.; Fischer, M.; Holm, J.; Beekhuizen, J. G.; Stolle-Smits, T.; Boeriu, C. Texture of cooked potatoes (*Solanum tuberosum*). 1. Relationships between dry matter content, sensory-perceived texture, and near-infrared spectroscopy. *J. Agric. Food Chem.* **2002**, *50* (18), 5082−5088.

(5) van Marle, J. T.; Stolle-Smits, T.; Donkers, J.; van Dijk, C.; Voragen, A. G. J.; Recourt, K. Chemical and microscopic characterization of potato (*Solanum tuberosum* L.) cell walls during cooking. *J. Agric. Food Chem.* **1997**, *45* (1), 50−58.

(6) McComber, D. R.; Horner, H. T.; Chamberlin, M. A.; Cox, D. F. Potato cultivar differences associated with mealiness. *J. Agric. Food Chem.* **1994**, *42* (11), 2433−2439.

(7) Burton, W. G. Varietal differences in growth, yield of tubers and percentage of dry matter in the tubers. In *The Potato*; Burton, W. G., Ed.; Longman Scientific and Technical: Harlow, U.K., 1989; pp 142−215.

(8) Jefferies, R. A.; Heilbronn, T. D.; Mackerron, D. K. L. Estimating tuber dry matter concentration from accumulated thermal time and soil moisture. *Potato Res.* **1989**, *32* (4), 411−417.

(9) Haase, N. U. Rapid estimation of potato tuber quality by near-infrared spectroscopy. *Starch/Staerke* **2006**, *58* (6), 268−273.

(10) Scanlon, M. G.; Pritchard, M. K.; Adam, L. R. Quality evaluation of processing potatoes by near infrared reflectance. *J. Sci. Food Agric.* **1999**, *79* (5), 763−771.

(11) Thybo, A. K.; Bechmann, I. E.; Martens, M.; Engelsen, S. B. Prediction of sensory texture of cooked potatoes from the raw material using uniaxial compression, near infrared spectroscopy and low field ^{1}H NMR spectroscopy. *LWT—Food Sci. Technol.* **2000**, *33* (2), 103−111.

(12) Belton, P. S. Can nuclear magnetic resonance give useful information about the state of water in foodstuffs? *Comments Agric. Food Chem.* **1990**, *2* (3), 179−209.

(13) Berendsen, H. J. C. Rationale for using NMR to study water relations in foods and biological tissues. *Trends Food Sci. Technol.* **1992**, *3*, 202−205.

(14) Thybo, A. K.; Andersen, H. J.; Karlsson, A. H.; Donstrup, S.; Stodkilde-Jorgensen, H. Low-field NMR relaxation and NMR-imaging as tools in differentiation between potato sample and determination of dry matter content in potatoes. *LWT—Food Sci. Technol.* **2003**, *36* (3), 315−322.

(15) Thygesen, L. G.; Thybo, A. K.; Engelsen, S. B. Prediction of sensory texture quality of boiled potatoes from low-field ^{1}H NMR of raw potatoes. The role of chemical constituents. *LWT—Food Sci. Technol.* **2001**, *34* (7), 469−477.

(16) Mortensen, M.; Thybo, A. K.; Bertram, H. C.; Andersen, H. J.; Engelsen, S. B. Cooking effects on water distribution in potatoes using nuclear magnetic resonance relaxation. *J. Agric. Food Chem.* **2005**, *53* (15), 5976−5981.

(17) Behrend, P.; Märcker, M.; Morgen, A. Ueber den zuzammenhang des specifischen gewichts mit dem stärkemehl- und trockensubstanz-gehalt der kartoffeln, sowie über die methode der stärkemehlbestimmung in den kartoffeln. *Landwirtsch. Vers.-Stn.* **1880**, *25*, 107−168.

(18) Simmonds, N. Relations between specific gravity, dry matter content and starch content of potatoes. *Potato Res.* **1977**, *20* (2), 137−140.

(19) Carr, H. Y.; Purcell, E. M. Effects of diffusion on free precession in nuclear magnetic resonance experiments. *Phys. Rev.* **1954**, *94* (3), 630−638.

(20) Meiboom, S.; Gill, D. Modified spin−echo method for measuring nuclear relaxation times. *Rev. Sci. Instrum.* **1958**, *29* (8), 688−691.

(21) Wold, S.; Martens, H.; Wold, H. The multivariate calibration problem in chemistry solved by the PLS method. In *Proceedings from Conference on Matrix Pencils*, 973rd ed.; Ruhe, A.; Kågström, B., Eds.; Springer Verlag: Heidelberg, Germany, 1983; pp 286−293.

(22) Provencher, S. W. CONTIN: A general purpose constrained regularization program for inverting noisy linear algebraic and integral equations. *Comput. Phys. Commun.* **1982**, *27* (3), 229−242.

(23) Marquardt, D. W. An algorithm for least-squares estimation of nonlinear parameters. *J. Soc. Ind. Appl. Math.* **1963**, *11* (2), 431−441.

(24) Bechmann, I. E.; Pedersen, H. T.; Nørgaard, L.; Engelsen, S. B. Comparative chemometric analysis of transverse low-field ^{1}H NMR relaxation data. In *Advances in Magnetic Resonance in Food Science*; Belton, P. S., Hills, B. P., Webb, G. A., Eds.; The Royal Society of Chemistry: Cambridge, U.K., 1999; pp 217−225.

(25) Pedersen, H. T.; Bro, R.; Engelsen, S. B. Towards rapid and unique curve resolution of low-field NMR relaxation data: Trilinear SLICING versus two-dimensional curve fitting. *J. Magn. Reson.* **2002**, *157* (1), 141−155.

(26) Engelsen, S. B.; Bro, R. PowerSlicing. *J. Magn. Reson.* **2003**, *163* (1), 192−197.

(27) Andrade, L.; Micklander, E.; Farhat, I.; Bro, R.; Engelsen, S. B. DOUBLESLICING: A non-iterative single profile multi-exponential curve resolution procedure—Application to time-domain NMR transverse relaxation data. *J. Magn. Reson.* **2007**, *189* (2), 286−292.

(28) Hansen, C. L.; Rinnan, A.; Engelsen, S. B.; Janhoj, T.; Micklander, E.; Andersen, U.; van den Berg, F. Effect of gel firmness at cutting time, pH, and temperature on rennet coagulation and syneresis: An in situ ^{1}H NMR relaxation study. *J. Agric. Food Chem.* **2010**, *58* (1), 513−519.

(29) Hills, B. P.; Lefloch, G. NMR studies of non-freezing water in cellular plant tissue. *Food Chem.* **1994**, *51* (3), 331−336.

(30) Straadt, I. K.; Thybo, A. K.; Bertram, H. C. NaCl-induced changes in structure and water mobility in potato tissue as determined by CLSM and LF-NMR. *LWT—Food Sci. Technol.* **2008**, *41* (8), 1493−1500.

Received for review April 8, 2010. Revised manuscript received September 2, 2010. Accepted September 4, 2010. The Danish Ministry of Food Agriculture and Fisheries and the Danish Agency for Science Technology and Innovation are greatly acknowledged for financial support to the project (FøSu Project: Gourmet Roots—The "Roots" of Wellness and Healthiness, JNR 3304-FSE-06-0504).

Paper VI

Using PARAFAC core-consistency to estimate the number of components in LF-NMR data - application to in-situ studies of mechanically induced gel syneresis in cheese production.

Accepted for publication in Magnetic Resonance in Food Science, proceedings for the 10th NMR in Food conference.

Using PARAFAC core-consistency to estimate the number of components in LF-NMR data - application to in-situ studies of mechanically induced gel syneresis in cheese production

C.L. Hansen, F. van den Berg and S.B. Engelsen

Quality & Technology, Department of Food Science, Faculty of Life Sciences, University of Copenhagen, Rolighedsvej 30, 1958 Frederiksberg C, Denmark

1 INTRODUCTION

A major challenge with low field NMR data analysis is estimation of the right number of exponential components. In this work we will demonstrate how PARAFAC core-consistency, using the so-called DoubleSlicing method *(1)*, can help to unambiguously determine the number of exponentials in the signal. The new approach will be demonstrated in a study where we investigate in-situ rennet induced milk gel formation and in-situ mechanically induced gel syneresis using low field nuclear magnetic resonance (LF-NMR) *(2)*.

In cheese manufacture the milk gel formation and syneresis processes are of major importance for the water content, texture and flavour properties of the final product. Several NMR relaxation studies have been reported that investigate milk gel formation *(3-6)* and syneresis *(4, 6, 7)*. The effect of milk gel syneresis on water proton relaxation has so far been studied on undisturbed gels that only exhibit spontaneous endogenous syneresis (i.e. syneresis caused by pressure being built up during network formation within the gel). This is however not representative for industrial cheese manufacturing where mechanical cutting of the gel into dices is an essential process step. Two inconsistencies exist in the interpretation of the water proton relaxation during milk gel formation and syneresis: (A) the development of the transverse relaxation time constant, T_2, and its corresponding proton population size during gel formation and (B) the number of proton populations (i.e. exponential terms) necessary to model water proton relaxation during cheese gel formation. Two studies have found no change in the relaxation time constant T_2 during milk gel formation *(4, 6)*, while other researchers *(3)* found small changes in the T_2 relaxation time during the gel formation. The latter study found (without providing explicit proof) that three populations of water protons were required to describe the relaxation during milk gel formation, while the former studies found that one proton population was adequate to describe the proton relaxation. There is however a general agreement that the onset of milk gel syneresis is associated with appearance of an additional water population with slower relaxation, which are the protons in the whey water *(2-4, 6)*.
One of the reasons for the discrepancy in number of proton components is related to the data analytical methods applied for studying the NMR relaxation data. The major challenge when analysing relaxation decay curves of LF-NMR experiments using multi-

exponential curve fitting is to decide the appropriate number of exponential terms that describe actual water populations present in the sample. A new exponential curve fitting method to assist in the determination of water populations called DoubleSlicing was introduced in 2003 by Micklander et al. *(8)*. Andrade et al. *(1)* further refined the method using the PowerSlicing scheme of Engelsen and Bro *(9)*. The DoubleSlicing technique utilizes the fact that different parts (slices) of a given multi-exponential decay curve consist of the same underlying exponential terms, but in a different quantities (concentrations). Because all underlying exponential terms are present in all slices of the DoubleSliced data cube, tensor models such as direct tri-linear decomposition (DTLD) or parallel factor analysis (PARAFAC *(10)*) can extract the individual exponential terms. These tensor methods have some unique possibilities for validating the solution (e.g. finding the appropriate number of water proton populations) and are surprisingly faster than conventional curve fitting methods.
The primary objective of this study was to investigate the effect of milk gel formation and in-situ mechanically induced gel syneresis on NMR proton relaxation. The secondary objective was to demonstrate DoubleSlicing as a method for determining the appropriate number of components in a semi-automated way. For these purposes the effect of milk gel formation and syneresis was studied using an experimental design with three factors: pH, temperature and gel firmness at cutting time. Time domain LF-NMR measurements were carried out in parallel with rheological measurements.

2 MATERIALS AND METHODS

2.1 Design of experiment

Rennet induced gel formation of skim milk and the subsequent syneresis process after gel cutting was studied by time domain LF-NMR. As experimental procedure rennet was added to skim milk in a bigger volume which was subsequently split into two fractions: one was immediately transferred into a 17mm diameter NMR tube and continuously analyzed inside a LF-NMR spectrometer; the other fraction was injected into a rheological instrument which continuously measured gel firmness during gel formation. The role of the rheological measurements was to ensure that the gels formed in the NMR tube for repeated experiments had the same, desired firmness at gel cutting time. A knife - consisting of a thin Plexiglass blade tightly matching the tube inner diameter - was used to cut the gel once over the entire length of the NMR tube as soon as the firmness of the gel in the twin sample had reached a pre-defined level (Figure 1).

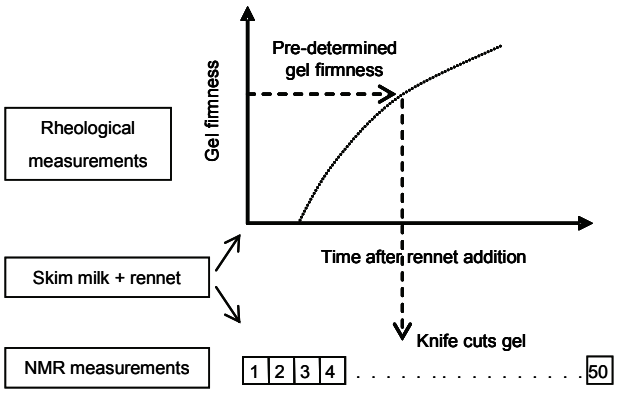

Figure 1 *Timing diagram of the study: Rennet was added to skim milk, which was split into a fraction for rheological analysis and a fraction for LF-NMR analysis. A knife cut the formed gel once over the entire length and inner diameter of the NMR tube, once the gel reached a pre-determined firmness. The LF-NMR spectrometer continued to analyse the gel, during the syneresis, which resulted in fifty snapshot/time-frames for each experimental run.*

During the gel formation and syneresis three experimental factors were investigated on two levels (a 2^3 factorial design). A pseudo centre point was added for the factors pH and gel firmness at cutting for the high temperature level (Figure 2). Each of the corner points in the design were run in duplicate, while the pseudo centre point was run in four replicates, resulting in a total of 20 experiments, carried out in random order.

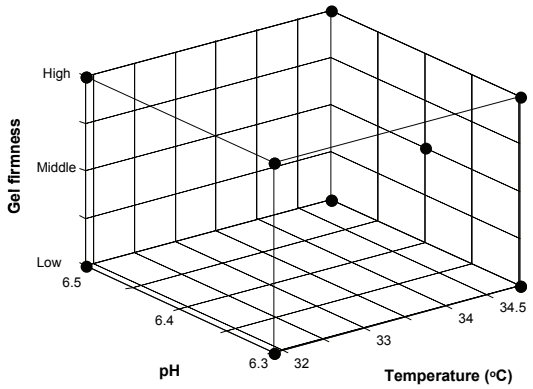

Figure 2 *The randomized 2^3 factorial design used to study gel formation and syneresis. The experimental factors varied were pH, temperature and gel firmness at cutting. The corner points in the design were run in duplicate, while the pseudo centre point (position selected due to experimental limitations) was run in four replicates, resulting in 20 experiments.*

2.2 NMR Spectroscopy

Time domain LF-NMR analysis was carried out on a benchtop 23.2 MHz Maran pulsed ^{1}H NMR spectrometer (Oxford Instrument, United Kingdom) equipped with a 17mm diameter variable temperature probe head. The CPMG (Carr-Purcell-Meiboom-Gill) pulse sequence was used to determine the relaxation behaviour. It was chosen because it minimizes the influence of magnetic field inhomogeneities, diffusion and chemical exchange *(11)*. A total of 8100 data points/echo times were acquired, with a 90–180 pulse spacing (τ) value of 500μs. Only the even numbered data points were used in the data analysis, resulting in 4050 data acquisition points per measurement. Prior to the first measurement the frequency of the instrument was adjusted on a 10mM CuSO4 standard sample. During gel formation four scans were accumulated with a relaxation delay between consecutive scans of 14 seconds. Prior to the four scans each measurement was preceded by two dummy scans leading to a total measurement time of 2 minutes and 12 seconds. Measurements were carried out continuously until a maximum of 100 minutes after cutting.

2.3 NMR data analysis by DoubleSlicing

Time domain LF-NMR data are commonly analyzed using multi-exponential fitting which applies non-linear iterative curve-fitting algorithms to extract and characterize the underlying pure exponentials from random noise in the data (Equation 1):

$$M(t) = \sum_{n=1}^{N} M_{0n} \cdot \exp\left(\frac{-t}{T_{2,n}}\right) + e(t) \qquad (1)$$

M(t) is the reduced magnetization at time t, M_{0n} is the concentration or magnitude parameter of the n^{th} exponential, $T_{2,n}$ is the corresponding transverse relaxation time constant and e(t) is the residual error. One of the pitfalls of curve fitting based on hard modelling to a functional form such as Equation 1 is that adding additional exponential components will per definition improve the fit (i.e. reduce the residual) even if only meaningless noise/none systematic variation is being fitted.
Micklander et al. *(1)* introduced an alternative non-iterative and rapid technique for curve resolution called DoubleSlicing. The technique pseudo-upgrades the single relaxation curve to become tri-linear data, by cutting the relaxation curve into slices (Figure 3). By selectively removing parts of the signal curve (slicing) and using the remaining curve along with the original curve, the relaxation curve can be transformed from a one-dimensional signal (a vector) into two-dimensional data (a matrix). By repeating this procedure on the matrix, the data is transformed to three-dimensional data (a cube or tensor). A DoubleSliced relaxation curve can be decomposed using tensor models such as DTLD or PARAFAC into (Equation 2):

$$\underline{X} = ABC^T + \underline{E} \qquad (2)$$

A, **B** and **C** are matrices and there outer product forms a model/approximation of **X**, while **E** holds the residual variation not explained by the model. If the **X** is decomposed using the right number of components, then matrix **B** will contain the true underlying mono-exponential components *(10)*. From the resolved mono-exponential components it is easy to determine T_2 and M_0 by using Equation 1.

Some major advantages in using tensor models are that they require no initial guesses and have unique possibilities for validation of the solution *(10, 12)*. Methods of solution diagnostics include relative reduction in root mean square error (RMSE), split-half validation and core-consistency. One general challenge of the DoubleSlicing method is to capture the fast relaxing protons, as these are rapidly attenuated in the relaxation curve. Andrade et al. *(1)* therefore further refined the DoubleSlicing method using the PowerSlicing scheme by Engelsen and Bro *(9)*. The PowerSlicing approach ensures that components with fast relaxing protons are present in sufficiently many of the slices by slicing more frequently at the short echo times, since the fast relaxing component only have a strong presence in the beginning of the curve (first echo times) .

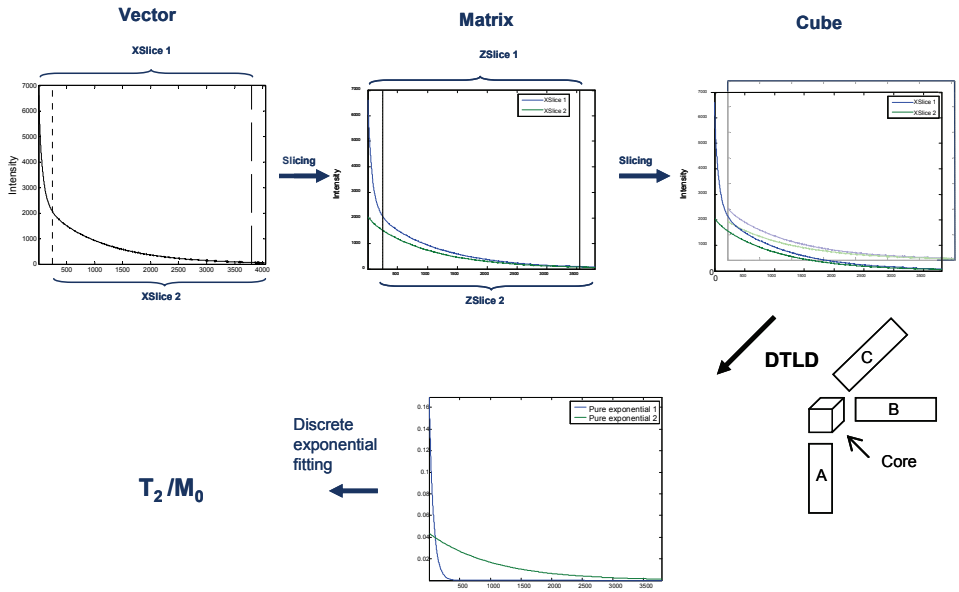

Figure 3 *Overview of the principle behind DoubleSlicing. The NMR signal is one-dimensional data (a vector) and a sum of N exponential decays corresponding to N water populations. The curve is divided in a number (here two for illustration purposes) of largely overlapping segments (X-slices) by removing the same number of first or last echo times. These two segments are placed in one matrix (2-dimentional) and the procedure is repeated to form (Z-slices) which are stacked behind each other to form a data cube (3-dimensional). This cube is decomposed by a DTLD factor model and the correct rank or dimensionality is then equal to N, the number of distinct water populations in the original signal. The profiles are from the DTLD decomposition (so-called loadings) are mono-exponential and can be used to estimate concentrations (M_0) and relaxation time constants (T_2).*

In the present study a step-wise DoubleSlicing algorithm was used as an extension to the Slicing algorithm by Pedersen et al. *(13)*. The DoubleSlicing algorithm slices the single relaxation curve 11 times at 1, 2, 4, 8, 16, 32, 64, 128, 256, 512, 1024 echo time variable (hence eleven X-slices compared to just two shown in Figure 3). The exponential increase in the slicing variable number is the so-called PowerSlicing approach and it ensures that fast relaxing components are present in sufficiently many slices. Subsequently, the eleven

slices are PowerSliced once again eleven times, which transform the single relaxation curve into a three-dimensional data cube. The three-dimensional data cube was decomposed by DTLD using one to four components. All the algorithms are available in MatLab code from www.models.life.ku.dk.

2.4 Estimation of the number of exponential components

Many methods have been evaluated for the determination of the appropriate number of exponential terms in Equation 1 or components in the tri-linear decomposition model. Obvious diagnostics criteria are loss in residual, explained variance, etc. However, the task remain difficult using these methods because the fit will always improve by adding more terms and the statistical or numerical evaluation on whether an additional term is justified is far from trivial, often giving conflicting information for different criteria. In this work we developed a semi-automated selection procedure for model complexity based on two-times-two evaluation criterion.
Bro and Kiers *(12)* proved that the core-consistency is a useful validation diagnostic for evaluating the appropriateness of fit of tri-linear models (Figure 4). The core-consistency is used to evaluate the tensor model in Equation 2. It expresses how close or far a model is from the assumed tri-linear structure. It is obtained by comparing the elements in an unconstrained or free core tensor with the element in a constrained (super-diagonal) tensor core (our target core). The core-consistency is expressed as the percentage , where a high percentage indicates that the unconstrained solution is close to or consistent with our desired modeling objective *(12)*. Thus, for a perfect tri-linear model the core-consistency is 100%, the desirable value, whereas e.g. negative percentages indicate a very poor model. Once the maximal appropriate number of components is exceeded, the core-consistency will typically drop dramatically. Core-consistency can thus be used as a diagnostic tool but it should always be used in combination with other diagnostics, because it sometimes leads to over-parameterized models. We therefore combine core-consistency with the loss of fit (RMSE).

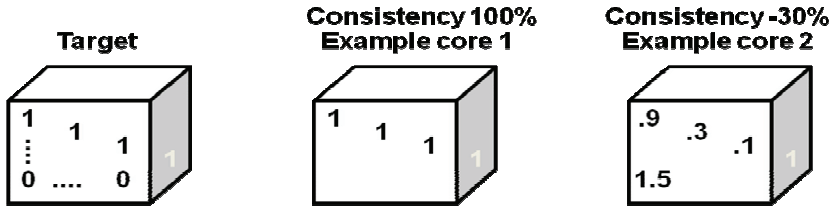

Figure 4 *Tri-linear core-consistency - if the core-consistency is much lower than 100% the tri-linear model is not appropriate i.e. it has the wrong number of components.*

In our model evaluation we construct tri-linear DTLD models with one to four components. Note that e.g. the first component is not the same for these four choices because tensor models are not embedded *(10)*. To justify inclusion of an additional component both criteria (Table 1) should be met. An advantage of the algorithm is that it can automatically find the appearance of additional components during the development of dynamic experiments such as gel formation and syneresis without any prior knowledge on the system. Also note that each LF-NMR relaxation measurement is modelled

independently (Figure 3). Hence any observation made over the time axis of the experiment can be based on sovereign measurement points, i.e. single relaxation curves.

Table 1 *Diagnostic methods and their corresponding threshold values used in the algorithm to validate the rank/number of components appropriate to describe each DoubleSliced relaxation curve.*

Diagnostic method	Threshold value for inclusion
Core consistency	> 60%
Loss of root-mean-squared-error[a] (RMSE)	> 10%

[a]Loss in root-mean-squared-error is relative to the model with one component less

3 RESULTS AND DISCUSSION

The raw CPMG data for a representative cheese batch is shown in Figure 5. The data show that the overall relaxation becomes systematically slower with experiment time after cutting of the milk gel. This implies that the proton populations progressively change as a result of the syneresis process, where water (i.e. whey) is expelled from the gel network. By visual inspection of the relaxation curves in Figure 5 it is not possible to observe any changes in the relaxation curves prior to cutting of the gel.

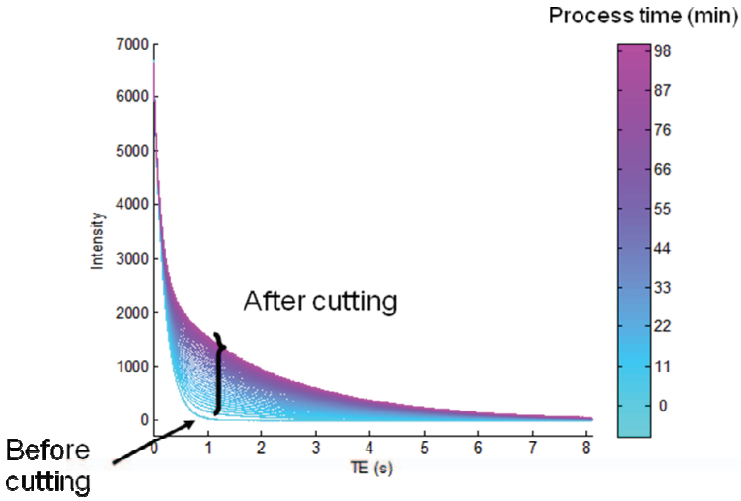

Figure 5 *NMR CPMG relaxation curves during gel formation and syneresis in one gel formation and syneresis experiment.*

The core-consistency and RMSE will be illustrated and evaluated using relaxation curves from one gel formation and syneresis experiment (pH = 6.3, T = 35^{o}C, low firmness at cut). Figure 6 shows how the core-consistency and loss in RMSE change as a function of the number of exponential terms included in the modeling of the relaxation curves. Since core-consistency is consistently 100% when the relaxation curves were fitted to two

exponentials, it is clear that at least two populations are present during the entire experimental run. Using three exponentials results in negative core-consistency during the initial phase, gel formation. The change from a core-consistency of 100% to negative values makes it easy to asses that only two components are present during gel formation, prior to cutting. In comparison, the loss in RMSE does not show strikingly different values when including three components. Mono-exponential fitting of the relaxation curves by DTLD before cutting yielded a RMSE of 0.045, while bi-exponential fitting results in a RMSE of 0.038 corresponding to a 15% reduction. Tri-exponential fitting resulted in a RMSE of 0.036 or a 4% reduction from a two component model (i.e. < 10%).

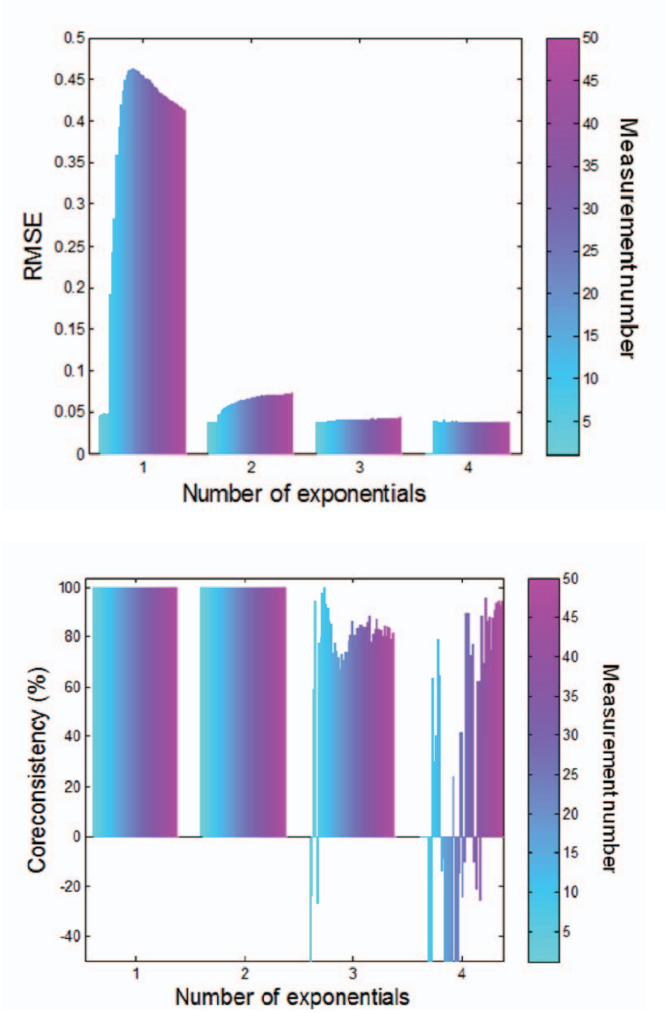

Figure 6 *Core-consistency and loss in RMSE change as a function of batch run-time and the number of exponential terms included in the modelling of a representative cheese batch (consisting of 50 NMR relaxation curves equals one batch of approximately 100 minutes).*

By comparing of the results of DoubleSlicing with traditional discrete exponential fitting of one relaxation curve before cutting (Figure 7) we see that two proton components are in

fact present in milk and the gel. This is evident from a plot of residuals after fitting one component (Figure 7B), which show that residuals are not random and equally distributed around zero as LF-NMR measurement noise should be. After fitting two components the residual become random (Figure 7C) showing that no more information is present in the data.

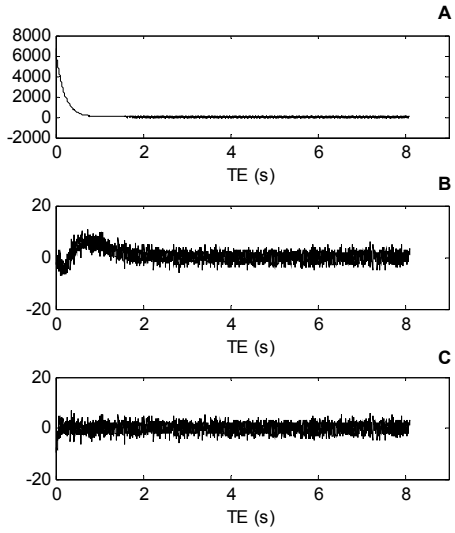

Figure 7 *(A) One CPMG relaxation curve, (B) residual after one component discrete exponential fitting and (C) residual after two components.*

When the appropriate number of proton components has been established the development in T_2 and population sizes can be calculated for each LF-NMR snapshot. The result for two representative batches is shown in Figure 8. The abrupt change at the cutting point and the otherwise smooth curves gives rise to high confidence in both the modelling approach and the automated method of model complexity determination. During gel formation and syneresis two proton populations with the characteristic transverse relaxation times $T_{2,1}$ and $T_{2,2}$ are present within the gel. The size of $T_{2,1}$ and $T_{2,2}$ show that proton population come from water associated with different parts/constituents of the gel. The data analysis clearly indicates that bi-exponential behaviour characterizes the system during gel formation and prior to cutting. Cutting unambiguously introduces a new component $T_{2,3}$ representing the whey.

The relative population sizes determined during modelling quantitatively shows how much water (protons) with different T_2's is present at a given time during the syneresis (Figure 8). The main portion of the (water) protons (relative contribution in total signal of 98.8%, SD = 0.2%) prior to cutting of the gel originate from a population which is characterized by an average $T_{2,1}$ of 180.7ms (SD = 5.1ms). The primary development can be summarized as follows: fast relaxing water ($T_{2,1}$ ~ 180ms) within the gel is mainly converted to slow relaxing water ($T_{2,3}$ ~ 2000 to 2200ms) situated outside the gel. A small fraction of the fast relaxing water protons is seemingly converted into water present within the gel with an intermediate relaxation rate ($T_{2,2}$ ~ 400 to 500ms). The rate by which the water leaves a cut milk gel (i.e. syneresis) can be described as a reaction of first order, meaning that the rate of water expulsion is dependent on the amount of water present at a given time *(14)*.

During syneresis the bulk proton population characterized $T_{2,1}$ steadily decrease to a level of ~ 50 – 70% of the water protons after 100 minutes. Assuming, this proton population is primarily associated to casein micelles as previously suggested *(15)*, then the decrease in population size initiated by cutting, suggest that the casein micelles are being steadily dehydrated.

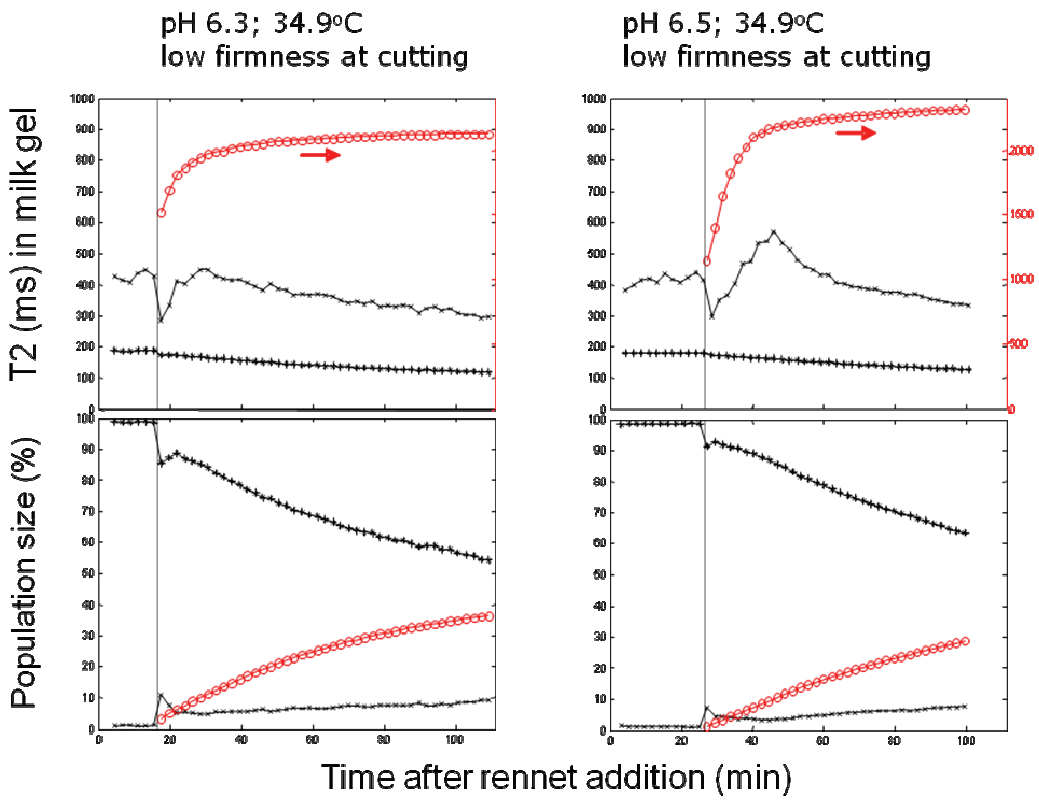

Figure 8 Development in T_2 (upper row) and relative population size (lower row) during gel formation and syneresis of two different cheese experiments with different pH-values. The vertical line indicates the time when the milk gel was cut.

4 CONCLUSION

LF-NMR was used to characterize skim milk gel formation and syneresis qualitatively and quantitatively using a new automated DoubleSlicing algorithm. Analysis of relaxation data using DoubleSlicing data proved to be precise in finding the appropriate number of underlying exponential components (i.e. proton populations) in single relaxation curves measured during gel formation and syneresis.

In-situ LF-NMR measurements have proven an excellent tool for studying rennet coagulation and syneresis. During coagulation two proton populations with distinct transverse relaxation times ($T_{2,1}$ = 181ms, $T_{2,2}$ = 465ms) were present in fractions (98.9%

and 1.1% respectively). Mechanical cutting of the gel in the NMR tube induced macro-syneresis, which led to the appearance of an additional proton population ($T_{2,3}$ = 1500 to 2200ms) identified as whey. The syneresis rate was found to be significantly dependent on pH in the range from 6.3 to 6.5 and temperature in the range from 32 to 35ºC. Gel firmness at cutting did not show any significant effect on syneresis rate *(2)*.

5 REFERENCES

Reference List

1. Andrade, L.; Micklander, E.; Farhat, I.; Bro, R.; Engelsen, S. B. DOUBLESLICING: A non-iterative single profile multi-exponential curve resolution procedure - Application to time-domain NMR transverse relaxation data. *J. Magn. Reson.* **2007,** *189* (2), 286-292.

2. Hansen, C. L.; Rinnan, A.; Engelsen, S. B.; Janhoj, T.; Micklander, E.; Andersen, U.; van den Berg, F. Effect of Gel Firmness at Cutting Time, pH, and Temperature on Rennet Coagulation and Syneresis: An in situ H-1 NMR Relaxation Study. *J. Agric. Food Chem.* **2010,** *58* (1), 513-519.

3. Hinrichs, R.; Bulca, S.; Kulozik, U. Water mobility during renneting and acid coagulation of casein solutions: a differentiated low-resolution nuclear magnetic resonance analysis. *International Journal of Dairy Technology* **2007,** *60* (1), 37-43.

4. Lelièvre, J.; Creamer, L. K. NMR-study of formation and syneresis of renneted milk gels. *Milchwissenshaft-Milk Science International* **1978,** *33* (2), 73-76.

5. Mariette, F.; Maignan, P.; Marchal, P. NMR relaxometry: A sensor for monitoring acidification of milk. *Analusis* **1997,** *25* (1), M24-M27.

6. Tellier, C.; Mariette, F.; Guillement, J. P.; Marchal, P. Evolution of water proton nuclear magnetic relaxation during milk coagulation and syneresis - structural implications. *J. Agric. Food Chem.* **1993,** *41* (12), 2259-2266.

7. Ozilgen, M.; Kauten, R. J. NMR analysis and modelling of shrinkage and whey expulsion in rennet curd. *Process Biochemistry* **1994,** *29* (5), 373-379.

8. Micklander, E.; Thygesen, L. G.; Pedersen, H. T.; van den Berg, F.; Bro, R.; Engelsen, S. B. Multivariate analysis of time domain NMR signals in relation to food quality. In *Magnetic Resonance in Food Science: Latest Developments* , Webb, G. A.; Belton, P. S.; Rutledge, D. N., Eds.; The Royal Society of Chemistry: 2003; pp 239-254.

9. Engelsen, S. B.; Bro, R. PowerSlicing. *J. Magn. Reson.* **2003,** *163* (1), 192-197.

10. Bro, R. PARAFAC. Tutorial and applications. *Chemom. Intell. Lab. Syst.* **1997,** *38*, 149-171.

11. Hills, B. P.; Takacs, S. F.; Belton, P. S. A new interpretation of proton NMR relaxation-time measurements of water in food. *Food Chem.* **1990,** *37* (2), 95-111.

12. Bro, R.; Kiers, H. A. L. A new efficient method for determining the number of components in PARAFAC models. *J. Chemom.* **2003,** *17* (5), 274-286.

13. Pedersen, H. T.; Bro, R.; Engelsen, S. B. Towards rapid and unique curve resolution of low-field NMR relaxation data: Trilinear SLICING versus two-dimensional curve fitting. *J. Magn. Reson.* **2002,** *157* (1), 141-155.

14. Fox, P. F.; McSweeney, P. L. H. *Dairy Chemistry and Biochemistry;* Klüwer Academic/Plenum Publishers: New York, 1998.

15. Le Dean, A.; Mariette, F.; Marin, M. H-1 nuclear magnetic resonance relaxometry study of water state in milk protein mixtures. *J. Agric. Food Chem.* **2004,** *52* (17), 5449-5455.

PhD thesis
ISBN 978-87-7611-390-2

CHRISTIAN BØGE LYNDGAARD

OPTIMIZATION OF DAIRY PROCESSES
APPLIED SPECTROSCOPY AND CHEMOMETRICS

SL grafik